EFFECT OF INSTABILITIES IN THE BUOYANCY-DRIVEN FLOW ON THE BOTTOM OXYGEN: APPLICATIONS TO THE LOUISIANA SHELF

A Dissertation

by

VALERIYA KISELKOVA

Submitted to the Office of Graduate Studies of
Texas A&M University
in partial fulfillment of the requirements for the degree of

DOCTOR OF PHILOSOPHY

May 2008

Major Subject: Oceanography

EFFECT OF INSTABILITIES IN THE BUOYANCY-DRIVEN FLOW ON THE BOTTOM OXYGEN: APPLICATIONS TO THE LOUISIANA SHELF

A Dissertation

by

VALERIYA KISELKOVA

Submitted to the Office of Graduate Studies of
Texas A&M University
in partial fulfillment of the requirements for the degree of

DOCTOR OF PHILOSOPHY

Approved by:

Chair of Committee,	Steven F. DiMarco
Committee Members,	Robert D. Hetland
	David Brooks
	Billy L. Edge
Head of Department,	Piers Chapman

May 2008

Major Subject: Oceanography

ABSTRACT

Effect of Instabilities in the Buoyancy-Driven Flow on the Bottom Oxygen: Applications to the Louisiana Shelf. (May 2008)

Valeriya Kiselkova, B.S., Far Eastern State Technical University;

M.S., Far Eastern State Technical University

Chair of Advisory Committee: Dr. Steven F. DiMarco

A combination of *in situ* sampling and numerical modeling was used to investigate the effects of mesoscale (<50 km) circulation patterns and stratification on the evolution of hypoxia on the Louisiana Shelf. Temperature, salinity, and dissolved oxygen concentrations records reveal the presence of an alongshelf meander, which is manifested vertically and horizontally as a wave-like distribution of the properties in the water column. The observations suggest the meander is a ubiquitous characteristic of the shelf with alongshore spatial scale approximately 50 km and less, which is consistent with the locations of sandy shoals along the coast and the local deformation radius.

Twelve numerical experiments using an idealized three-dimensional shelf circulation model were performed to evaluate the relative importance of the variable bottom topography and freshwater forcing on the development, evolution, and scales of the dynamic instabilities. The inclusion of the shoals into the bottom topography showed the development of the dynamic instabilities as the flow passed over the shoals and downstream. Introduction of fresh water onto the shelf resulted in greater salinity differences, and, as a consequence in the formation of the dynamically unstable salinity fronts along the plume edge. The combination of the freshwater forcing and shoaling topography produced competing and complex interactions.

Six numerical experiments were analyzed in order to investigate the effect of dynamic instabilities on spatial and temporal patterns of dissolved oxygen

concentrations along the shelf. Although a linear relationship between Brunt-Väisälä frequency and dissolved oxygen deficit was expected, a nonlinear loop-like relationship was discovered that reflects the response of biochemical properties to the alongshelf variability of the density field. Comparison of the numerical modeling runs to observations of density and dissolved oxygen concentrations on the Louisiana Shelf reinforces the importance of physical processes such as topographic steering and/or freshwater forcing on the alongshore distribution of physical and biochemical properties. It suggests that the time scales of respiration (~3 days) and buoyancy transfer processes (~5-7 days), associated with the physical processes that are responsible for water column stability and ventilation, are similar to the time scales associated with the benthic respiration rates.

DEDICATION

To my husband Ilya Pavlenko
and
my mother Natalia Kiselkova

ACKNOWLEDGEMENTS

I would like to thank my committee members: Dr. Steven DiMarco for his superb advising and careful review of the manuscript; Dr. Robert Hetland for his creative ideas and assistance with the programming; Dr. David Brooks and Dr. Billy Edge for their suggestions and comments.

I also would like to express my heartfelt thanks to my husband Ilya Pavlenko for his endless love, incredible patience and support during the entire study. Sincere thanks go to my grandmother and whole family for their encouragement and inspiration.

Last, but not least, my special thanks go to David Shepler for being a true friend through the hard times and always.

This study was supported by NOAA's Center for Sponsored Coastal Ocean Research, under the grant numbers NA03NOS4780039 and NA06NOS4780198.

TABLE OF CONTENTS

CHAPTER Page

LIST OF FIGURES

LIST OF FIGURES (continued)

LIST OF FIGURES (continued)

FIGURE Page

LIST OF FIGURES (continued)

FIGURE Page

LIST OF FIGURES (continued)

FIGURE Page

LIST OF TABLES

CHAPTER I

INTRODUCTION

1.1 Hypoxia in the Northern Gulf of Mexico and other regions around the world

Hypoxia in aquatic systems refers to the waters where dissolved oxygen concentration is below 1.4 $ml \cdot L^{-1}$ or 2 $mg \cdot L^{-1}$ [*Rabalais et al*., 2001; *Rowe and Chapman*, 2002]. Hypoxic (low oxygen) and anoxic (no oxygen) waters have existed throughout geologic time and presently occur in many of the ocean's deeper environments, such as oxygen minimum layers, deep basins, and fjords [*Kamykowski and Zentara*, 1990; *Diaz*, 2001; *Osterman et al*., 2005]. The occurrence of hypoxia and anoxia in shallow, coastal and estuarine areas appears to be increasing, possibly accelerated by human activities [*Diaz and Rosenberg*, 1995; *Diaz*, 2001; *Rabalais et al*., 2002b].

As on land, oxygen is vital in the marine environment to sustain life in fish and invertebrates. Oxygen introduced into the water from the atmosphere and from phytoplankton, helps to maintain the respiration needs of all animals, including those that swim or move above the bottom and those that reside in sediments. When the oxygen consumption rate exceeds resupply, oxygen concentrations may decline below levels that sustain most animal life [*Diaz*, 2001]. When the oxygen level remains low for prolonged time periods, marine organisms suffer, and ecosystem is altered, resulting in the forced migration, decrease in food supply, increase in mortality, and reduction of biodiversity [*Rabalais et al.*, 2001; *Rabalais et al*., 2002b]. Fish population studies by *Wu et al.* [2003] showed that chronic exposure to hypoxia in some aquatic environments cause a disruption in the endocrine system and reproductive impairment. Hypoxia is a stressful condition in aquatic ecosystems, and can have disastrous effects [*Diaz and Rosenberg*, 1995; *Diaz*, 2001; *Rabalais et al.*, 2002b].

This dissertation follows the style of *Journal of Geophysical Research*.

The second largest zone of oxygen-depleted waters in the world is found on the northern Gulf of Mexico continental shelf adjacent to the outflows of the Mississippi and Atchafalaya Rivers [*Diaz*, 2001; *Rabalais et al.*, 2002a]. The combination of high freshwater discharge, wind mixing, regional circulation, and summer warming controls the strength of stratification that goes through a well-defined seasonal cycle. The physical structure of the water column and high nutrient load that enhance primary production lead to an annual formation of the hypoxic waters that is dominant from spring through late summer [*Pokryfki and Randall*, 1987; *Rabalais et al*., 2002b; *Rowe and Chapman*, 2002]. Paleoindicators in dated sediment cores indicate that hypoxic conditions likely began to appear around the turn of the last century [*Osterman et al*., 2005] and became more severe since the 1950s as the nitrate flux from the Mississippi River to the Gulf of Mexico tripled [*Rabalais et al.,* 2002a]. Referred to as the "Dead Zone" in the press and literature, the areal extent of the severe oxygen deficiency has averaged over 15000 km^2 annually since 1993, and reached a record size of 20700 km^2 in mid-summer 2001 [*Rabalais et al*., 2001].

Several studies examined the effect of hypoxia on living organisms in the northern Gulf of Mexico. During the summer of 1981 *Gaston* [1985] found hypoxia on the inner shelf south off Cameron, Louisiana, and that population of most macrobenthos species were significantly reduced. While mobile species may escape the low-oxygen waters, benthic species such as tube dwellers and some surface feeders are severely affected by hypoxic events [*Gaston*, 1985]. *Rabalais and Harper* [1992] described a decline in species abundance as water conditions changed from oxygenated in the spring to hypoxic in summer. *Cruz-Kaegi and Rowe* [1992] explained the low benthic macrofauna biomass to high sediment loading from the Mississippi River system and seasonal hypoxia. *Harper et al*. [1981] documented a decrease in species diversity and abundance over the Texas shelf associated with the 1979 summer hypoxia off Freeport, Texas. *Zimmerman et al.* [1995] examined shrimp catch per unit fishing effort over the Louisiana Shelf and found no relationship with percent of area that is hypoxic. Most of the research investigating the effects of eutrophication and hypoxia in the Northern Gulf

of Mexico has emphasized the potential loss of marine flora and fauna in general.

There is general agreement that two principal factors are required for the development and maintenance of coastal hypoxia on the Texas-Louisiana Shelf. First, the water column must be stratified so that the bottom layer is isolated from the surface layer and the diffusion of dissolved oxygen from surface to bottom is inhibited. Both salinity and temperature are important in influencing the strength of stratification in the Northern Gulf of Mexico [*Rabalais et al*., 1991; *Wiseman et al*., 1997]. Fresh waters derived from rivers and seasonally warmed surface waters are less dense than, and reside above, the saltier, cooler and more dense water masses near the bottom. Stratification on the Louisiana shelf goes through a seasonal cycle that generally exhibits maximum stratification during the summer and weakest stratification during the winter months [*Wiseman et al*., 1997; *Rabalais et al*., 2002b]. This cycle is due to the strength and phasing of river discharge, wind mixing, regional circulation and air-sea heat exchange processes.

Typically, hypoxia occurs in waters shallower than 30 m along the Texas-Louisiana Shelf between 89.5^{o}W and 94^{o}W [*Rabalais et al*., 1999], and found in the lower half or two-thirds of the water column, although in the western regions of the shelf, hypoxia can be confined to the lower 1-2 m.

On the Texas Shelf occurrences of hypoxia are believed to be less frequent, shorter lived, and more limited in extent than those over the Louisiana shelf. Hypoxic event along the Texas coast was first documented in June and July of 1979 [*Harper et al.,* 1981]. The hypoxia extended from Freeport, Texas, northeast to Sabine Pass in 10- to 33-m depth. On the inner shelf between Galveston Bay and Matagorda Bay, seasonal sampling (4 times per year) revealed scattered low-oxygen concentrations in July 1973 [*Oetking et al.,* 1974]. Data recently available seems to indicate that Texas hypoxia may be more persistent and frequent than previously held [*DiMarco*, pers. comm.].

The northwestern estuaries of the Gulf of Mexico are also known to experience episodic hypoxic conditions. Hypoxia has been documented in the southern part of Corpus Christi Bay, in Texas, every summer since 1998 [*Ritter and Montagna,* 1999].

Hypoxia also has occurred in parts of Galveston Bay [*Seiler et al.,* 1991] and other Texas estuaries such as in Matagorda Bay, Aransas Bay, and Laguna Madre [*U.S. Environmental Protection Agency*, 1999].

There are few documented occurrences of hypoxia over the northeastern Gulf shelf between the Mississippi River Delta and the west Florida shelf. *Rabalais* [1992] reported hypoxic waters off Mississippi Sound and Mobile Bay following high river discharge in 1991. *Waller* [1998] also reported hypoxia off the Mississippi Sound and Mobile Bay following the 1993 Mississippi River flood. Most reported occurrences in this region are in years of high river discharge. *Brunner et al.* [2006] analyzed the foraminiferal proxies of hypoxia collected in 1951-1956 in the Mississippi Bight. The results show apparent, recurrent low-oxygen to hypoxic bottom water on the inner shelf at hotspot locales seaward of the Mississippi-Alabama barrier islands and the eastern distributaries of the Balize delta.

Estuaries and bays in the northeastern Gulf of Mexico also experience hypoxia. *Schroeder* [1977] reported hypoxic waters in Mobile Bay in 1973 following flooding by the Mobile River. It has been noted that migration of a high number of fish and invertebrates to the shore of the Mobile Bay is related to the occurrences of hypoxia [*Martin et al.,* 1996]. Hypoxia has been recorded in Tampa, Sarasota, and Hillsborourgh Bays and Charlotte Harbor, Florida [*Martin et al.,* 1996; *Gray et al.,* 2002].

Many other regions around the world, similar to the Mississippi River Delta, i.e. near the mouths of the world's major river systems have experienced hypoxic or anoxic conditions [*Degens et al*., 1991; *Diaz and Rosenberg*, 1995; *Glausiusz*, 2000; *Joyce*, 2000; *Diaz*, 2001]. The Rhine River in the North Sea [*Bennekom and Wetsteijn*, 1990], the Pearl River [*Yin et al*., 2004] and Changjiang River [*Wei et al.,* 2007] in China are notable examples. *Gray et al*., [2002] listed bays (Kiel, Germany; Viliane, France; Tokyo, Japan; Chesapeake, USA) and estuaries (Port Hacking, Australia; Pamlico, Pappahannock, and York River, USA) around the world with observed hypoxia or anoxia.

The reduction of the subpycnocline dissolved oxygen concentrations in many of these ecosystems has been attributed to an increase in nutrient loading. The increase in the nutrient loading has been linked to the growth of the human population and industrialization of these areas, development of the modern agriculture and related loss of inland wetlands [*Earles*, 2000]. *Diaz* [2001] compared the Louisiana Shelf to three other hypoxic regions – the Kattegat, the Black Sea, and the Baltic Sea. He found that the northwestern Gulf of Mexico is the only system in which there is no documented decline in fisheries.

In many locations hypoxia results from the factors other than high nutrient loading. For example, in the Rappahannock and York Rivers estuaries, tidal mixing and close proximity to the hypoxic waters of Chesapeake Bay control the occurrence of hypoxia. *Walsh* [1998] and *Stoddard and Welsh* [1986] showed that hypoxic events in the York Bight were related to the unusual hydrographic and/or climatic conditions such as warm winter with large terrestrial runoff, a low frequency of spring storms, persistent southerly summer winds. They suggested that anoxic events might occur without any allochthonous input of organic carbon and that climatic conditions are extremely important in driving the event.

Hypoxia occurs naturally in the world major upwelling areas [*Demaison and Moore*, 1980]. In these cases, the hypoxia is driven by mesoscale variability changes often depended on the wind field. In the Agulhas Bank, south of Africa, hypoxia develops without fresh water input from the few rivers along the southern coast of South Africa. Summer solar heating and limited water movement result in the establishment of a strong pycnocline that assists the development of hypoxia [*Chapman and Shannon*, 1987; *Carter et al.,* 1987].

The lack of flushing of the deep basins of the Baltic Sea has been identified as a primary cause for the observed anoxic conditions [*Conley et al.,* 2002]. The anoxia within the deep interior basins of Black Sea also is a result of the limited ventilation, however, the hypoxic conditions on the northwestern shelf of the Black Sea during the

summer-autumn months are mostly attributed to the intense phytoplankton blooms and organic matter generation and recycling [*Oguz*, 2006].

Hypoxia or anoxia occurrences result from a combination of multiple factors, including weather (e.g. frontal passages, winds, rainfall, temperature), oceanic conditions (e.g. stratified or mixed areas, areas with a sill or without, tidal mixing, currents, waves, upwelling), and anthropogenic forcing (e.g. sewage, agricultural and forestry runoff). Therefore, there is no simple model of oxygen depletion that can fit all forms of variability [*Belabbassi*, 2006].

1.2 Physical description of the Louisiana Shelf

The region historically affected by seasonal hypoxia covers inner Louisiana Shelf west of the Mississippi delta and part of the Texas Shelf at the depth range between 5-60 m [*Belabbassi*, 2006; *Rabalais et al.,* 2007]. The Texas-Louisiana Shelf belongs to the northern shelves of the Gulf of Mexico that are naturally divided into eastern and western regions by the Mississippi River Delta which protrudes seaward from the coast to a narrow shelf edge (Figure 1.1). The shelf width, as defined by the 200-m isobath, is about 200 km at its widest point (near the Texas-Louisiana border) but narrows to about 90 km off the Rio Grande Delta (at the border between Mexico and Texas) and virtually disappears off the Mississippi Delta (near the Louisiana-Mississippi border). The area encompassed by these boundaries is approximately 105 km^2 [*Etter et al.*, 2004]. The Louisiana Shelf extends from the Mississippi Bight to the Texas border.

The Gulf of Mexico is a semi-closed basin with broad and narrow continental shelves surrounding a deep abyss reaching ~3800 m and is connected to the world ocean through entrances at the Yucatan and Florida Straits. The circulation processes of the deep Gulf of Mexico combined with the local processes of wind forcing, river runoff, and other processes are responsible for the vertical and horizontal density structure, and distribution of freshwater and biochemical properties.

Figure 1.1. Map of the Northern Gulf of Mexico showing bathymetry and key geographic locations. The 10, 20, 30, 40, 50, 60, 200 m isobaths are shown.

The physical dynamics, biochemical activity, and geomorphologic processes on the Louisiana Shelf are highly affected by the Mississippi-Atchafalaya River System discharge. The annual combined outflow of the Mississippi-Atchafalaya River system averages about 530 km^3 of water and introduces 210 x 10^9 m^3 of sediment [*Milliman and Meade,* 1983]. This discharge constitutes 55% of the total freshwater input to the Gulf of Mexico [*Solis and Powell*, 1999]. The Mississippi River enters the Louisiana Shelf through the bird-foot delta via three large passes and numerous smaller channels along a 40 km peninsula at about 89°W, 29°N. The mean annual discharge of the Mississippi River at Tarbert Landing, LA, is approximately 13,500 $m^3 \cdot s^{-1}$. The Atchafalaya River flow discharges through Atchafalaya Bay near Morgan City, LA at about 91.5°W, 29.3°N. Since 1976, the Atchafalaya River outflow has been constrained to 30% of the total Mississippi-Atchafalaya discharge, and combined with 50% of Mississippi River flow that goes west, introduces large amount of freshwater onto Louisiana Shelf.

The freshwater volume exhibits an annual cycle that is dominated by the spring flood of Mississippi and Atchafalaya Rivers [*Dinnel and Wiseman*, 1986]. Maximum shelf freshwater volume occurs approximately one month after peak spring runoff; minimum freshwater volume occurs just prior the spring maximum. *Etter et al.* [2004] constructed monthly mean freshwater budgets for the Texas-Louisiana Shelf for the period May 1992 to November 1994 using the hydrographic data, supplemented by meteorological data. The freshwater flux divergence indicates a persistent divergence of fresh water over the area in agreement with the baseline climatology. Filling and flushing times are balanced by reducing the westward-directed fraction of the Mississippi River discharge to 47%, supporting the statement that approximately half of the long-term Mississippi River discharge is directed westward upon entering the Gulf of Mexico.

The realistic modeling study of Mississippi-Atchafalaya River outflow dynamics shows two dynamically distinct plumes [*Hetland and DiMarco*, 2008]. The Mississippi River plume enters the shelf near the shelf edge, forms a recirculating gyre in Louisiana

Bight [*Ichiye*, 1962], and typically does not interact directly with topography. The Atchafalaya River plume is more diffuse, enters a broad shelf at the coast, and interacts with the shallow coastal topography. Both plumes are strongly affected by winds, and tend offshore during the mean summer upwelling winds.

The quasi-annual low-frequency circulation over the Texas-Louisiana Shelf is primarily wind driven. For most of the year, the low frequency circulation on the shelf consists of an elongated cyclonic gyre, with westward flow near the coast and eastward flow near the shelf break about 200 m isobath [*Cochrane and Kelly*, 1986; *Cho et al.,* 1998; *Nowlin et al.,* 2005]. The downwelling favorable non-summer (approximately September through June) winds drive the currents downcoast, toward Texas, transporting the freshwater away from Louisiana. A directional shift in the mean wind stress during the summer months (approximately June through September) from predominantly westward to north and northeast disrupts the gyre and results in a current reversal to eastward flow over the shelf starting in June [*Nowlin et al.,* 1998; *Wang et al.,* 1998]. Another shift in the prevailing wind direction back to the west allows for the re-establishment of the gyre in August-September.

The circulation patterns of the outer shelf in the northern Gulf of Mexico are associated with motions of the Loop Current and its eddies [*Nowlin et al.,* 2001; *Sturges and Lugo-Fernandez,* 2005]. The Loop Current interacts with the currents on the outer edge of the eastern continental shelf through the phenomenon of Loop Current Eddy formation and associated cyclones. The eastern region near Mississippi Canyon shows the estimates of kinetic energy in the mesoscale band of the spectrum, corresponding to the mesoscale circulation features like eddies [*Nowlin et al.,* 2005]. The offshore circulation features are episodic in nature due to the chaotic character of the Loop Current intrusions into the northern Gulf of Mexico and the separation of periods of the Loop Current eddies [*Sturges and Leben,* 2000; *Leben*, 2005].

The tides in the Gulf of Mexico are considered to be small compared to oceanic tides. *DiMarco and Reid* [1998] described the principal tidal current constituents from 81 current meter measurements deployed on the Texas-Louisiana Shelf from 1992-

1994. Tides in the region are predominantly diurnal. The dominant tidal constituents are found to be K1, O1, and M2. The largest tidal surface current of about 9 $cm \cdot s^{-1}$ was found at the northeast corner of the shallow shelf near the Atchafalaya Bay, and decreased to about 2 $cm \cdot s^{-1}$ at the shelf edge [*DiMarco and Reid*, 1998].

The inertial currents on the Texas-Louisiana Shelf are driven by the passages of atmospheric fronts, hurricanes and tropical storms [*Nowlin et al.,* 1998; *Nowlin et al.,* 2005]. The amplitudes of inertial oscillations can reach 15 $cm \cdot s^{-1}$ for a weak front passage and are typically surface trapped above the pycnocline [*Chen et al.,* 1996; *DiMarco et al.*, 2000; *Zhang et al.*, 2008 submitted]. The Texas-Louisiana Shelf is also influenced by a diurnal sea breeze due to differential heating and cooling of the land and ocean [*Hsu*, 1988]. The 30^{o}N latitude of the shelf combined with the diurnal wind forcing results in a near-resonant response of the surface currents to the wind stress. The 24-hour anticyclonic currents can reach 60 $cm \cdot s^{-1}$ and represent the largest non-storm induced high-frequency currents on the shelf [*DiMarco et al.,* 2000]. These currents possibly can enhance shear mixing across the pycnocline and reduce stratification [*Zhang et al.*, 2008 *submitted*].

The severity and frequency of storms and frontal passages increases during the nonsummer months [*Nowlin et al.,* 1998]. The stratification of the water column is broken through the action of the surface gravity waves and shear mixing processes. In summer, scarce atmospheric fronts allow the shelf to remain stratified and inhibit downward mixing. Therefore, the seasonal pattern of storms propagation contributes to the summertime conditions favorable for the water column stratification on the Louisiana Shelf. The amplitude and period of surface gravity waves in the Gulf of Mexico are considerably smaller than those found in the open ocean or larger basins. The typical wave conditions over the inner Texas–Louisiana Shelf have mean significant wave heights of less than one meter with average periods of about six seconds [*DiMarco et al.,* 1995]. Strong winds during the passage of hurricanes and tropical storms produce significant wave heights that mix the water column from the surface to the bottom.

In terms of sediment transport, the Texas-Louisiana Shelf is considered a storm-dominated environment experiencing relatively low energy levels resulting from winds and wave processes except for the winter passages of cold fronts and the summer occurrence of hurricanes and tropical storms [*Boyd and Penland*, 1988]. The Holocene Mississippi River delta plain is located in southeast Louisiana and occupies ~400 km of the coastline in the Northern Gulf of Mexico [*Williams et al.,* 2006]. There are only two active delta complexes within the delta plain, the Modern and the Atchafalaya. At the present time the Mississippi delta undergoes the transgressive phase of its evolution, the late stages of which are characterized by the barrier islands submergence and reworking as sandy shoals [*Boyd and Penland*, 1988]. Facies found on bathymetric highs of the Atchafalaya delta as shallow as 5 m water depth consist of highly consolidated relict sand and mud, and associated with subaqueous sand shoals formed in the early Holocene [*Neill and Allison*, 2005]. The modern Atchafalaya delta has at least two distinct topographic features along the coast, the Trinity Shoal and the Ship Shoal (Figure 1.2).

1.3 Study motivation

Because of the significant implications of the hypoxia on the marine ecosystem, fisheries, and public health, the problem has received an increased attention from the scientific community over the past 20 years. The occurrence of the hypoxia on the Louisiana shelf has been documented since 1973 [*Harris et al*., 1976; *Ragan et al*., 1978; *Pokryfki and Randall*, 1987; *Boesch and Rabalais,* 1991; *Rabalais et al*., 2002b]. The extent of the hypoxic zone along the Texas-Louisiana coast varies from year to year (Figure 1.3). Most of these studies are based on the eutrophication paradigm which suggests that the widespread hypoxia on the Louisiana shelf is a product of extensive nutrient loading brought with the river runoff into the shelf, thus the limitation of the nutrients source would reduce the extent and intensity of hypoxia off Louisiana [*Turner and Rabalais,* 1994; *Rabalais et al.,* 2002a].

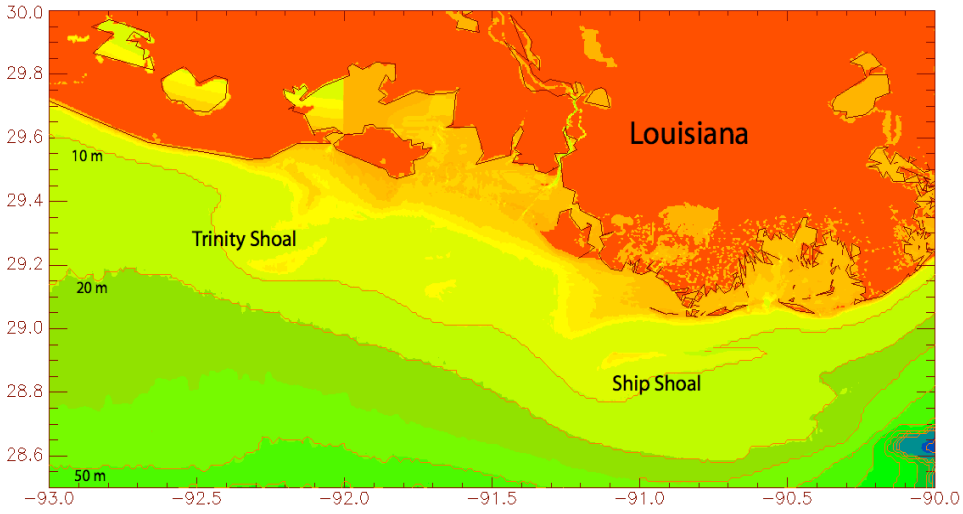

Figure 1.2. The bottom bathymetry of the Louisiana Shelf. Locations of 10, 20, and 50 m isobaths are indicated. (Figure courtesy of M. K. Howard)

To better our understanding of the hypoxic zone dynamics and to enhance the predictive capabilities, a number of modeling studies have been conducted [*Rowe*, 2001; *Justic et al.,* 2002; *Scavia et al*., 2003; *Turner et al*., 2005; *Hetland and DiMarco*, 2008].

The hindcasts and predictions of the hypoxic areal extent are mostly based on the statistical relationship between freshwater flux to the shelf, nutrient loading, respiration, and primary productivity. *Justic et al.* [2002] use a vertical two-layer model, and do not account for horizontal variability of the water column. *Scavia et al*. [2003] propose a model that uses a westward drift of oxygen-depleted waters at depth from the river source of the freshwater and nutrient supply. *Turner et al.* [2005] implement a statistical relationship between freshwater discharge and near-shore nitrogen concentrations, and link it to the area of hypoxia. All these models support the hypothesis that riverine nutrient fluxes, via their influence on the net productivity of the upper water column, play a major role in controlling bottom water hypoxia.

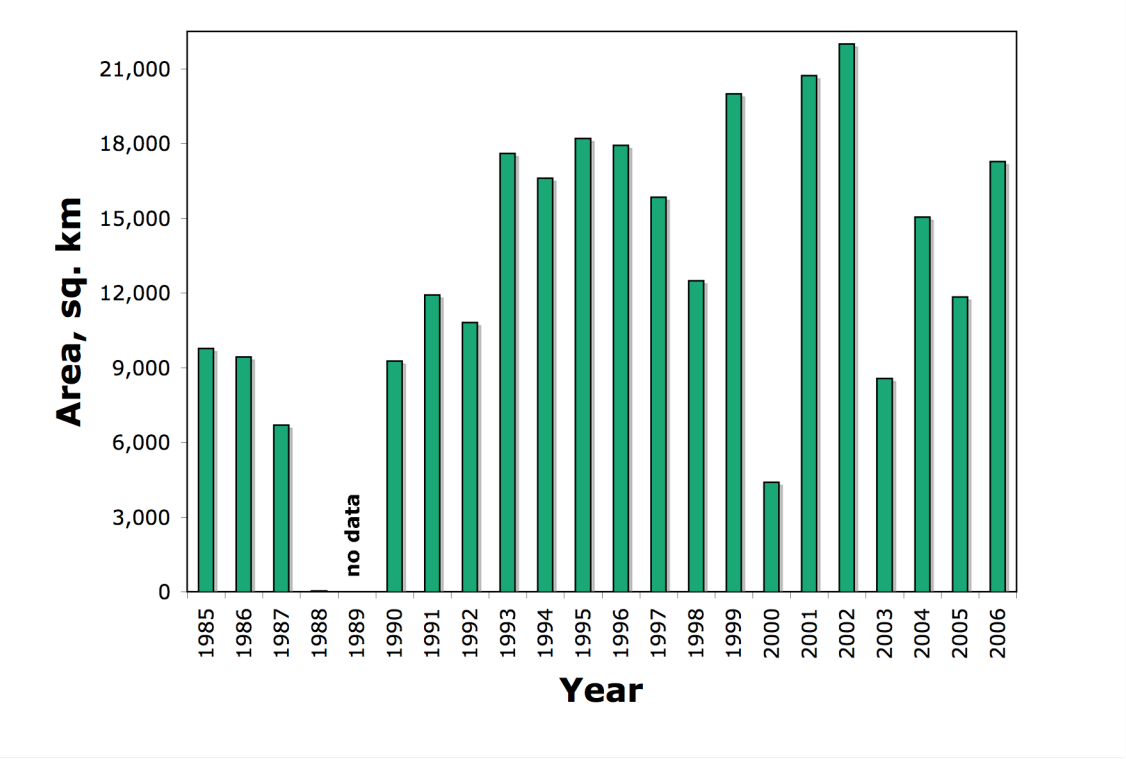

Figure 1.3. Mid-summer areal extent of hypoxic waters in the Northern Gulf of Mexico between 1985 and 2006. (Data source: N. N. Rabalais, LUMCON)

Hetland and DiMarco [2008] take a different approach. They apply simple, idealized models of biological respiration to a complex three-dimensional hydrodynamic model of coastal circulation. They showed that the formation of the hypoxia is primarily a vertical process, which is dependent on the local respiration and dispersed by vertical mixing, and different respiration processes tend to dominate in different geographical regions. The biological processes responsible for producing hypoxia change from east to west, with the shelf region south of Terrebonne Bay being the approximate dividing line between water column respiration predominantly causing hypoxia to the east and benthic respiration causing hypoxia to the west.

Rowe [2001] uses a non-steady state, time-dependant numerical simulation model to compare biological and physical processes with shipboard measurements and continuous near-bottom records. He summarized biological processes that consume or

produce oxygen in a budget, and later uses that to quantify the degree to which consumption in deep waters and in sediments exceeds net production and thus the time it takes to reach hypoxic conditions following the spring onset of stratification. The simulations illustrate possible variations in oxygen concentrations on time scales of hours and months, which match much of the variability in the direct observations at time scales of days to weeks.

Texas-Louisiana Shelf can be described as a region of freshwater influence (ROFI). The distinctive feature of all ROFI systems is the input of significant amounts of buoyancy as freshwater from river sources [*Dagg et al.,* 2004; *Geyer et al.,* 2004]. This input tends to drive a coastal-parallel flow, which without frictional effects is subject to baroclinic instability. These baroclinic instabilities induce large meanders and eddies in the flow that can be stabilized by the stirring introduced as the action of wind and waves, or tidal flow [*Simpson*, 1997].

Field measurements show evidence of large-amplitude, shelf-scale disturbances in the distribution of hydrographic properties across the Louisiana Shelf [*DiMarco et al.,* 2007a, *submitted*]. These wave-like instabilities were also seen in satellite imagery (MODIS, SeaWifs) throughout the year (Figure 1.4), which leads to a conclusion that formation of the meander is common in this region. The position of the meander is consistent with the location of the shallow sandy shoals, which are remnant subaqueous deltaic features along the Louisiana Shelf. This meander also is seen in the vertical distribution of physical properties in the water column. Vertical displacements of isopycnals were as large as 10 m in 20 m total depth and an estimated along shelf wavelength of about 50 km. Observations indicate that dissolved oxygen concentrations are increased at the bottom where the break down in stratification occurs; as stratification weakens, it allows for vertical mixing to ventilate the lower layers of the water column [*DiMarco et al.,* 2007a, *submitted*].

Belabbassi [2006] showed a significant correlation in summer between Brunt-Väisälä frequency and near-bottom dissolved oxygen concentration on the Texas-Louisiana Shelf, and found that hypoxia did not occur at Brunt-Väisälä frequencies less

than 40 cycles/hour. Her further investigations covered the entire northern Gulf of Mexico revealed that Brunt-Väisälä frequencies greater than 40 cycles·h^{-1} were rare outside of eastern Texas-Louisiana Shelf. This finding suggests that the absence of the strong stratification plays a part in the rare occurrences of hypoxia on these shelves.

Hydrodynamic instabilities in the buoyancy-driven flow and other problems, related to this phenomenon, have been investigated by a number of scientists (*Clarke and Brink*, 1985; *Barth*, 1989; *Haine and Marshall*, 1997; *Lentz and Helfrich*, 2002; *Wolfe and Cenedese*, 2006).

The baroclinic waves as a result of baroclinic instabilities are important agents of buoyancy transport through the ocean mixed layer [*Haine and Marshall*, 1997]. The intensity of the baroclinic response of the shelf waters is dependant on the stratification strength, slope of the continental shelf, and Coriolis parameter, and hence is a direct product of the hydrographic regime and topographic features of the shelf [*Clarke and Brink*, 1985]. The degree of stratification is usually defined in terms of stratification (Brunt-Väisälä) frequency. Brunt-Väisälä frequency is the natural frequency of oscillation of a water parcel displaced adiabatically from its rest position [Väisälä, 1925; *Brunt*, 1927]. The higher the stratification the more water column resists vertical mixing.

Orlanski [1969], and also *Xue and Mellor* [1992] have examined the role of bottom topography on the stability of baroclinic flow. They demonstrated that the topographic slope is a stabilizing factor, while the height of the topography is a destabilizing factor. *Wolfe and Cenedese* [2006] investigated the hypothesis that rapid changes in the bathymetric slope could induce instability and eddy formation by a buoyant coastal current. Laboratory experiments have shown that currents only form eddies over steep bathymetry, and that eddying currents were stabilized as they moved onto gently sloping topography. These results are consistent with theoretical studies by *Lentz and Helfrich* [2002]. The development of the wave-like disturbances has been also observed along the coastal upwelling fronts [*Barth*, 1989; *Glenn et al*., 2004].

September 16, 2004

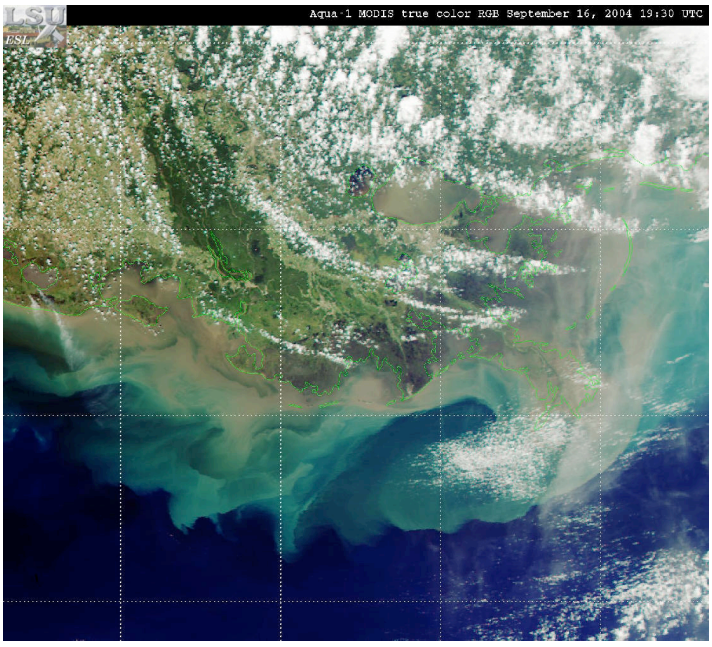

October 25, 2005

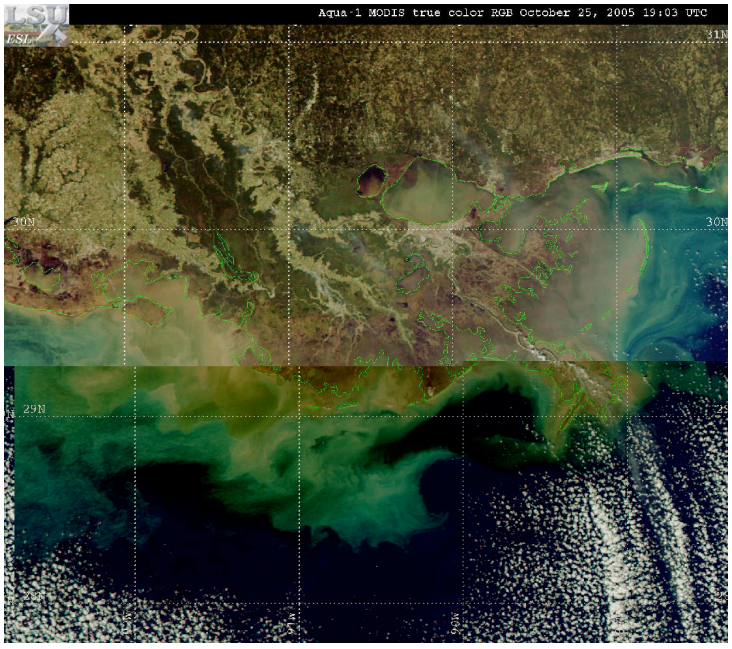

Figure 1.4. Ocean color from Aqua-1 MODIS on September 16, 2004 and October 25, 2005. (Source: Nan Walker, ESL).

A theoretical and modeling study of alongshore variability of the coastal upwelling fronts suggests that these meanders are rather produced by hydrodynamic instability than alongshore topographic variations [*Barth*, 1989]. A comparison between the model predictions and observations from three different coastal upwelling regions showed a reasonable agreement suggesting that observed alongfront variability can be explained in terms of the instability.

Glenn et al. [2004] tested the hypothesis that hypoxia on the New Jersey inner shelf is more related to the coastal upwelling rather than nutrient load from the rivers. Their idealized numerical model, initialized with typical midsummer density profile and constant upwelling wind, showed the development of a broad coastal jet meandering along the coast, that formed downstream at each topographic high. The model simulations suggested that topographic variations redistribute the upwelled water unevenly along the coast, and enhanced the biochemical impacts at the specific locations.

1.4 Study objectives

The primary objective of this study is to investigate how local topographic conditions and physical water column processes contribute to the occurrence and distribution of low dissolved oxygen concentrations in coastal ecosystems particularly that of the Louisiana shelf. This study is focused on the influence of buoyancy driven instabilities on the bottom dissolved oxygen concentrations along the shelf. The goal is to find a linkage between the transfer of buoyancy through the water column along and across the shelf and dissolved oxygen concentrations at the bottom. To achieve this goal the following objectives, divided into observational and modeling components, will be completed:

Observational Component

- Describe and analyze the hydrographic data collected in the region of study;

- Obtain a quantitative relationship between stratification (Brunt-Väisälä) frequency, which is taken to represent the stability of water column, and dissolved oxygen concentrations along the coast;

Modeling Component

- Evaluate the relative importance of the freshwater discharge and shelf topographic features on the development of dynamic instabilities along the shelf;

- Examine the effect of instabilities on the dissipation of the bottom hypoxic waters;

- Investigate the influence of shoaling topography on the sustainment of the hypoxic waters on the shelf.

The overall purpose of the proposed research is to better our understanding of how physical processes can affect biochemical processes in coastal ecosystems. The consequences of hypoxia lead to the long-lasting negative effects on the environment and economy. It is expected that this study will contribute to the present debate whether the reduction of the nutrients alone as a management strategy will lessen the occurrence of hypoxia on the Louisiana Shelf. The use of an idealized numerical circulation model will simplify the overall complex coastal system, and help to separate the processes responsible for the generation of dynamic instabilities. The inclusion of the simple chemical tracer into the model will allow to determine how the local physical processes affect the distribution of the chemical and biological properties of the water. It is also hoped that the outcome of this study will be sufficiently compelling to other researchers interested in similar problems in different regions of the world, for example Changjiang Estuary (Yangtze River).

1.5 Organization

Chapter II presents the overview of the data and research methods used in this study. The general description of the MCH data sets, numerical model, and numerical experiment setup is provided.

Chapter III covers the results from the MCH observations by season and region. First, the detailed description of the temperature, salinity, and dissolved oxygen concentrations is given. Next, the effect of local stratification on the occurrence of low oxygen bottom waters is investigated.

Chapter IV discusses the results from numerical modeling. The relative importance of the freshwater discharge and bottom topography on the development of dynamic instabilities is examined. Also the influence of shoaling topography and dynamic instabilities on distribution of the hypoxic waters is investigated.

Chapter V summarizes results presented in Chapters III and IV and provides the conclusions.

CHAPTER II

DATA AND RESEARCH METHODS

As indicated by the research objectives, a combination of *in situ* sampling and numerical modeling is used to investigate the effects of mesoscale circulation patterns and stratification on the evolution of hypoxia on the shelf. The field observations of hydrographic properties sampled during the program specifically designed to address the occurrence of hypoxia on the Louisiana Shelf, are used for the description of the hypoxic environment in the region, data analysis, and qualitative verification of the numerical model. The purpose of the numerical experiment is to isolate the impact of the shelf topography and freshwater input on the development of the dynamic instabilities along the coast, and also to demonstrate the influence of the shoaling bottom profile on the longevity of hypoxic conditions.

2.1 Description of the MCH data sets

The principal data sets used are from research cruises sponsored by the National Oceanic and Atmospheric Administration (NOAA) and conducted by Texas A&M University as part of the program "Mechanisms Controlling Hypoxia on the Louisiana Shelf" (MCH). The MCH program was conducted along the eastern Texas-Louisiana Shelf from September 2003 through August 2005. In this study, the data from the seven cruises from April 2004 through August 2005 is used. The start and end dates of the cruises are given in Table 2.1. The timing of the cruises was planned according to the temporal scales of hypoxia, including periods typical for the onset, duration, and dissipation of the hypoxic conditions on the shelf.

The sampling plan was initially based on a hypothesis proposed by *Rowe and Chapman* [2002], stating that different biological processes are in control of hypoxia in the different physical regimes. They introduced the idea of three zones around the Mississippi (and Atchafalaya) River mouth (Figure 2.1). The first (brown) zone, nearest

to the river mouth, is controlled by the deposition of sedimentary material, light- and production-limited. The second (green) zone is the region occurs immediately offshore-alongshore from zone 1. In this zone, the light penetration is increased, and dissolved nitrate and silicate concentrations are high, as is photosynthesis. The third (blue) zone, which mostly affected by the volume of water delivered by the rivers, is one where stratification plays the most important role. The euphotic zone is nitrogen limited, and production is thought to be controlled by regenerated nitrogen.

Table 2.1. Cruise identifiers and their corresponding dates.

Cruise ID	Start date	End date
M1	2 April 2004	8 April 2004
M2	26 June 2004	1 July 2004
M3	19 August 2004	26 August 2004
M4	22 March 2005	29 March 2005
M5	18 May 2005	25 May 2005
M6	6 July 2005	12 July 2005
M7	17 August 2005	24 August 2005

The cruise tracks for M1-M6 cruises were similar and designed to obtain measurements from the three regions of the shelf: close to the Mississippi River Delta (zone A), near the C6 monitoring station location operated by LUMCON and south of Terrebonne Bay (zone B), off Atchafalaya Bay, LA (zone C). The basic station plan is shown in Figure 2.2.

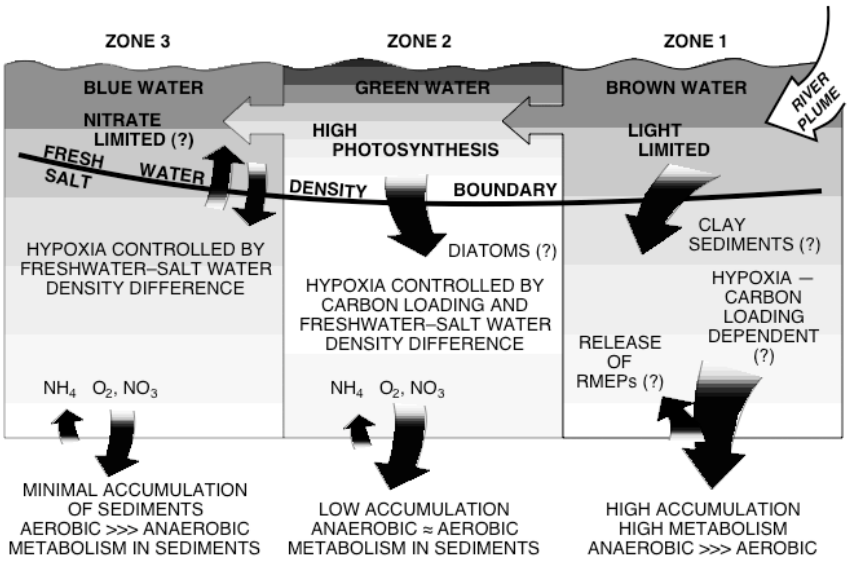

Figure 2.1. A paradigm describing the controls on hypoxia in the three regions. (From *Rowe and Chapman*, 2002).

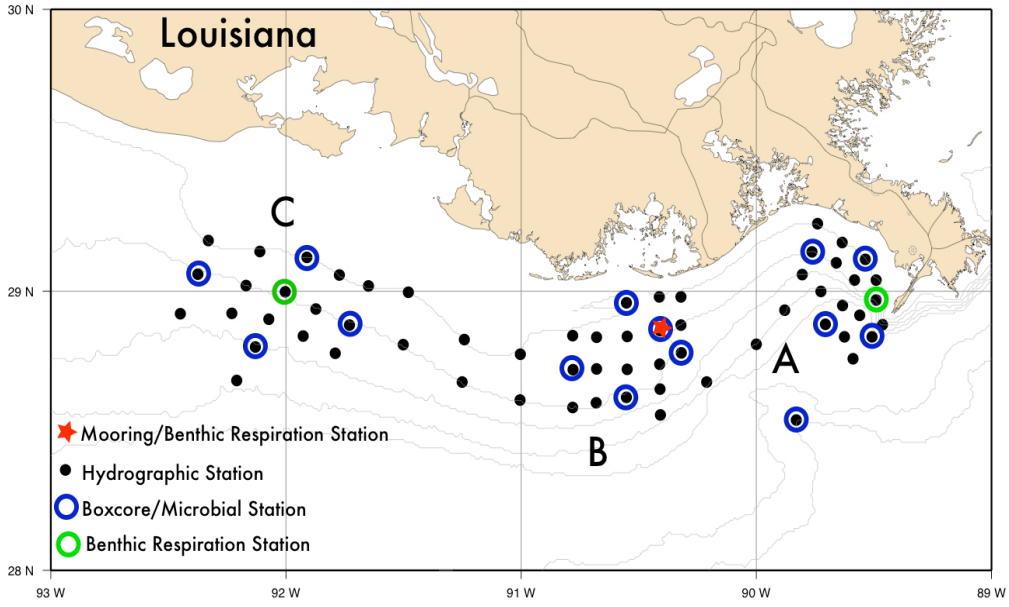

Figure 2.2. Stations plan for 2004-2005 NOAA-MCH Cruises (M1-M6). Shown are CTD/bottle stations (black dots), mooring location (red stars), and boxcore stations (blue circles). Bathymetric lines are drawn for 10, 20, 30, 40, 50, 200, and 500 m. (Figure courtesy of Steven F. DiMarco)

The cruises during 2005 were significantly impacted by weather and required adaptive sampling strategies while at sea. During M4 a strong squall forced the abandonment of several stations towards the end of the cruise. During M6, the treat of Hurricane Dennis forced the station sampling to be altered and the addition of 30 stations in the western study region, named zone D (downstream open shelf between Texas border and Atchafalaya Bay). This alteration influenced the stations plan for the M7 cruise, as those stations were revisited. The actual CTD/bottle stations for each cruise are shown in Figure 2.3.

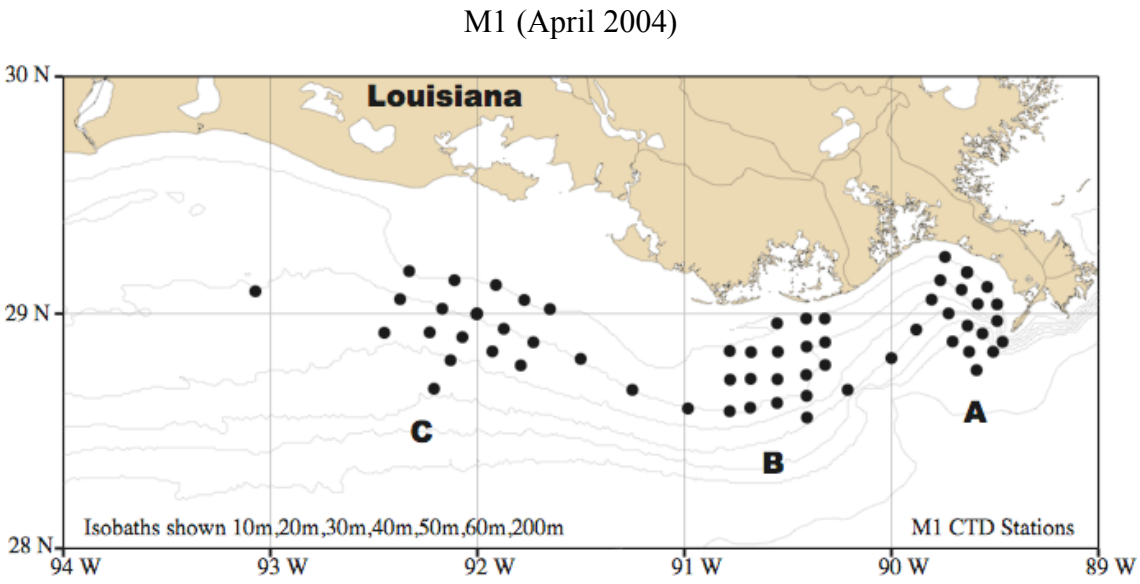

Figure 2.3. Actual CTD/bottle stations (black dots) for 2004-2005 NOAA-MCH cruises (M1-M7). Bathymetric lines are drawn for 10, 20, 30, 40, 50, 200, and 500 m.

M2 (June/July 2004)

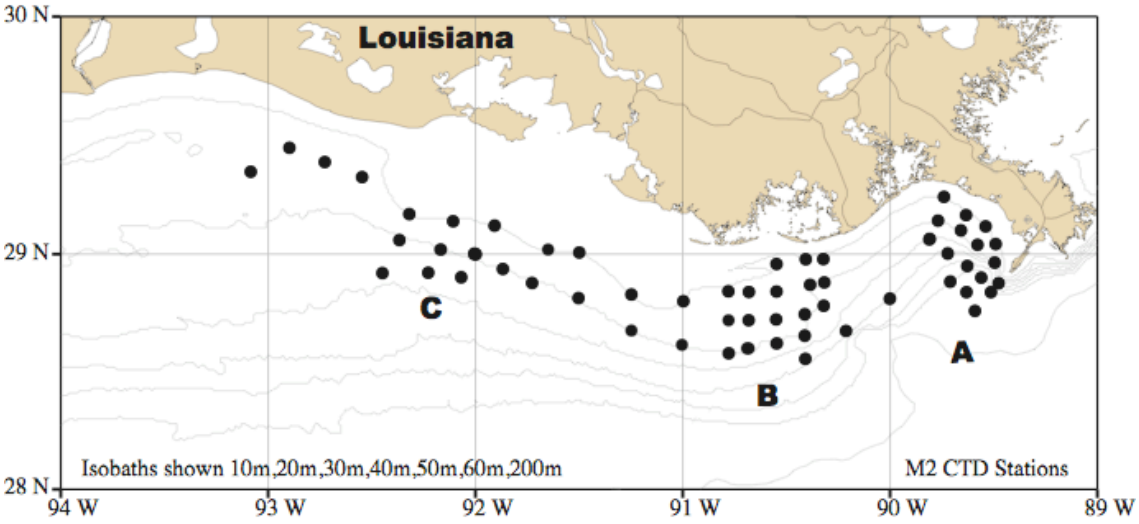

M3 (August 2004)

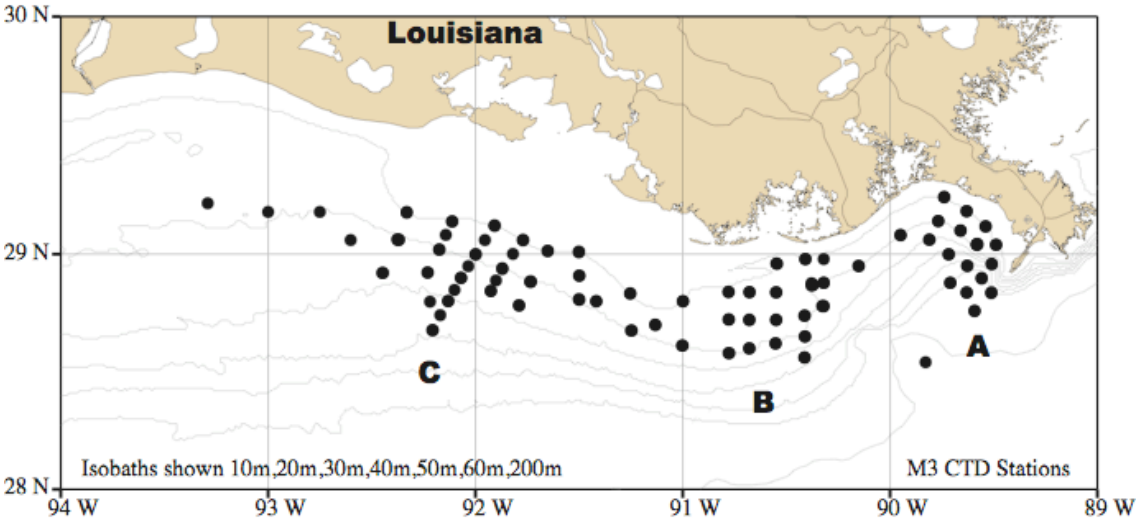

Figure 2.3. Continued.

M4 (March 2005)

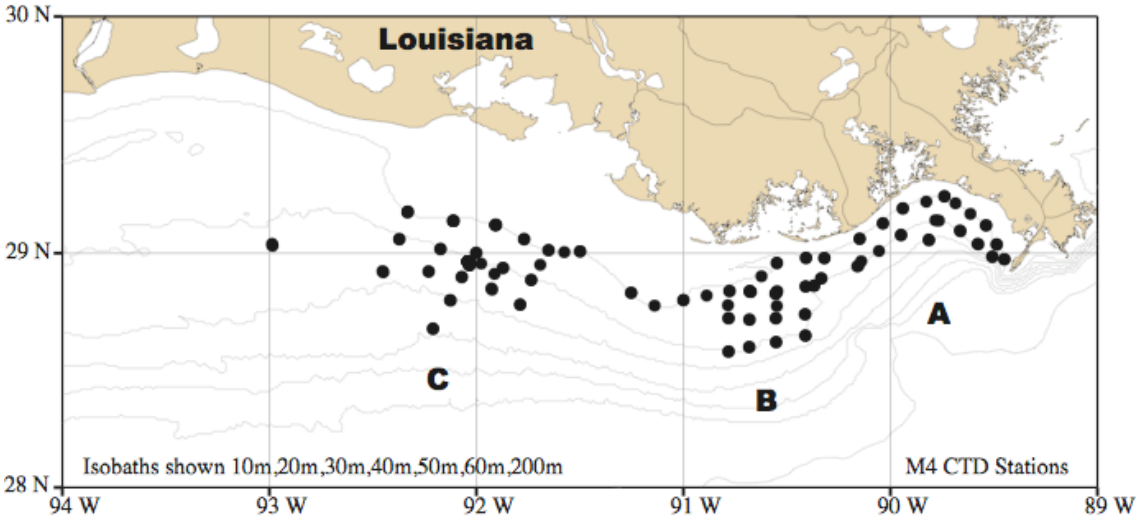

M5 (May 2005)

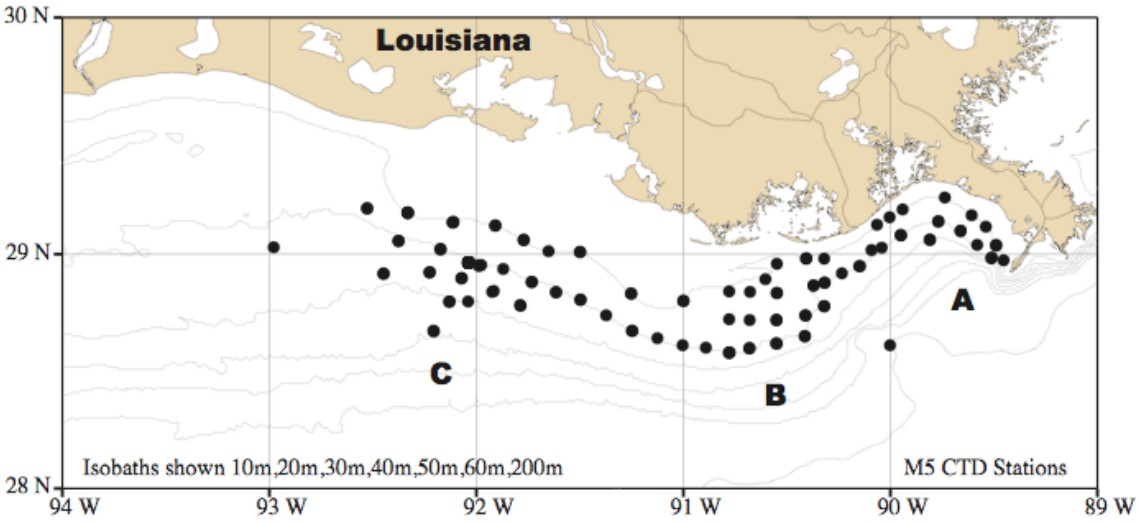

Figure 2.3. Continued.

M6 (July 2005)

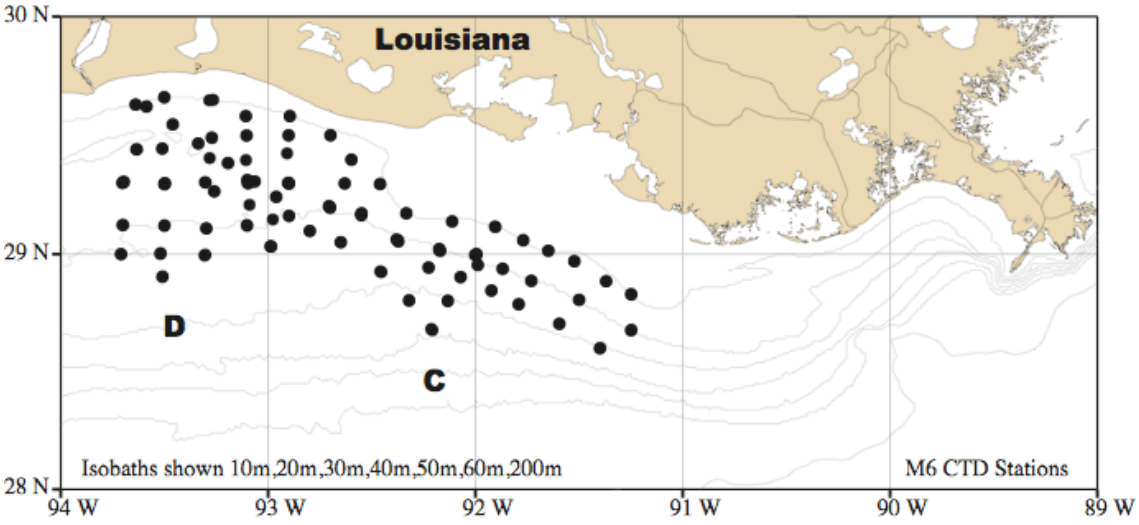

M7 (August 2005)

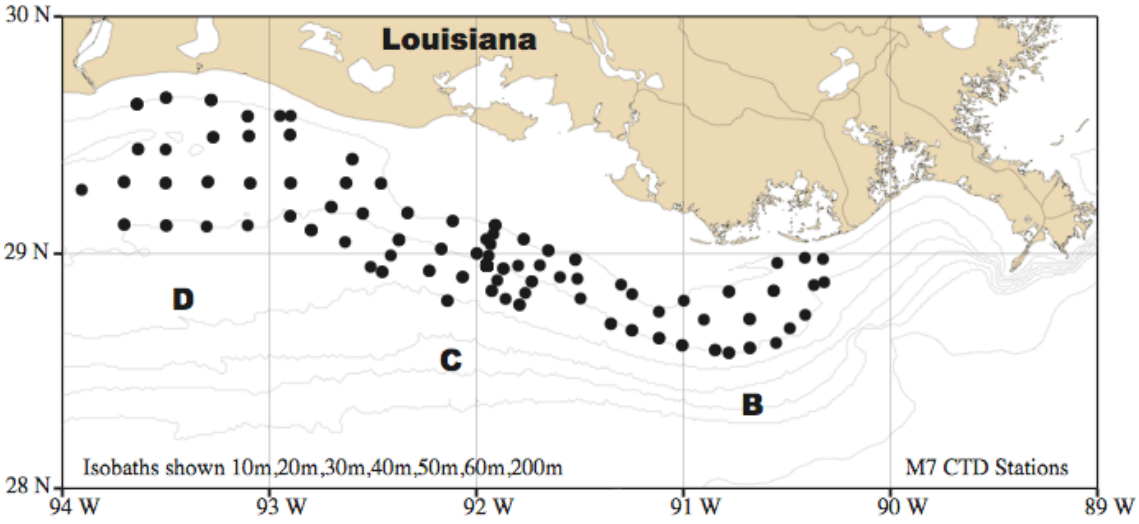

Figure 2.3. Continued.

The data collection, represented by a wide range of measurements, includes records of: salinity, temperature, dissolved oxygen concentrations, nutrients contents in the water, current velocities, benthic respiration rates, chlorophyll, dissolved carbon concentrations and more. The observations of salinity, temperature, pressure, and dissolved oxygen concentrations across and along the shelf were used in this study. A brief description of the data used is given below. For detailed information on the sampling methods refer to report by *DiMarco* [2007a].

The data used in this study also include continuous vertical profiles of: salinity, temperature, dissolved oxygen concentration, and pressure recorded at all stations with the CTD (Model: Sea-Bird SBE-911-Plus) casts. The vertical separation distance of data on these profiles after processing raw records is 0.5 m. Discrete bottle samples were taken using a 12-bottle rosette. Vertical resolution of the bottles is typically 5 m. A 1.5-1 bottle was attached to the CTD frame to ensure the collection of water samples within 0.5 m of the bottom. Flow-through sensors provided two-minute measurements of 3-m salinity, temperature, and chlorophyll. This translates into 1-3 km spatial resolution while underway. A small rosette (nicknamed Pogo) equipped with four Nisken Bottles and self contained CTD and transmissometer was used to take samples within 0.5 m of the bottom. Nisken bottle samples of dissolved oxygen were analyzed at sea with Winkler titration method; a salinometer system was mostly run at sea; some of the salinity samples were frozen and analyzed on shore in the lab. A shipboard 150-kHz ADCP was used on all cruises to provide estimates of current velocity along the ship track. The summary for the data collection used in this study is summarized in Table 2.2.

Table 2.2. Data type and number of stations for each MCH cruise in 2004-2005.

Data type	M1	M2	M3	M4	M5	M6	M7
CTD cast	61	60	64	105	105	76	127
Pogo cast	61	60	71	94	67	80	108
Nisken Bottles	392	368	364	398	469	365	576
ADCP	Yes	Yes	Yes	Yes	Yes	Yes	Yes
Thermosalinography	Yes	Yes	Yes	Yes	Yes	Yes	Yes

2.2 Numerical modeling

A free-surface, hydrostatic, primitive-equation regional ocean model (ROMS) was used in this study to model mesoscale flow over a subaqueous delta. ROMS is an updated and expanded version of the S-coordinate Rutgers University Model (SCRUM) described by *Song and Haidvogel* [1994]. ROMS is widely used by a rapidly growing user community for applications from the basin to coastal and estuarine scales [*Haidvogel et al*. 2000; *Marchesiello et al.* 2001; *Peliz et al.,* 2003; *DiLorenzo,* 2003*, Dinniman et al.,* 2003; *Wilkin et al.,* 2005]. ROMS solves the primitive equations using finite-difference approximations on orthogonal curvilinear coordinates in the horizontal and a stretched, terrain-following coordinate in vertical planes. Model computational algorithms are described in detail by *Shchepetkin and McWilliams* [1998, 2003, 2005]. For computational economy, the hydrostatic primitive equations for momentum are solved using a split-explicit time-stepping scheme. This scheme requires special treatment and coupling between barotropic (fast) and baroclinic (slow) modes. A finite number of barotropic time steps, within each baroclinic step, are carried out to evolve the free-surface and vertically integrated momentum equations. In order to avoid the errors associated with the aliasing of frequencies resolved by the barotropic steps but unresolved by the baroclinic step, the barotropic fields are time-averaged before they replace those values obtained with a longer baroclinic step. A cosine-shape time filter, centered at the new time level, is used for the averaging of the barotropic fields

[*Shchepetkin and McWilliams*, 2005]. Careful formulation of the time-stepping algorithm allows both exact conservation and constancy preservation for tracers, while achieving enhanced stability and accuracy in coastal applications where the free surface displacement is a significant fraction of the total water depth [*Shchepetkin and McWilliams,* 2005]. In the vertical, the primitive equations are discretized over variable topography using stretched terrain-following coordinates [*Song and Haidvogel*, 1994]. The stretched coordinates allow increased resolution in the surface and/or bottom boundary layers.

2.2.1 Model description

The Regional Ocean Modeling System (ROMS) is configured to use third-order upstream horizontal advection of tracers, conservative parabolic splines to calculate vertical gradients, and generic length-scale mixing turbulence closure with horizontal smoothing of buoyancy/shear. The surface and bottom temperature and salinity fluxes are solved analytically.

The model is initialized with a horizontal salinity gradient and uniform temperature, and is forced with a spatially uniform weak idealized onshore/offshore wind (~1 $m \cdot s^{-1}$). The simulations were run for 45 days. The fixed parameter values used in the simulations are summarized in Table 2.3.

The currents extracted from the hydrodynamic simulations are used to advect a tracer representing the dissolved oxygen deficit in the water column, initialized to be zero (the water column is fully saturated) everywhere. The no-gradient east and west boundary conditions are nudged toward zero, where the model is pushed gently toward desired boundary conditions in such a way that noise is minimized. This usually consists of adding a time-dependent nudging coefficient to the model equation [*Kalnay*, 2006].

Oxygen consumption is parameterized using the simple benthic respiration biological model. The functional form is:

$$DO(t) = DO(t) + {}^{dt}\!/_{\tau} \cdot \left(1.0 - DO(t)\right), \tag{2.1}$$

where *DO(t)* is the oxygen deficit at the given time step; *dt* is time step in seconds; τ is respiration time scale in seconds.

Table 2.3. Listing of the fixed parameters used for the simulations.

Fixed Parameters	**Units**	**Value**
Gravity	$m \cdot s^{-2}$	9.8
Coriolis Parameter	s^{-1}	6.6E-5
Temperature	^{o}C	25
Barotropic Time Step	s	300
Baroclinic Time Step	s	9000
Mean Density	$kg \cdot m^{-3}$	1025
Averaging frequency	timesteps	72
Quadratic bottom drug coefficient		3.0E-3
Respiration time scale	days	3

The negative values correspond to the deficit of the dissolved oxygen or undersaturation of the waters. The dissolved oxygen values at the surface are constrained to be zero (fully saturated) at all time steps. The oxygen advection model assumes no other sources of the dissolved oxygen into the system.

2.2.2 Numerical experiment setup

A set of twelve numerical experiments was performed to investigate the influence of the freshwater discharge and shelf topographic features on the development of dynamic instabilities on the shelf.

The numerical simulations are conducted in an idealized coastal domain represented as a rectangular box, 384 km long in the east-west direction, and 96 km long on the north-south direction. The domain is bounded by a coastline on the northern and southern sides and the open ocean on eastern and western edges. The grid resolution of the domain is 3 km in the *x*-direction (east-west), and 1 km in the *y*-direction (north-south). Ten vertical levels result in ~0.1 m vertical resolution at the coast, where the minimum depth is set to 1 m, and ~10 m resolution offshore in the deepest regions of the domain.

Each experiment is drawn from the 2x2x3 matrix of combinations made from two bottom profiles, two values of the continental shelf slope, and three values of the freshwater discharge. The variable parameter values used in the experiments are summarized in the Table 2.4.

The topographic features used to represent the shelf are: continental shelf slope and bottom bathymetry. The submarine delta off Atchafalaya River (Figure 1.2) is represented by two idealized topographies: sloping bottom, and sloping bottom with three distinct shoals spaced by 50 km in the north-south direction (Figure 2.4). The continental slope magnitude, *S*, is varied in order to represent two cases of the shelf: with the gradual slope, and with the steep slope.

The freshwater discharge, *Q*, is varied to produce three different river runoff regimes: drought, moderate discharge, and flooding. The amount of the freshwater introduced onto the shelf affects the strength of the stratification, and is used to evaluate the importance of density gradients on the hydrodynamic instabilities. The freshwater plume enters the domain over 10 grid cells in the *x*-direction, which is equivalent to 30 km. The amount of the freshwater entering the domain in the vertical direction decreases exponentially with depth.

Table 2.4. Listing of the variable parameters used for the twelve experiments.

Slope, *S*	**Bottom**	**Freshwater Discharge, *Q***		
		None	Moderate 7500 $m^3 \cdot s^{-1}$	Large 15000 $m^3 \cdot s^{-1}$
Steep 0.0007	No shoals Shoals	*a* *c*	*e* *i*	*g* *k*
Gradual 0.0005	No shoals Shoals	*b* *d*	*f* *j*	*h* *l*

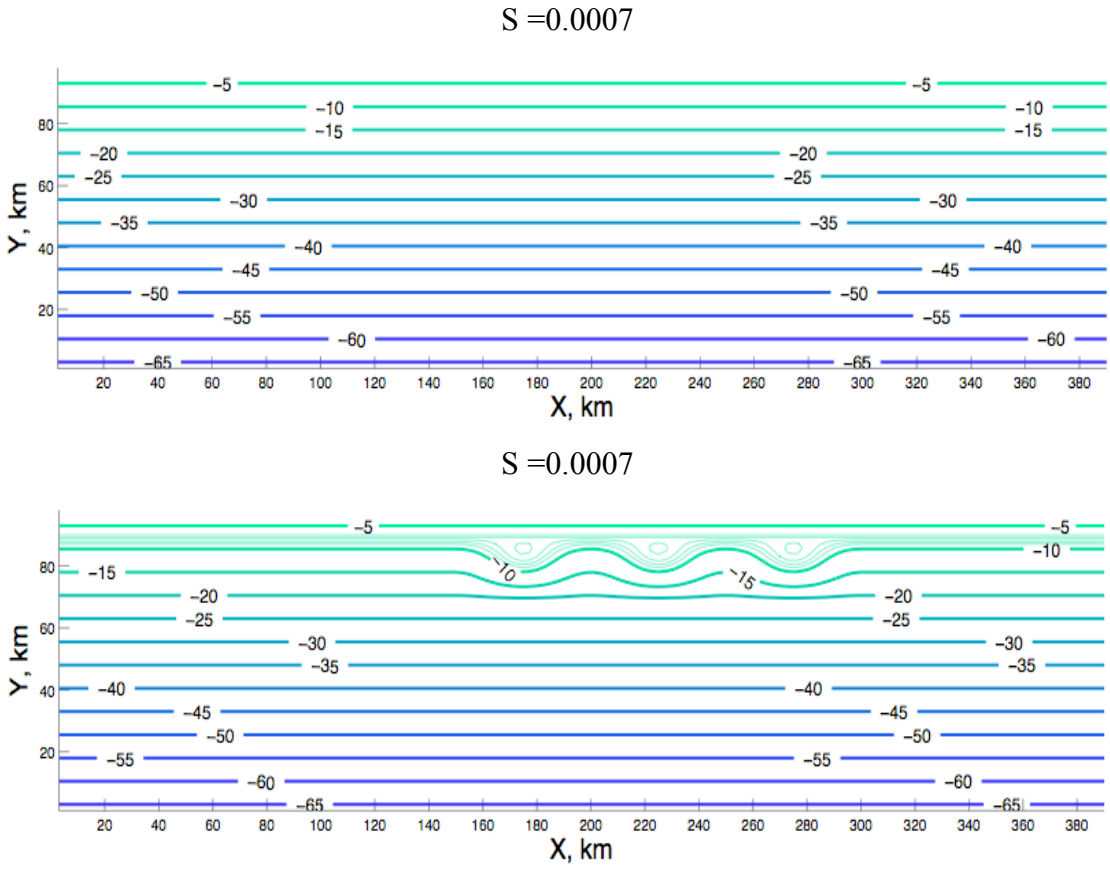

Figure 2.4. Two-dimensional representation of the idealized domain showing bottom topography: sloping bottom (upper panel) and sloping bottom with shoals (lower panel). Depth contours are labeled.

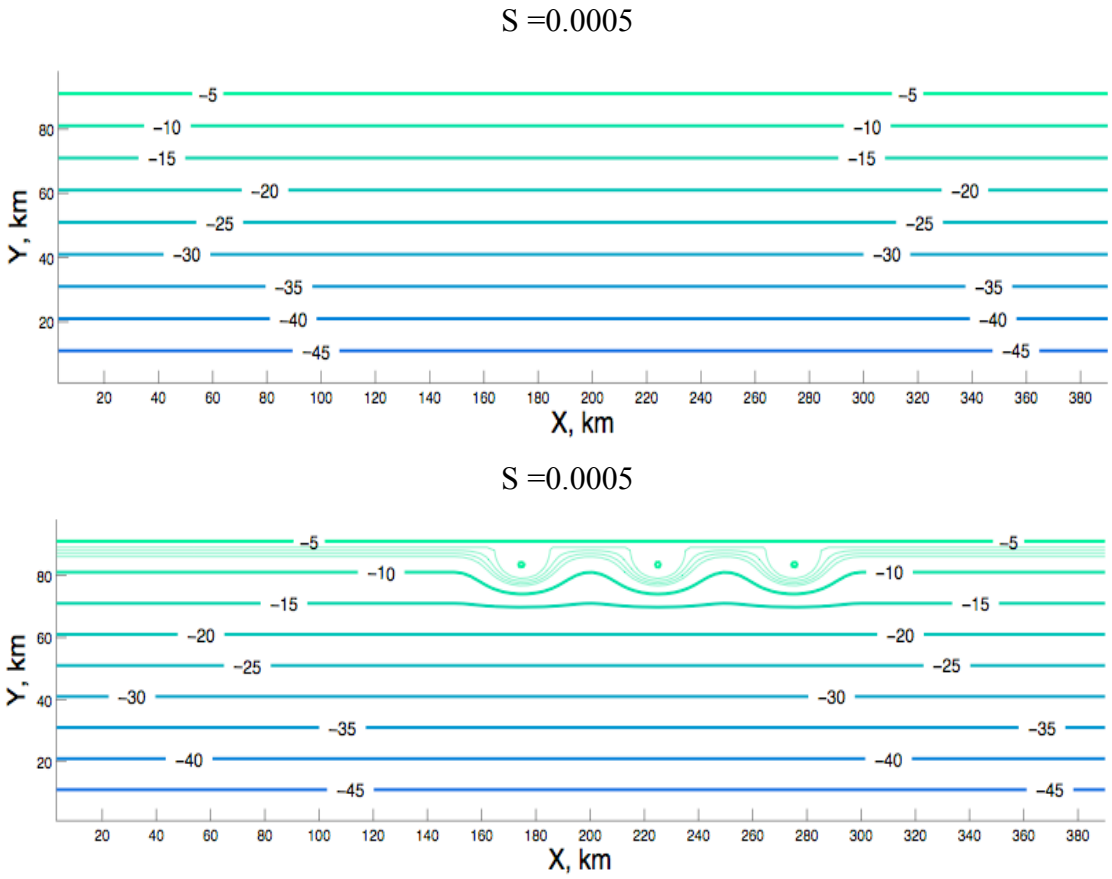

Figure 2.4. Continued.

The east-west periodic boundary conditions are applied for the experiments with no shoals bottom topography and no freshwater discharge. In all other cases, the radiation conditions are used for the three-dimensional velocities, a *Flather* [1976] condition is used for the two-dimensional velocities, a *Chapman* [1985] condition is used for the free surface, and the clamped condition is used for the tracers on the eastern edge. For the western edge, the gradient conditions are used for the three-dimensional velocities, a *Flather* [1976] condition is used for the two-dimensional velocities, a *Chapman* [1985] condition is used for the free surface, and the clamped condition is used for the tracers.

CHAPTER III

EFFECT OF STRATIFICATION ON THE BOTTOM OXYGEN CONCENTRATIONS

Local conditions and processes that are responsible for coastal hypoxia reflect the complex interaction of one or more regional physical and biochemical processes, such as air-sea interactions, vertical mixing, advection, diffusion, respiration, photosynthesis, remineralization, denitrification, and nitrification. Unraveling the relative contribution of each process requires extensive data collection of property values related to those processes. This requires a good understanding of the density structure of the water column and the processes that can alter that structure. The investigation of the alongshore structure of density can reveal much about the character of physical processes that occur in the coastal ocean. Fortunately, MCH cruises routinely performed station lines along the 20 m isobath. I will focus the discussion on the property distributions found along these lines.

Layering of the water column, commonly known as stratification, is a local condition that acts to limit vertical mixing. Change in the heating and/or freshening of surface waters result in a change of the density structure and formation of the layers. On the Louisiana Shelf, vertical mixing between the upper surface and the lower layer depends directly on the regional wind and indirectly on solar heating and freshening of surface waters by river runoff.

Surface waters are normally near saturated values of dissolved oxygen concentrations mainly balanced through air-sea exchange and photosynthesis inputs. At the air-sea interface, oxygen concentrations are affected by parameters such as: wind speed, air and sea temperatures, salinity, surface films, wave action, and bubble injection rates [*Millero*, 2005]. The well-oxygenated surface waters are vertically mixed through the surface layer as a result of winds but may be influenced by other processes such as horizontal advection, internal wave breaking, and current shear. The waters in the lower

layer are usually less saturated with oxygen because those waters are not in direct contact with the atmosphere and local biochemical processes remove oxygen faster than the replenishment needed to maintain saturation (ventilation rate). The lower layer of the water column receives dissolved oxygen mainly through vertical diapycnal mixing. When there is a sufficient amount of light and nutrients in the lower layer, phytoplankton can add oxygen locally through the process of photosynthesis.

Other local physical processes associated with advection, mixing, downwelling, and upwelling, import and export dissolved oxygen in both layers [*Wiseman et al*., 1997; *DiMarco et al*., 2007a, *submitted*]. The processes associated with these water movements may offset the results of the local biological processes and redistribute the dissolved oxygen over the region.

In this chapter, I discuss the relationship of the density structure with the dissolved oxygen concentrations in the water column from observations taken on the MCH cruises in 2004 and 2005. First, I give a description of the spatial distribution of the temperature and salinity the Louisiana Shelf with a focus on their importance to the alongshore variability of the water column stratification. Then, I describe the distribution of dissolved oxygen concentrations on the shelf. Finally, I examine the effect of local vertical stratification on the occurrences of hypoxic waters.

3.1 Temperature and salinity distributions on the Louisiana Shelf

The horizontal and vertical structure and distribution of density on the Louisiana Shelf is controlled by several physical processes, including river freshwater discharge, solar heating, and wind mixing. The density of seawater is determined by temperature, salinity, and pressure. Therefore, by understanding the distribution of these physical properties in the water column and along the coast I plan to establish a link between the density structure and locations of low-oxygen waters.

The water column temperature and salinity sections along the 20 m isobath on MCH spring and summer cruises in 2004 and 2005 are shown in Figures 3.1-3.2.

The temperature records demonstrate the general characteristic seasonal trend of spring and summer warming. In early spring (Figures 3.1), the temperature distribution is mostly uniform throughout the water column and along the coast. The temperature difference between the surface values (2 m below the surface) and values at the bottom (0.5 m above the bottom) is ~2^{o}C in the early spring cruises M1 and M4. As the seasonal heating progresses, significant vertical temperature variations can be seen during the late spring and early summer cruises M2 and M5. The difference in temperature between surface and bottom layers reaches ~8^{o}C during M5 cruise.

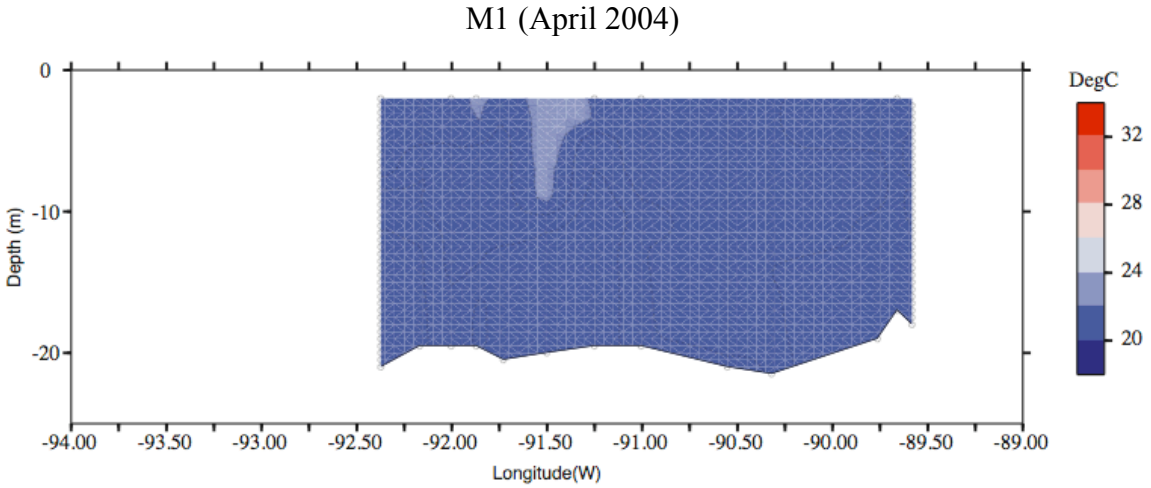

Figure 3.1. Water column temperature profiles from continuous CTD (Model: Sea-Bird SBE-911-Plus) casts with vertical intervals of 0.5 m along the 20 m isobath on MCH cruises (M1-M7) in 2004-2005.

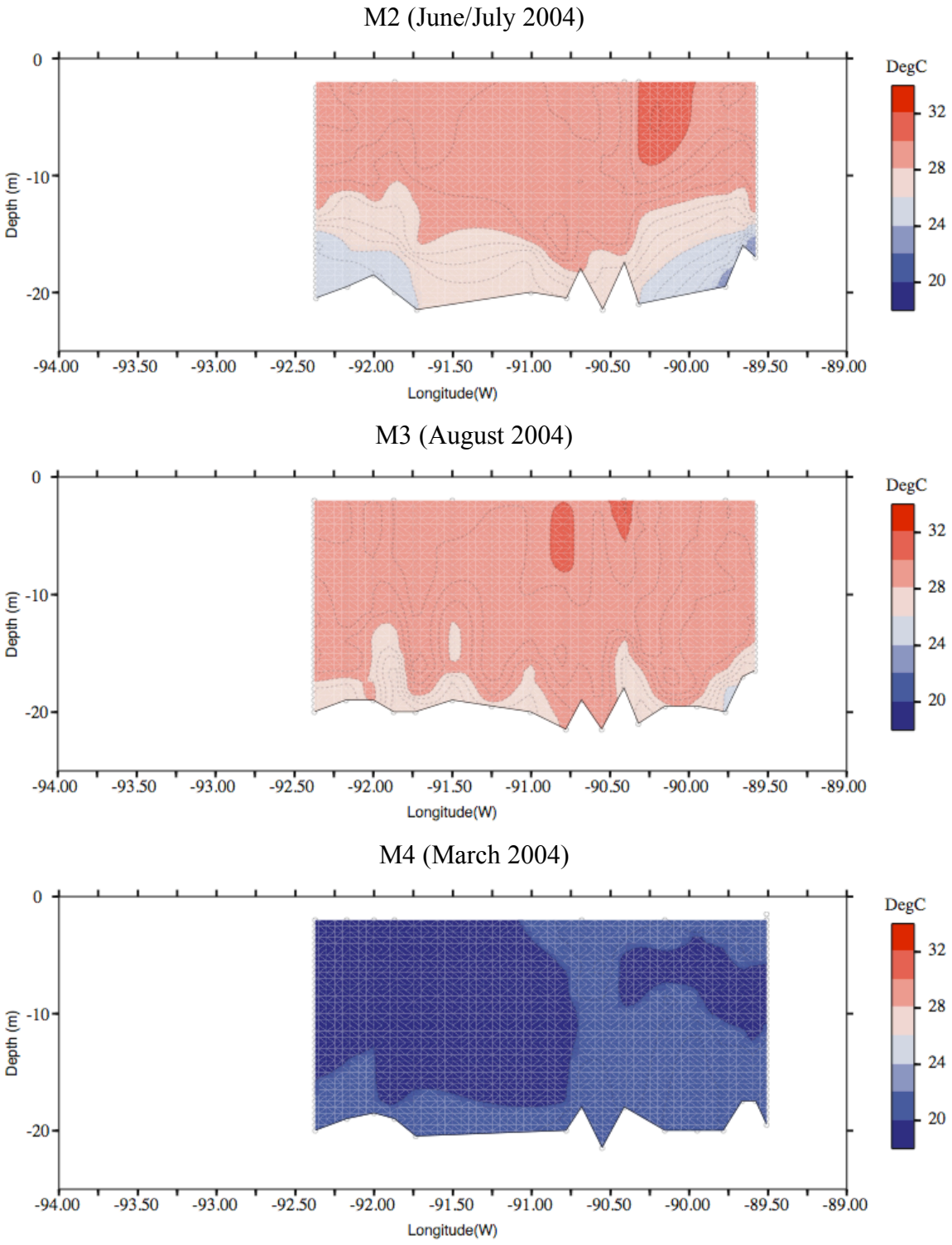

Figure 3.1. Continued.

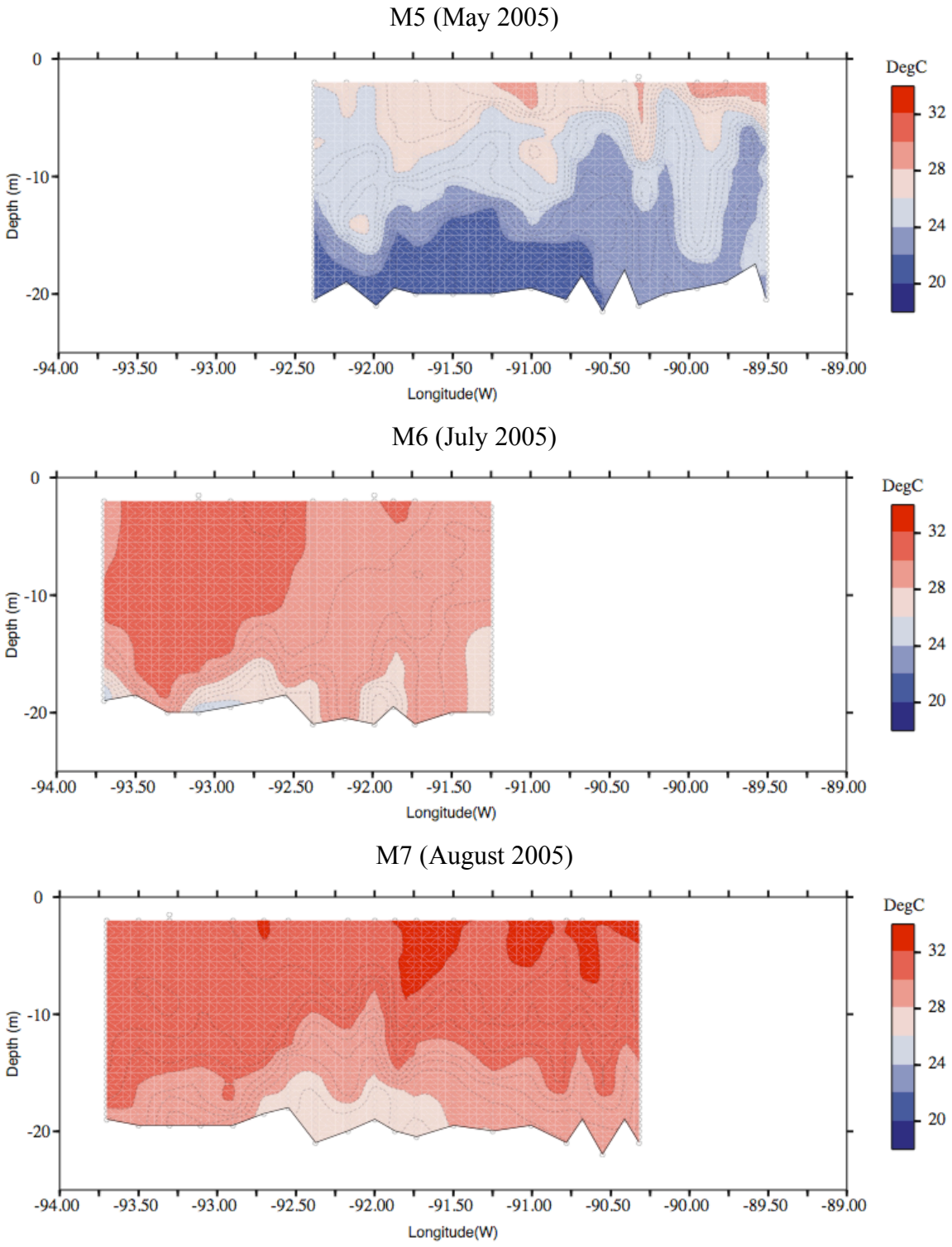

Figure 3.1. Continued.

The absence of the strong vertical mixing due to the general weakening of the winds during the summer months also contribute to the development of a pronounced thermocline. As summer continues, the water column exhibits a nearly uniform distribution throughout the water column and along the shelf. In general, the spring temperatures are ~4^{o}C at the bottom and ~8^{o}C at the surface cooler than those in late summer when the sea surface temperatures usually reach their annual maximum. Therefore, temperature is thought to have a stronger affect on controlling density structure in spring and almost no affect in summer.

The water column salinity records along the Louisiana Shelf (Figure 3.2) show distinctive signatures of two plumes: the Mississippi River plume and Atchafalaya River plume. The plumes, defined as large bodies of less saline than ambient water, can be clearly seen in salinity profiles in cruises M1-M2, and M4-M5. During M3 and M6-M7 cruises, the plume signatures are less pronounced due to the decrease in the Mississippi-Atchafalaya River system discharge and intensification of the wind mixing.

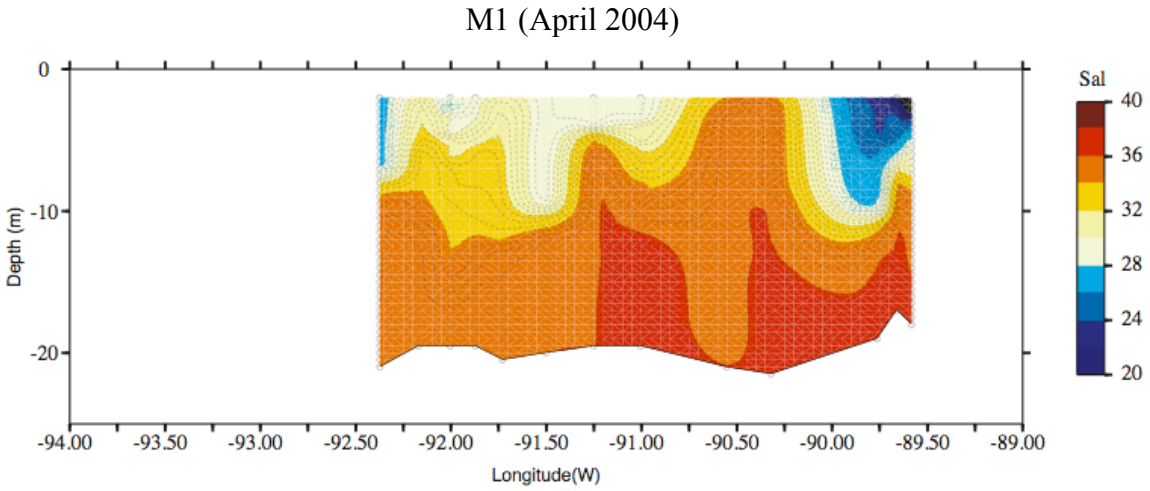

Figure 3.2. Water column salinity profiles from continuous CTD (Model: Sea-Bird SBE-911-Plus) casts with vertical intervals of 0.5 m along the 20 m isobath on MCH cruises (M1-M7) in 2004-2005.

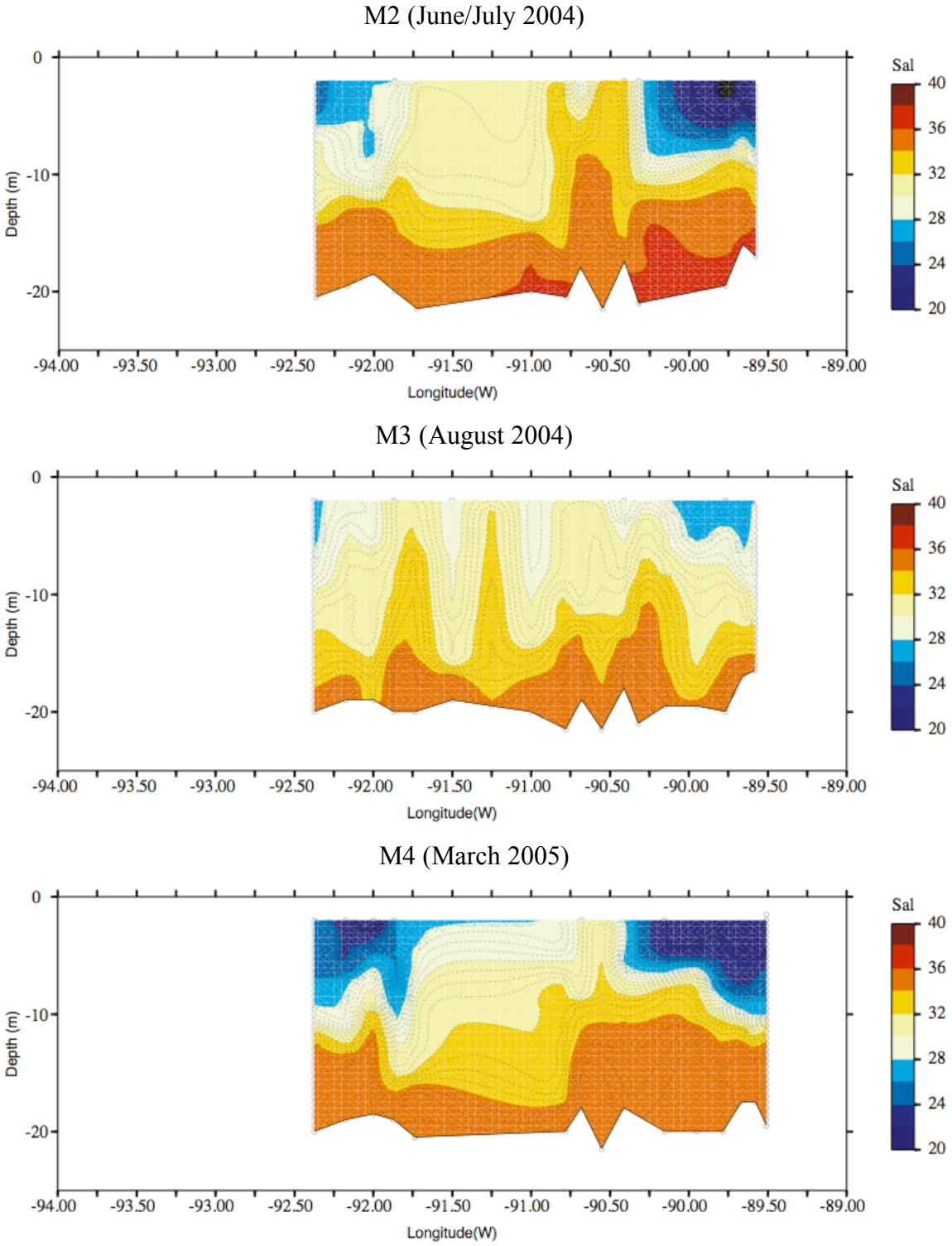

Figure 3.2. Continued.

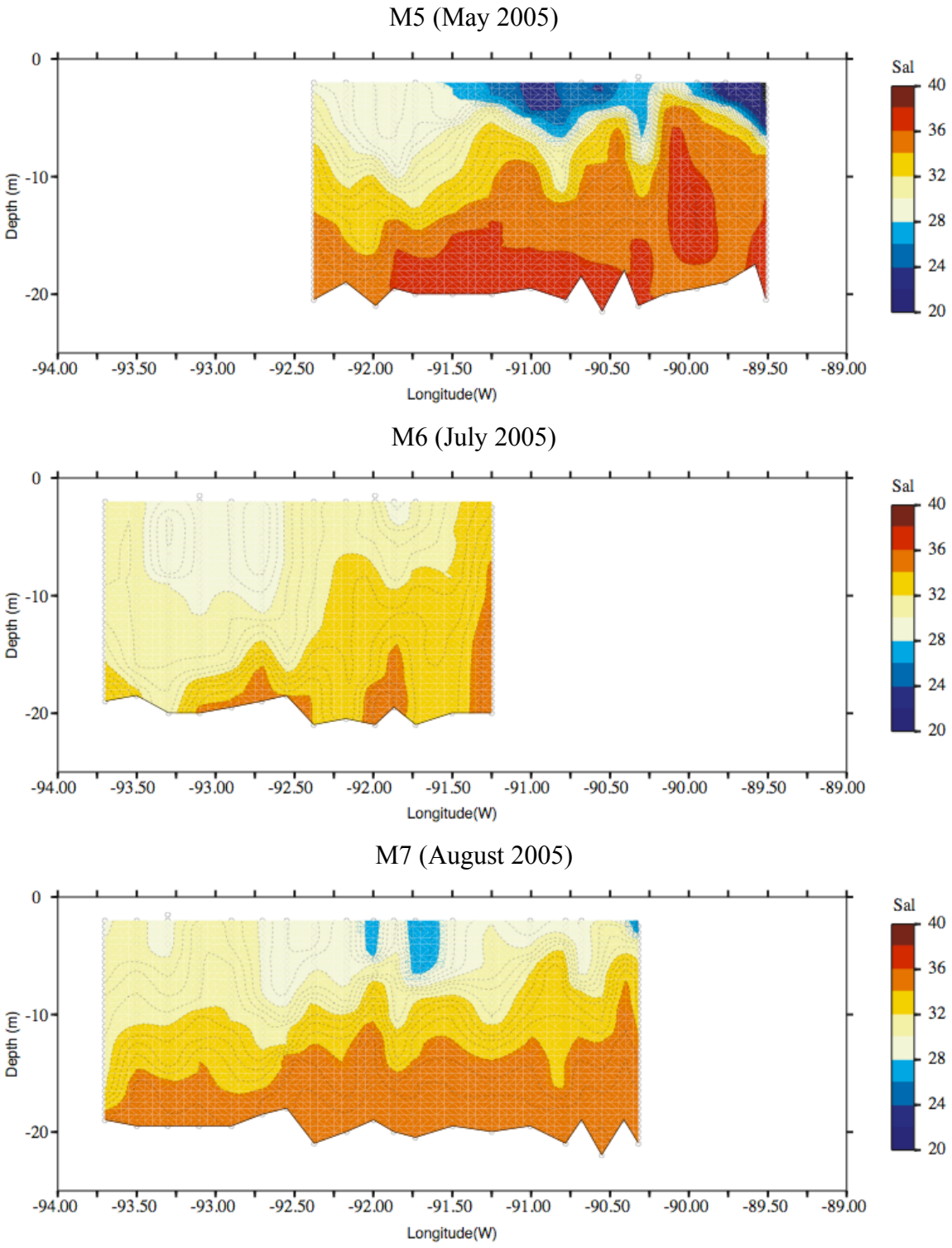

Figure 3.2. Continued.

The size and spatial spread of the plumes greatly varies seasonally and interannually, and can be related to the river discharge. The Mississippi-Atchafalaya River System discharges the majority of the fresh water onto the Louisiana Shelf [*Solis and Powell*, 1999]. Plots of the annual discharge for the Mississippi-Atchafalaya River System in 2004 and 2005 are shown in Figure 3.3. The Mississippi and Atchafalaya discharge records have a high coherence due to the reasons stated in the introduction (Chapter I). A simple comparison of the time series of Mississippi-Atchafalaya River outflow from 2004 and 2005 reveals that discharge during the period from January to April in 2005 was greater than in 2004, and as a result, larger bodies of the less saline than ambient oceanic water are present in the salinity sections along the shelf in 2005.

Another prominent feature found in each of the water column temperature and salinity sections is the wave-like disturbance along the Louisiana Shelf. The feature is less noticeable in the temperature records, but is pronounced in the salinity structure. The amplitude of disturbance varies from 1 m up to 10 m in total 20 m depth with the approximate wavelength around 50 km. The origin of this feature can be attributed to the processes associated with buoyancy transfer in the water column. Fresh waters from Mississippi-Atchafalaya System enter the shelf and trigger development of the instabilities due to the density difference of river plume and ambient oceanic waters [*Simpson*, 1996]. Another possible cause for the formation of instabilities along the shelf is the deviation in the flow controlled by topography [*Orlanski*, 1969; *Xue and Mellor*, 1992; *Wolfe and Cenedese*, 2005]. The posterior development of meanders, as deviations of the water property front along the coast, can be set by depth variations. Sandy shoals along the Louisiana shelf off Atchafalaya River Delta pose an abrupt change in the water depth from 10 m up to 5 m (Figure 1.2). Dynamic instabilities produced by the density differences and topographic steering may interact with one another, resulting in a highly irregular wave-like distribution of the water properties along and across the shelf.

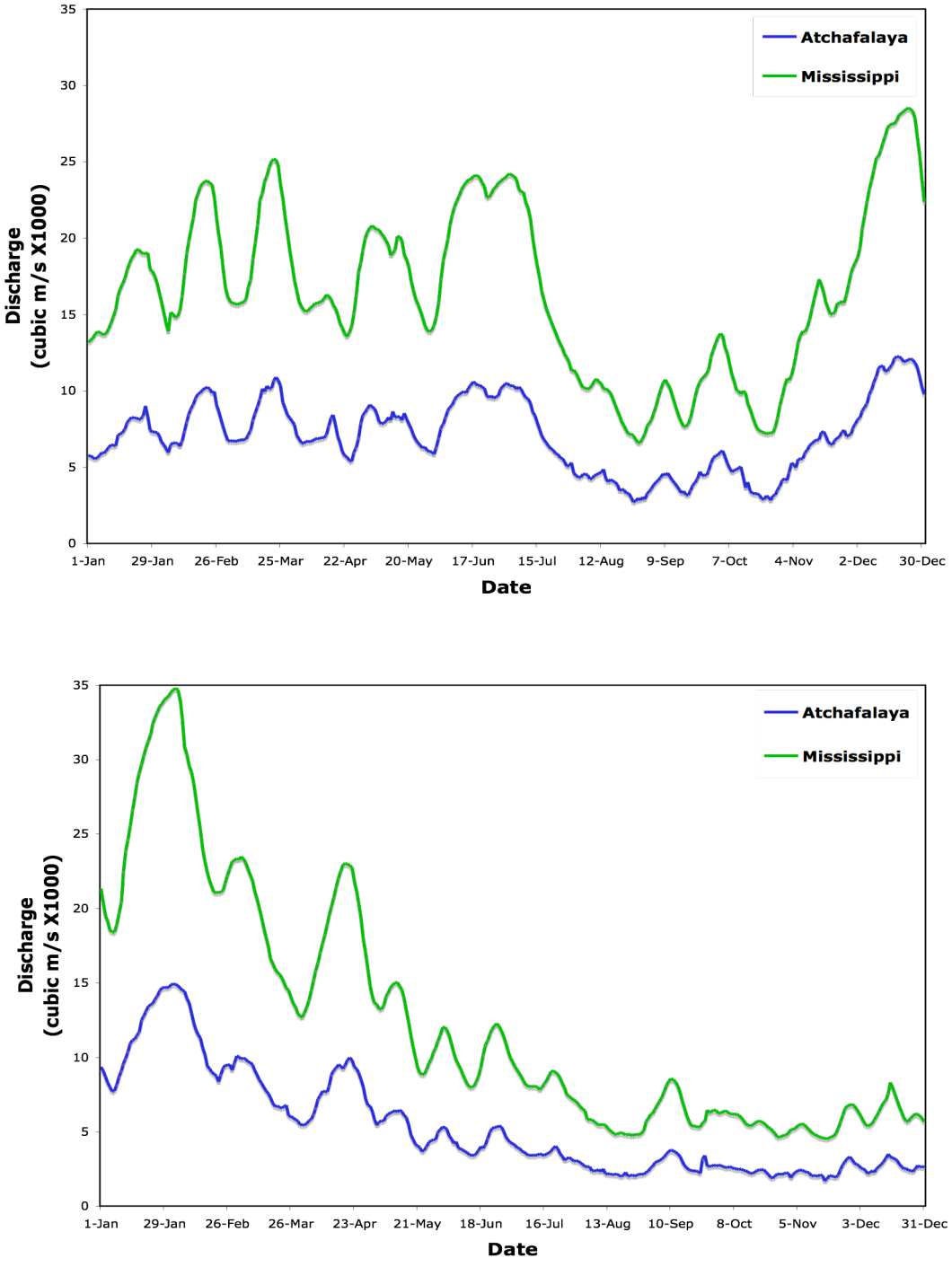

Figure 3.3. The Mississippi River discharge at Tarbert Landing, MS, and Atchafalaya River discharge at Simmesport, LA, in 2004 (top) and 2005 (bottom). (Data source: US Army Corps of Engineers)

The horizontal distributions of river-derived low-salinity water over the Louisiana Shelf by cruise are shown in Figure 3.4.

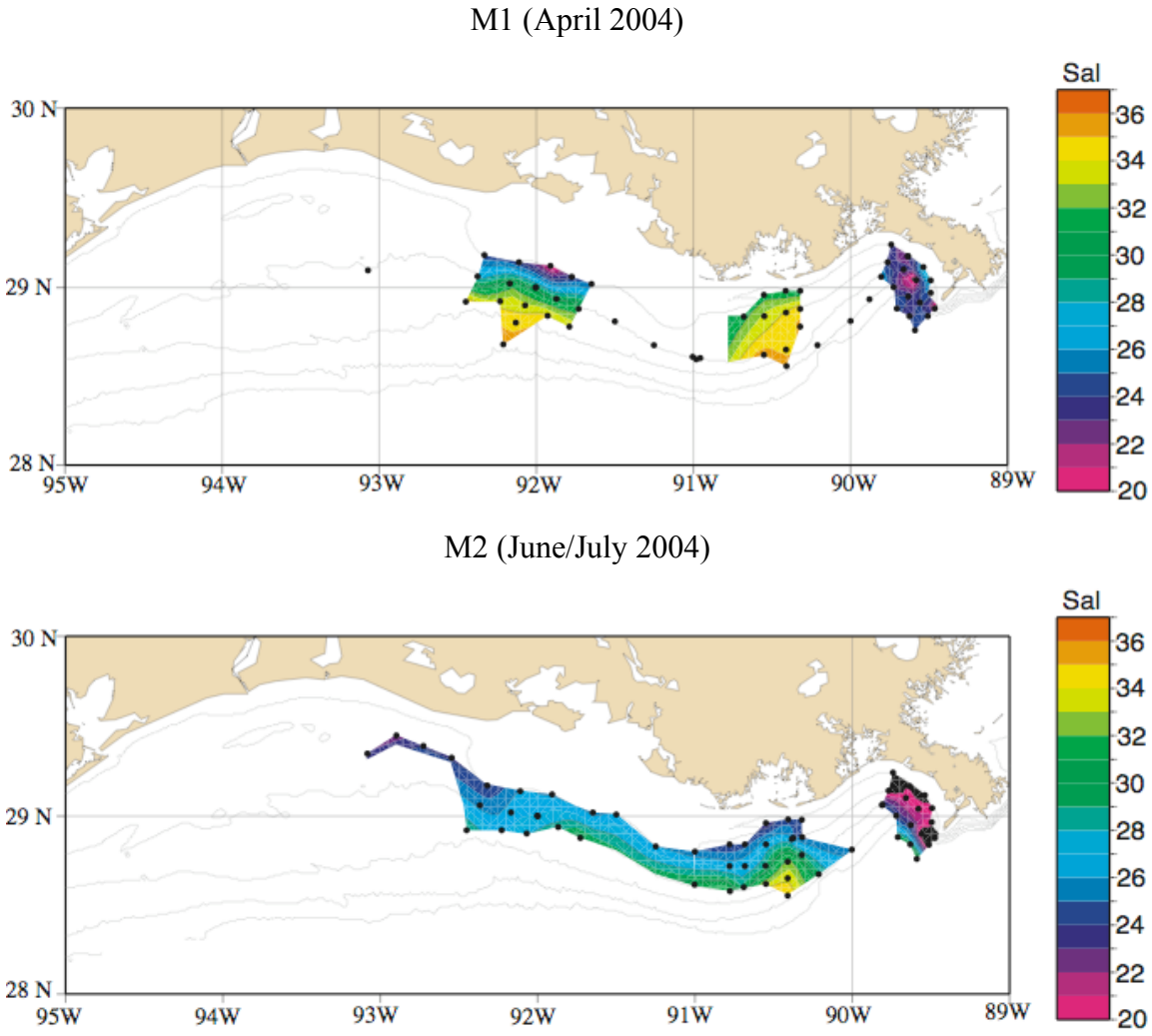

Figure 3.4. Near-surface salinity (3 m below surface) from Nisken bottles on MCH cruises (M1-M7) in 2004-2005. Dots represent station locations.

M3 (August 2004)

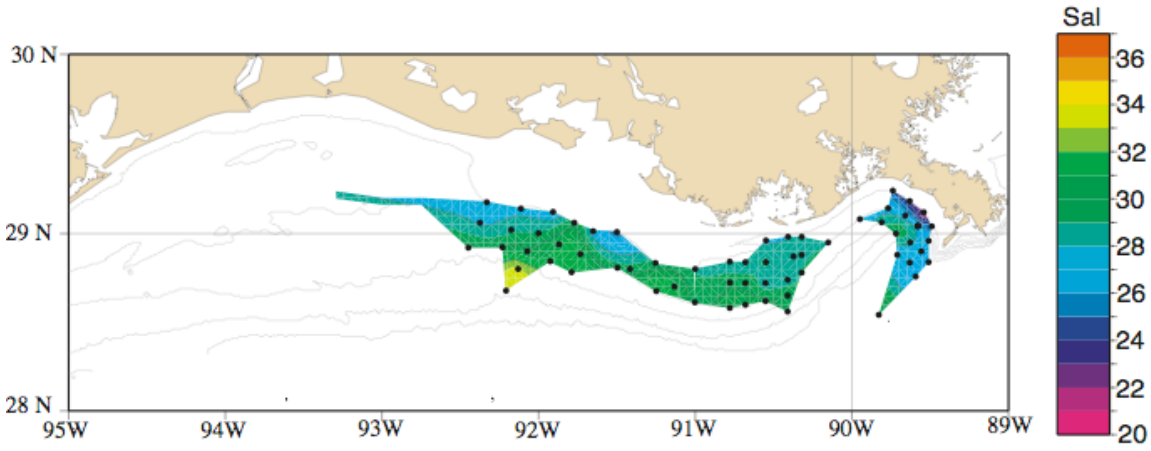

M4 (March 2005)

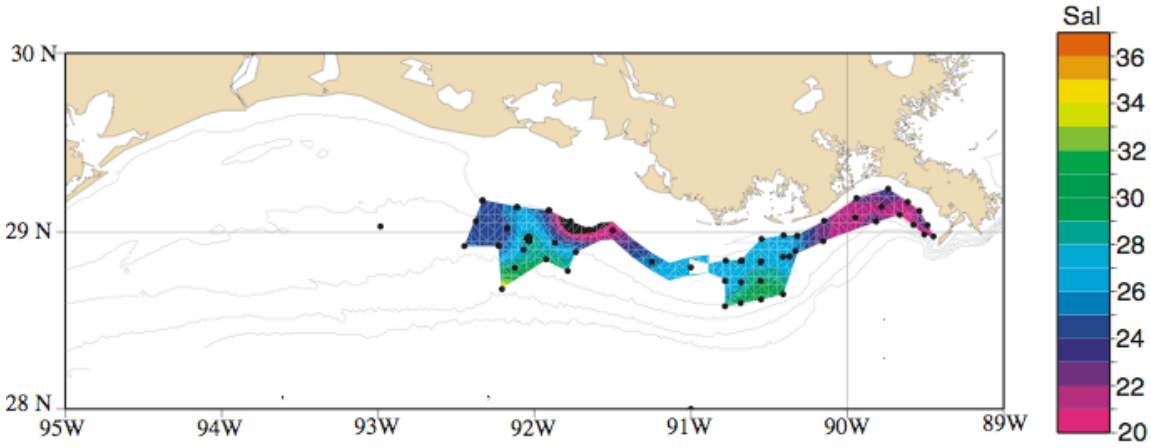

M5 (May 2005)

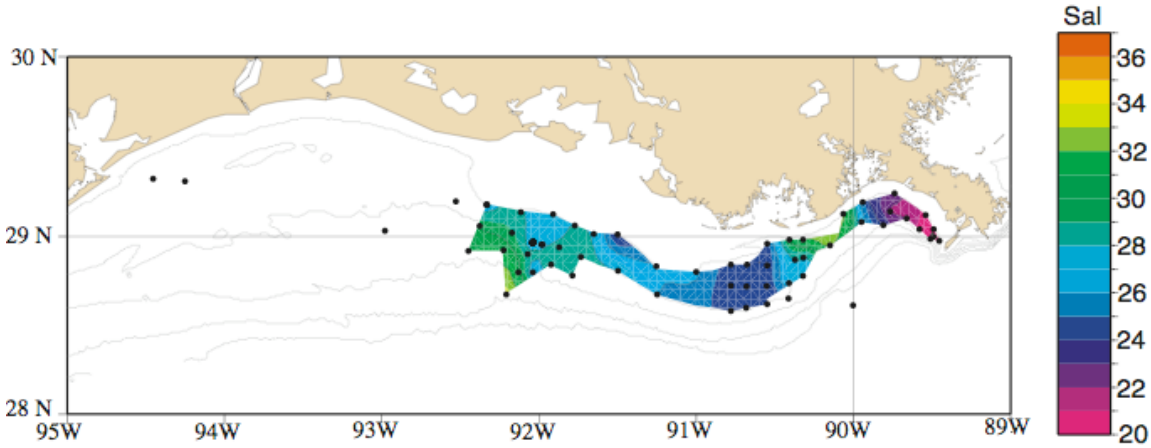

Figure 3.4. Continued.

M6 (July 2005)

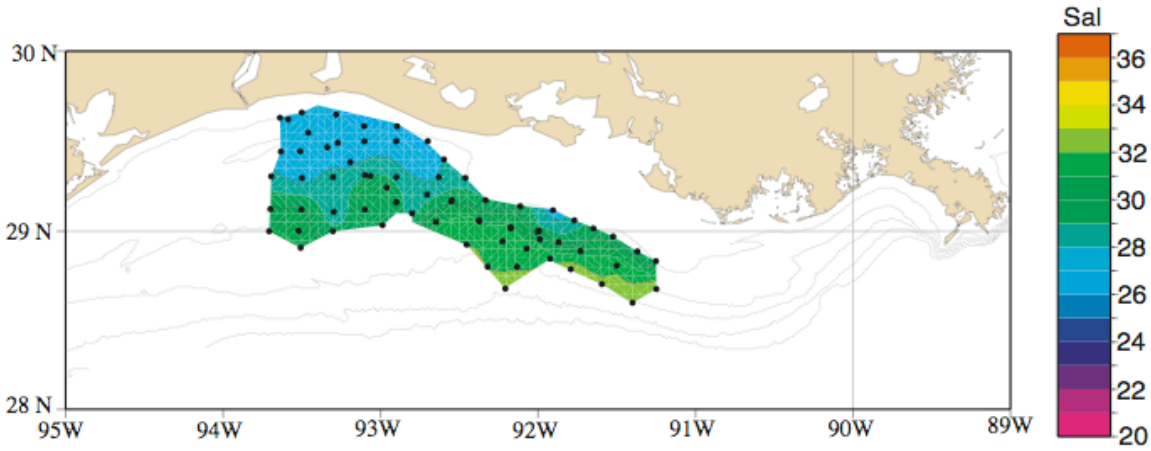

M7 (August 2005)

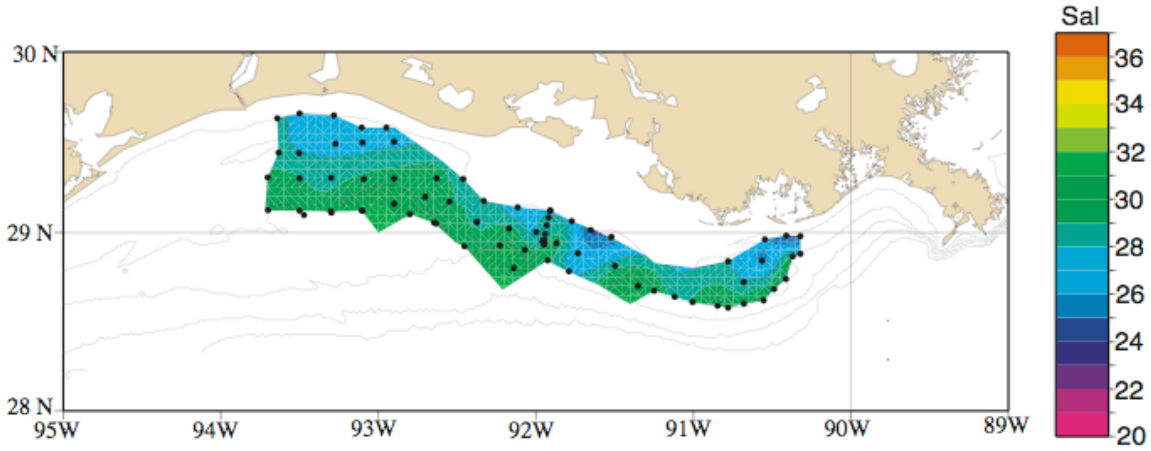

Figure 3.4. Continued.

The wind-driven annual pattern of low-frequency circulation over the Texas-Louisiana shelf directly affects the local stratification. In spring during cruises M1 and M4, the downcoast currents (Figure 3.5) driven by downwelling favorable winds (upper panels of Figure 3.6) advect low-salinity water along the near shore areas of the Louisiana Shelf. As a result, during those cruises, the salinity gradient over the Louisiana Shelf is directed offshore with the lowest salinity waters inshore and the highest salinity waters offshore. In summer, the circulation conditions are different from those in spring as prevailing winds acquire an upcoast component [*Nowlin et al.*, 1998]. Therefore, water discharged from the Mississippi-Atchafalaya River System typically pools in the region rather than being transported out of the area by downcoast flow [*Nowlin et al.*, 2005]. Prevailing winds were upwelling favorable (lower panels of Figure 3.6) and allowed for the spread of the low-salinity water over much of the inner shelf during cruses M2 and M5 (Figure 3.4).

Although infrequent during the summer months, atmospheric storms and hurricanes bring strong winds that can break down the stratification on the shelf and promote the ventilation of the water column. Tropical Storm Matthew on 12 of August 2004 (several days before the M3 cruise) passed through the eastern edge of the shelf bringing significant winds (~10 $m \cdot s^{-1}$) and surface waves. This condition combined with generally low river discharge and downwelling advection of water masses during the summer months led to the relatively weaker salinity gradient over the Louisiana Shelf as observed during the M3 cruise. A similar pattern is seen in the surface salinity during the M7 cruise in 2005. Swells generated by the Hurricane Dennis during M6 cruise most likely contributed to the vertical mixing of the water column and the breakdown of the vertical stratification.

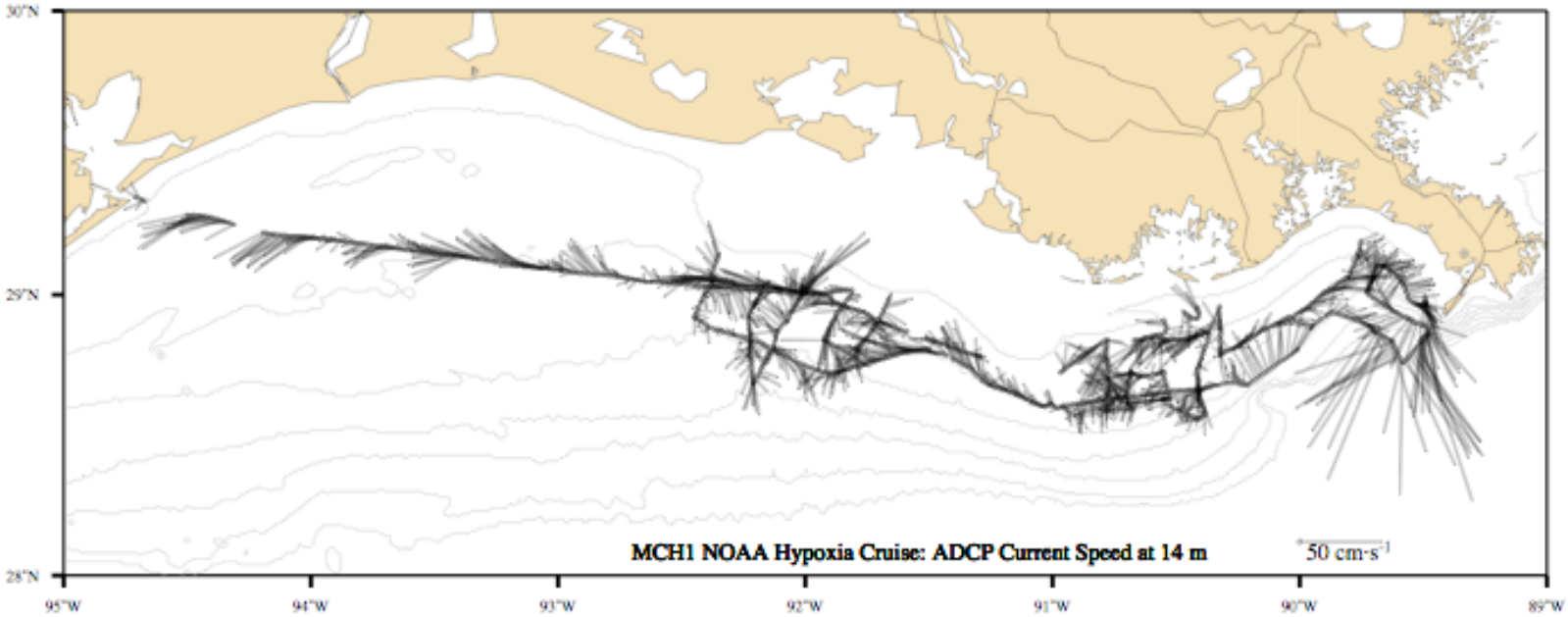

Figure 3.5. Current velocity at 14 m depth from shipboard 150-kHz ADCP on MCH cruise M1 in 2004.

M1 (April 2004)

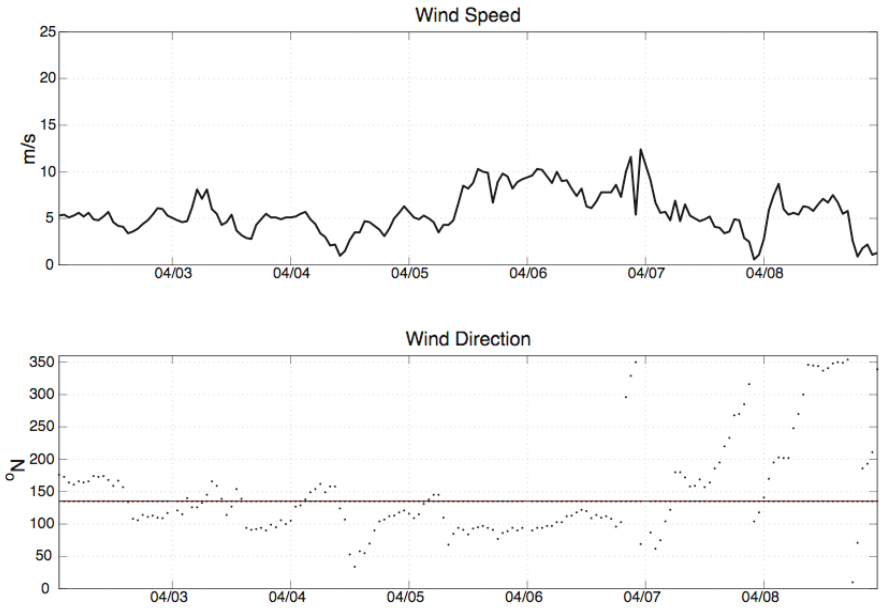

M2 (June/July 2004)

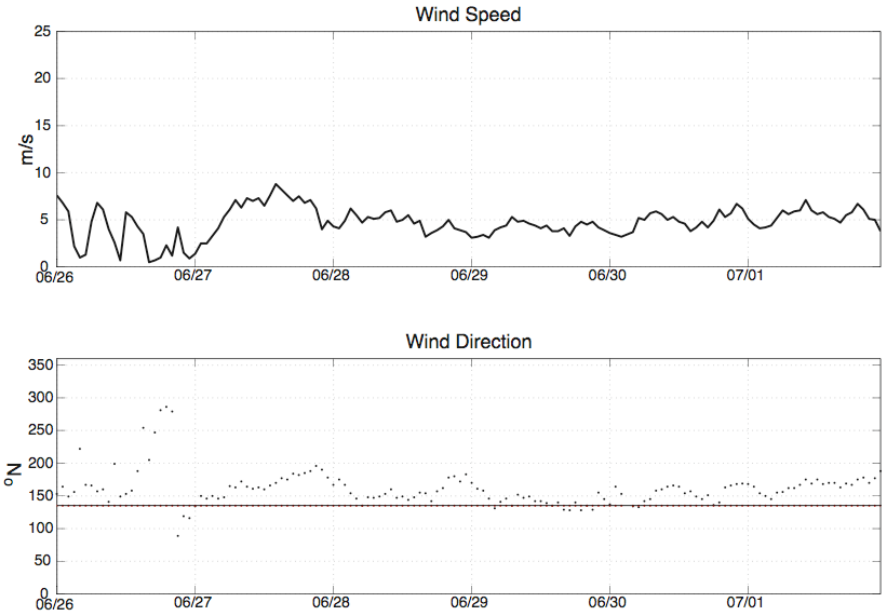

Figure 3.6. Wind speed and direction from station 42035 located at 29°13'54"N 94°24'48"W during MCH cruises in 2004-2005. (Data source: National Data Buoy Center).

M4 (March 2005)

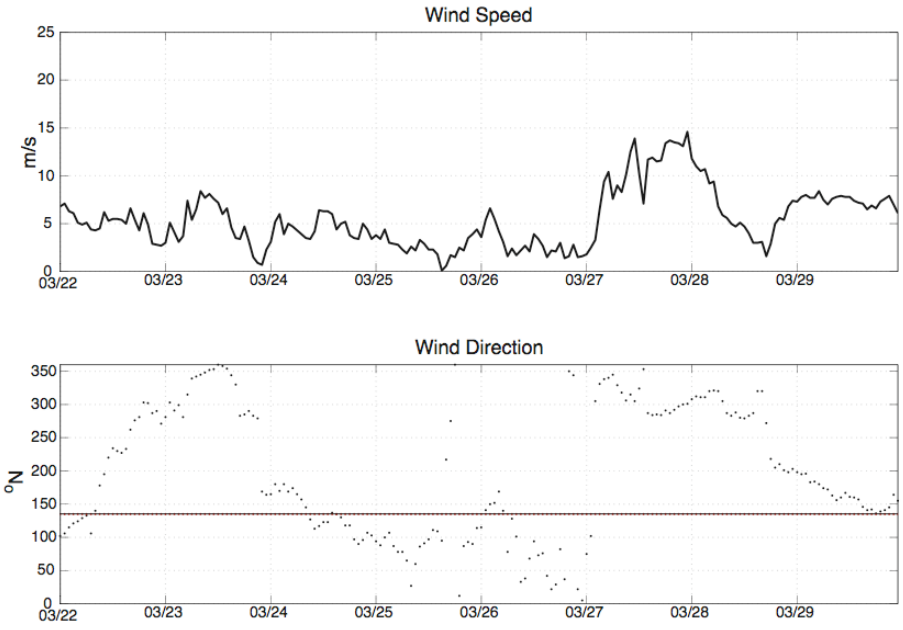

M5 (May 2005)

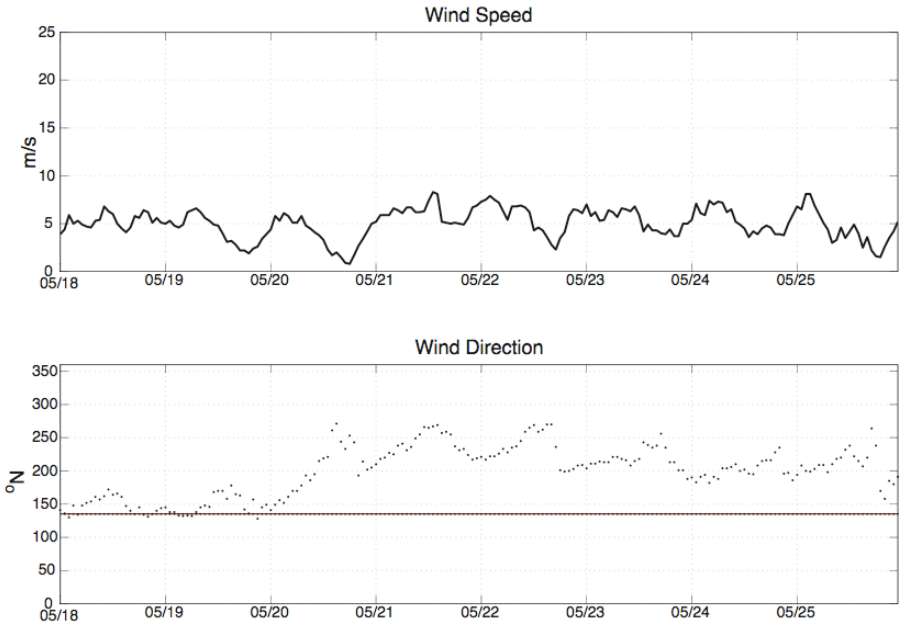

Figure 3.6. Continued.

In general, the high river discharge in the end of winter and/or early spring corresponds with the high freshwater content on the shelf, causing strong horizontal and vertical salinity gradients on the shelf. The mean halocline depth varies seasonally being closer to the surface at ~5-10 m depth in spring due to the peak freshwater discharge. In late summer as river discharge decreases, winds also dramatically decrease leading to a deeper mixed layer depth of 13-17 m.

A T/S diagram comparing temperature and salinity for all MCH cruises shows a noticeable separation by season (Figure 3.7). The summer cruises exhibit the greater temperature differences due to the substantial solar heating. The salinity differences are significant for the all cruises being greater in the spring and early summer as a result of spring flooding. The temperature and salinity records provide evidence that salinity has a greater effect than temperature on the density structure along the Louisiana Shelf. Most of the density stratification is due to the vertical salinity gradient, however the stratification is enhanced by seasonal thermocline during the early summer cruises.

3.2 Dissolved oxygen concentrations on the Louisiana Shelf

The annual cycle in the development of hypoxia on the Louisiana Shelf usually described as follows [*Rabalais et al*., 1999]. During winter and early spring months, hypoxic waters are usually not found on the shelf in the water depths range of 10-60 m. The Mississippi-Atchafalaya River System carries large amounts of fresh water, sediments, dissolved and particulate materials onto the shelf, especially during peak spring discharge. The nutrients delivered with the river runoff support the primary production across the Texas-Louisiana Shelf [*Lohrenz et al.,* 1994]. Often a phytoplankton bloom becomes a large source of fixed carbon for decomposition by aerobic bacteria [*Rabalais et. al*., 1999]. The process of decomposition removes dissolved oxygen from the water column, causing the development of hypoxia during the spring and summer months. The concurrent effect of the weak upwelling-favorable winds during this time of the year and freshwater discharge produces the intense stratification and promotes the development of bottom hypoxia on the shelf. Very often,

the severe weather conditions alter the distribution of hypoxic waters along the Texas-Louisiana shelf. The passages of tropical storms and hurricanes, starting usually in July, disrupt the stratification of the water column and oxygenate the bottom layers. Seasonal reversal of winds to downwelling-favorable in the late summer also contributes to the weakening of stratification and the ventilation of hypoxic bottom waters. Strong mixing events, decline in the river discharge and decomposition of organic matter lead to dissipation of hypoxia in the fall, and the virtual absence of hypoxia during the winter [*Rabalais et al.,* 2007].

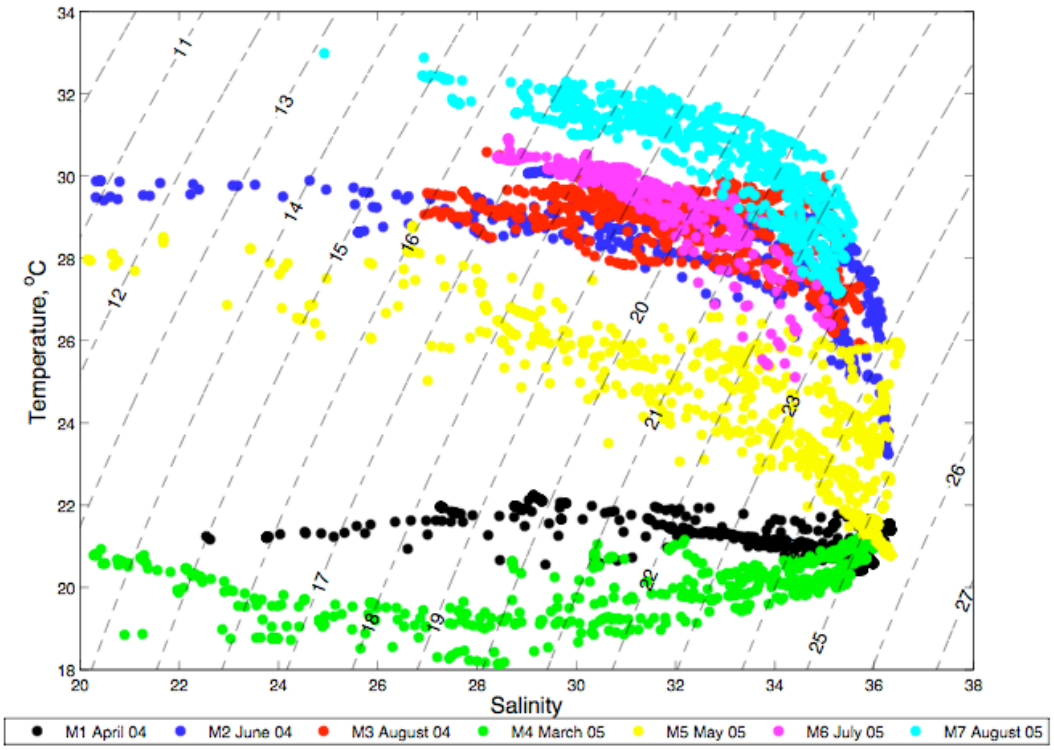

Figure 3.7. Temperature versus salinity from continuous CTD (Model: Sea-Bird SBE-911-Plus) casts with vertical intervals of 0.5 m at all stations on all MCH cruises in 2004-2005. Contours represent potential density (sigma-theta, $kg \cdot m^{-3}$).

The horizontal distribution of near-bottom dissolved oxygen concentration over the Louisiana Shelf and vertical distribution of dissolved oxygen concentration in the water column along the 20 m isobath on MCH cruises (M1-M7) are shown in Figure 3.8 and Figure 3.9.

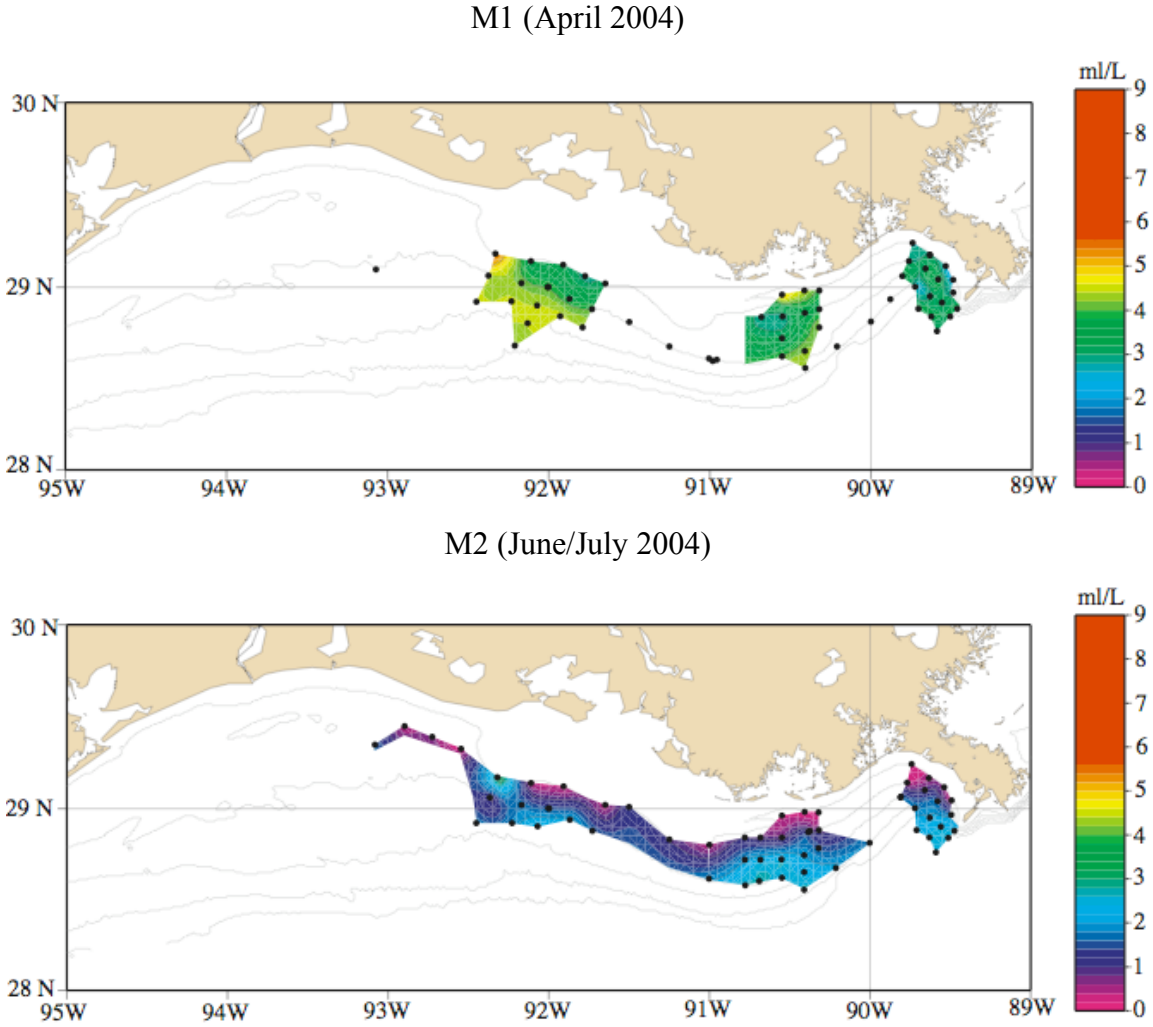

Figure 3.8. Near-bottom (~0.5 m above bottom) dissolved oxygen concentration from Nisken bottles on MCH cruises (M1-M7) in 2004-2005. Dots represent station locations.

M3 (August 2004)

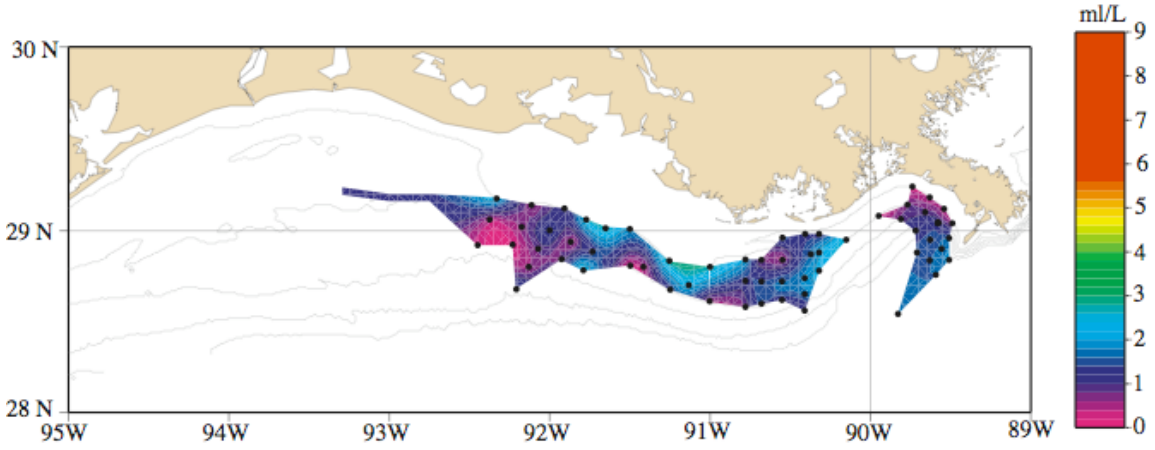

M4 (March 2005)

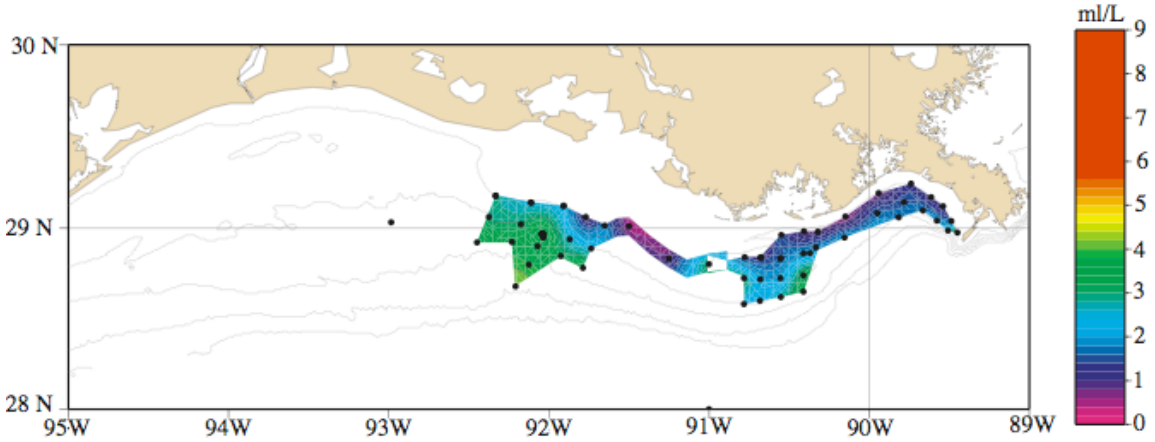

M5 (May 2005)

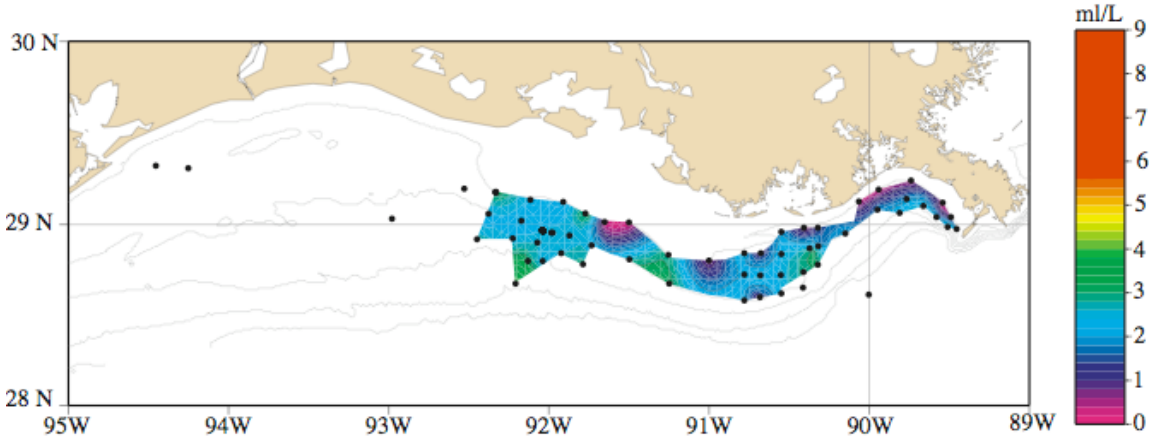

Figure 3.8. Continued.

M6 (July 2005)

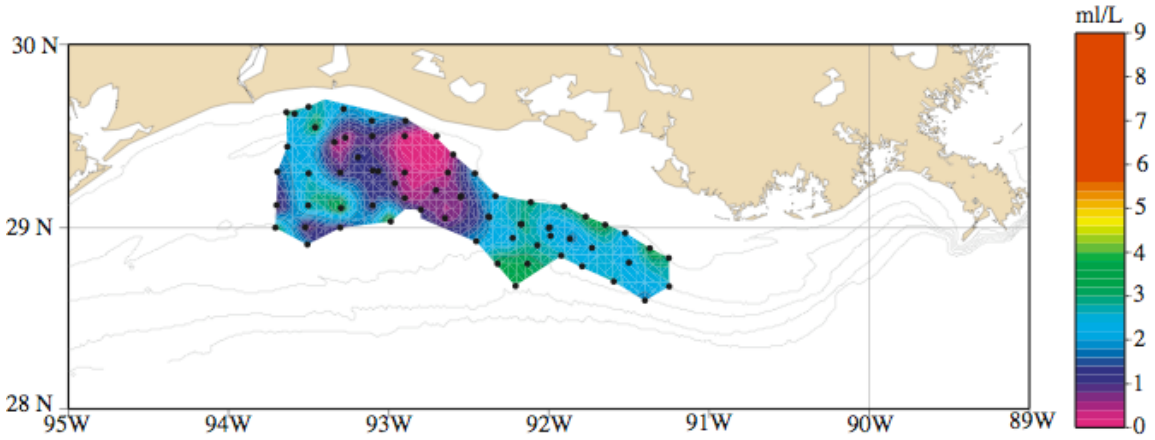

M7 (August 2005)

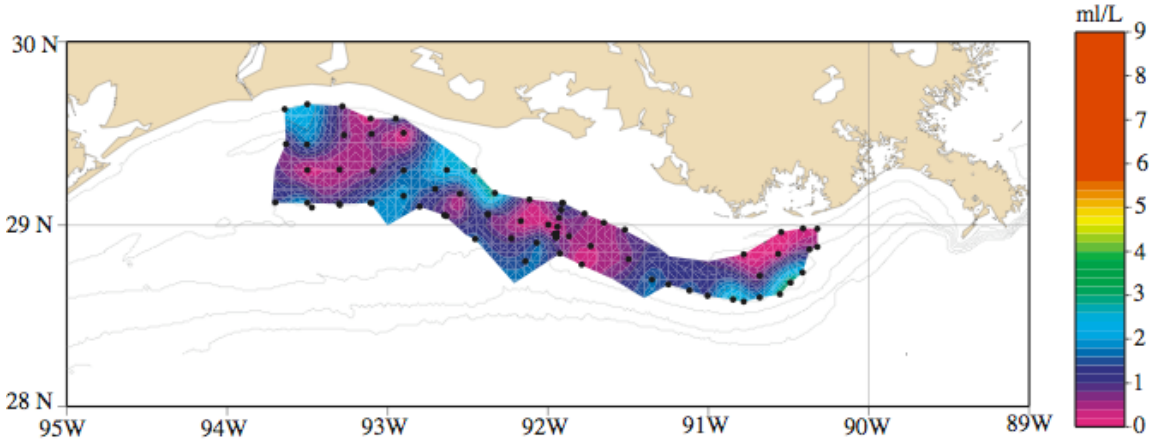

Figure 3.8. Continued.

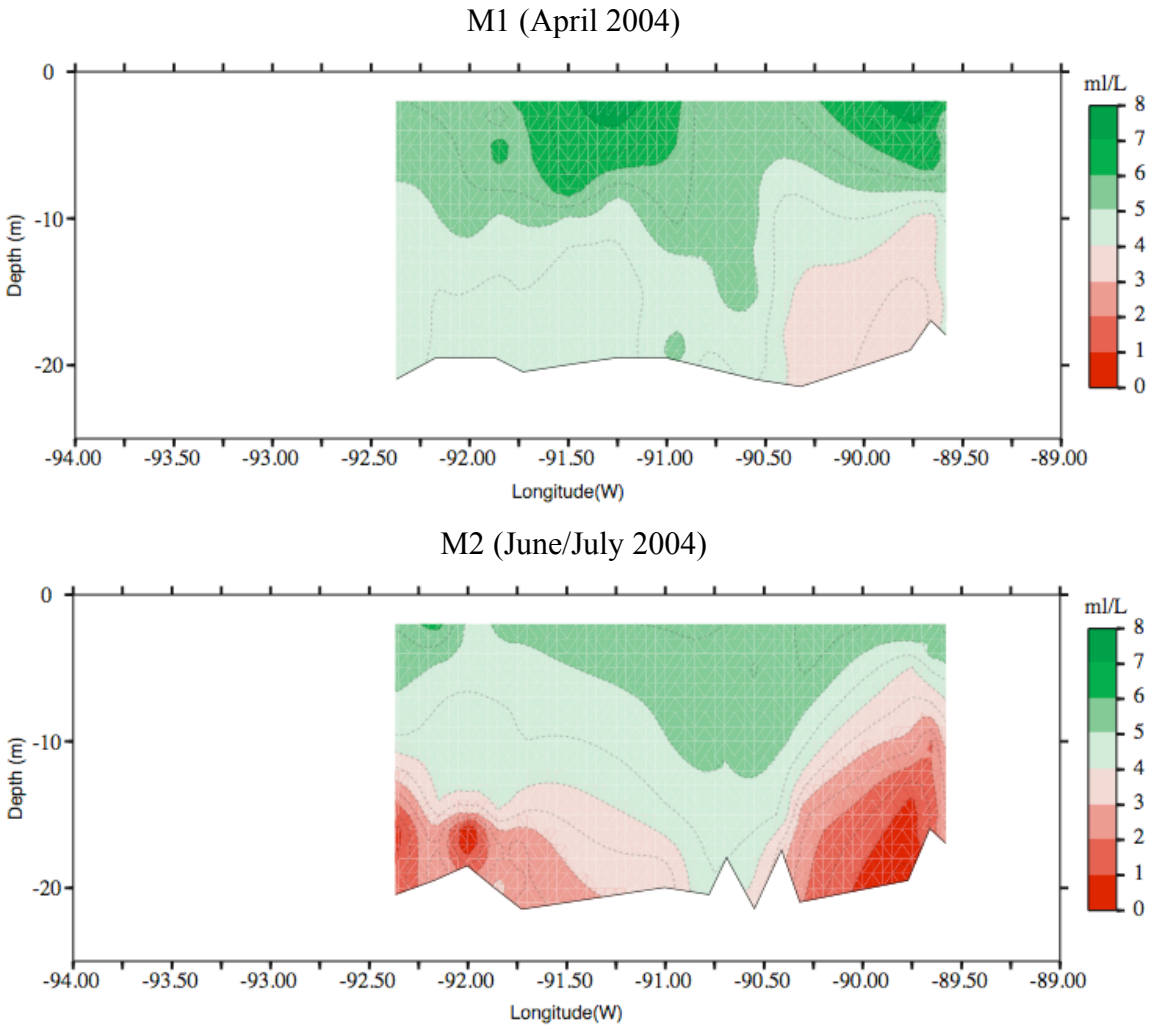

Figure 3.9. Water column dissolved oxygen concentration profiles from Nisken bottles along the 20 m isobath on MCH cruises (M1-M7) in 2004-2005.

M3 (August 2004)

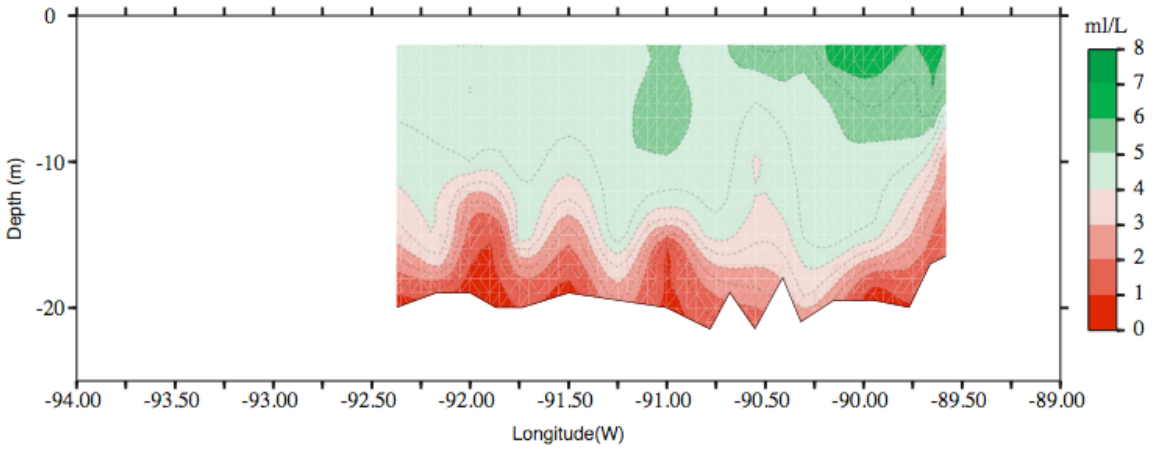

M4 (March 2005)

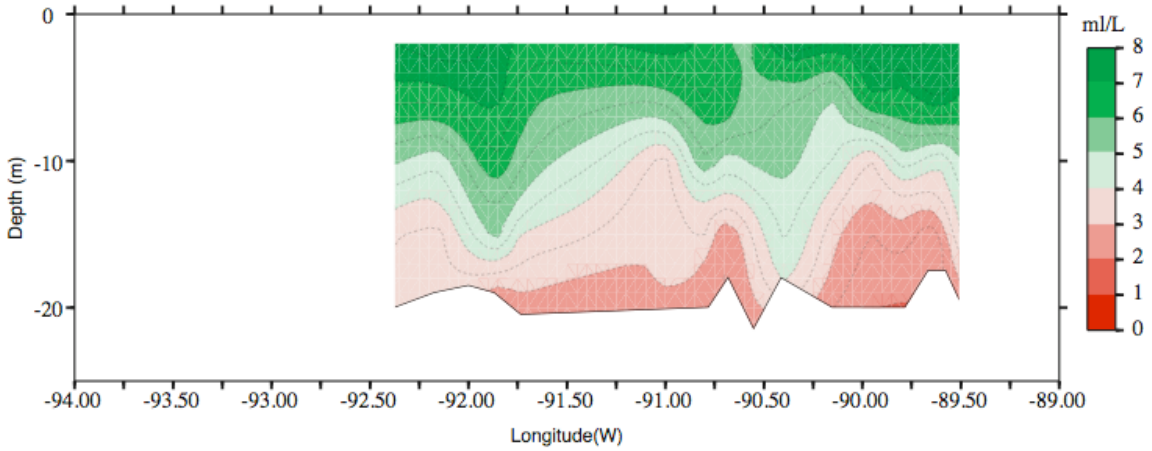

M5 (May 2005)

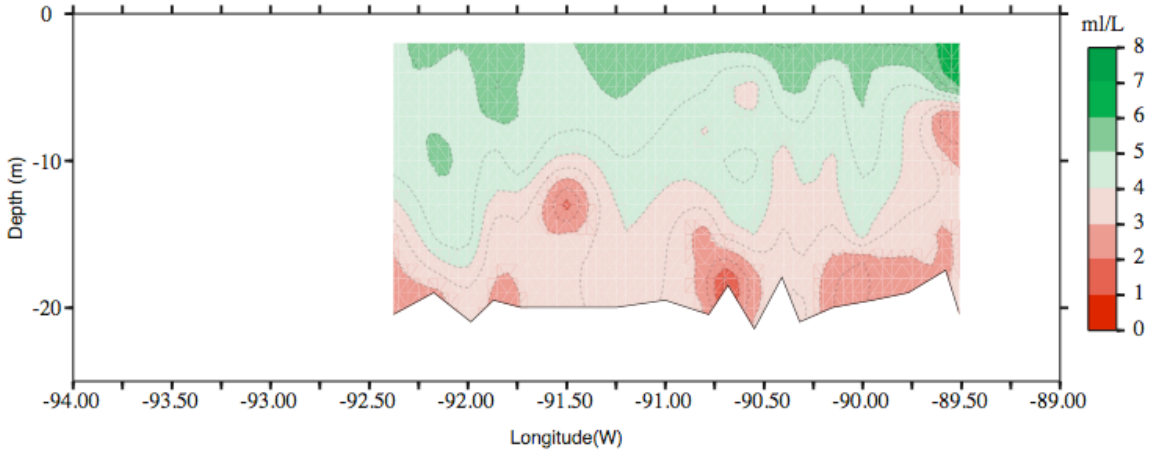

Figure 3.9. Continued.

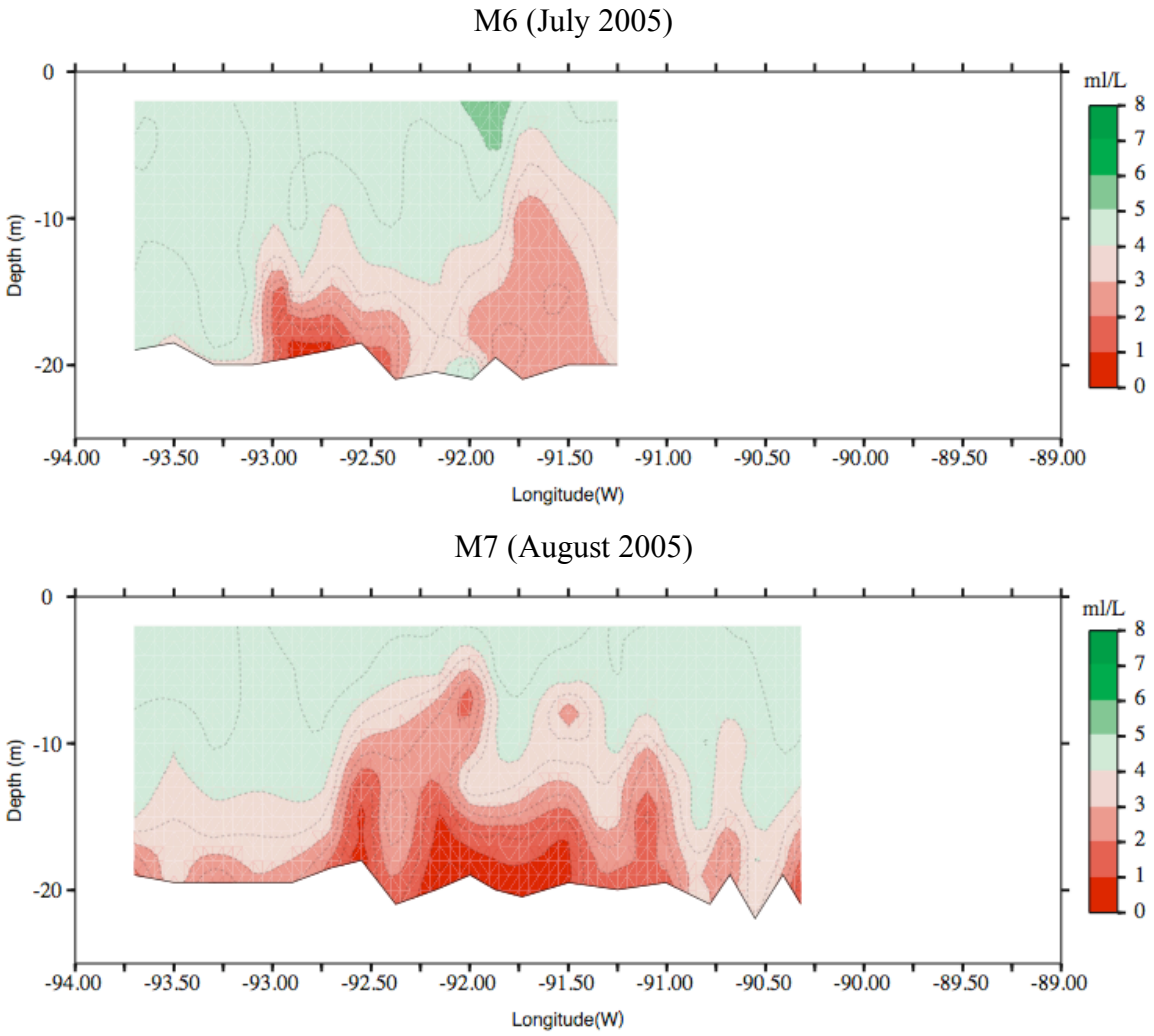

Figure 3.9. Continued.

The sequence of dissolved oxygen concentrations observed on MCH cruises, illustrate that 2004 was largely typical in the development and evolution of hypoxic conditions. During the M1 cruise, the bottom waters were only slightly depleted at all stations. Near-bottom dissolved oxygen concentrations (Figure 3.8) ranged from 3.5-5.5 $ml \cdot L^{-1}$, which are below saturation values but well above hypoxic values (i.e., less than 1.4 $ml \cdot L^{-1}$). During M2 cruise, upwelling-favorable winds and high river discharge allowed for the development of a highly stratified water column over much of the inner

shelf (Figure 3.1), resulting in the hypoxic near-bottom dissolved oxygen concentrations at most of the stations in 10-15 m of total water depth. During the M3 cruise, low near-bottom dissolved oxygen concentration water has moved offshore to 15-30 m of total water depth, particularly south of Atchafalaya River. Near-bottom waters at inshore stations (10-15 m of total water depth) were no longer hypoxic. The overall spatial distribution of the near-bottom dissolved oxygen shows that bottom hypoxia has broken into a series of patches along the shelf.

The vertical distribution of dissolved oxygen concentrations (Figure 3.9) also exhibits a wave-like structure compatible to those in temperature and salinity records described above. The estimated wavelength of this feature is ~50 km along the shelf and amplitude (peak to trough) is ~ 5 m is the 20 m of total water depth. The similarity of spatial scales seen in the salinity, temperature, and dissolved oxygen distributions along the shelf, suggests that the feature is most likely a characteristic of the water movements associated with physical processes on the shelf rather than biochemical processes.

Slightly different conditions were encountered during the early spring cruise in 2005. Near-bottom dissolved oxygen concentrations (Figure 3.8) ranged from 1.0-4.0 $ml \cdot L^{-1}$. The high Mississippi-Atchafalaya River system discharge in January and February was most likely to cause the overall low near-bottom oxygen over the shelf with the few inshore hypoxic stations off the Atchafalaya Bay. Similar hypoxic conditions were observed during the M5 cruise. Due to the previously described severe weather conditions during the M6 cruise, the sampling plan was altered and covered mostly the western region of the Louisiana Shelf near the Texas and Louisiana border. The hypoxic near-bottom waters were found west of Atchafalaya Bay at inshore and offshore stations. During the M7 cruise the hypoxic waters were found at inshore (10-15 m of total depth) and offshore (15-30 m of total depth) stations. The near-bottom dissolved oxygen concentrations pattern in August 2005 demonstrates the similar wave-like structure to those in August 2004. The wave is also seen in the vertical section along the 20 m isobath (Figure 3.9). The estimated wavelength of the meander is ~50 km along shelf and amplitudes vary from ~2 m to ~7 m in the 20 m of total water depth.

3.3 Brunt-Väisälä frequency versus apparent oxygen utilization

As mentioned previously, the term stratification refers to the strength of the vertical density gradient. The Brunt-Väisälä frequency, *N*, is often used to define the degree of stratification. Large values of N correspond to strong vertical density gradient.

In this study, the Brunt-Väisälä frequency was calculated over 0.5 m depth intervals for each hydrographic station on MCH cruises. The method used for computing is given in *Millard et al.* [1990]:

$$N^2 = \rho \cdot g^2 \cdot \left[-\alpha \cdot \left({dT}/{dp} - \Gamma \right) + \beta \cdot \left({dS}/{dp} \right) \right] \text{ (radians/s)}, \qquad (3.1)$$

where T is the temperature (^{o}C),

S is the salinity,

p is the pressure (decibars),

ρ is the density (kg·m^{-3}),

g is the gravity acceleration (m·s^{-2}),

α is the thermal expansion, $\alpha = -\left({1}/{\rho} \right) \cdot \left({\partial \rho}/{\partial T} \right)$ (^{0}C^{-1}),

β is the saline contraction, $\beta = \left({1}/{\rho} \right) \cdot \left({\partial \rho}/{\partial S} \right)$,

Γ is the adiabatic lapse rate, $\Gamma = -\left(T_a / C_p \right) \cdot \left({\partial v}/{\partial T} \right)$,

v is the specific volume, $v = {1}/{\rho}$,

T_a is the absolute temperature, $T_a = T + 273.15$ (Kelvin),

C_p is the specific heat.

Figure 3.10 shows vertical profiles of Brunt-Väisälä frequency along the 20 m isobath on MCH cruises. All cruises exhibit strongly stratified water column along the shelf. Stratification is generally higher during the spring (cruises M1, M4, and M5) and early summer (cruise M2). There is a noticeable patchiness in the Brunt-Väisälä frequency distribution along the shelf. The highest values of Brunt-Väisälä frequency appear immediately under the river plumes in the upper layer of the water column. Main pycnocline depth varies seasonally being closer to the surface at ~5-10 m during the M1,

M2, M4, and M5 cruises, and ~14-16 m during M3, M6, and M7 cruises. There are also regional differences in the Brunt-Väisälä frequency distribution along the shelf. During the M2 cruise, as the distance from the freshwater source increases, the stratification weakens due to diffusion, resulting in lower values of the Brunt-Väisälä frequency and greater pycnocline depths.

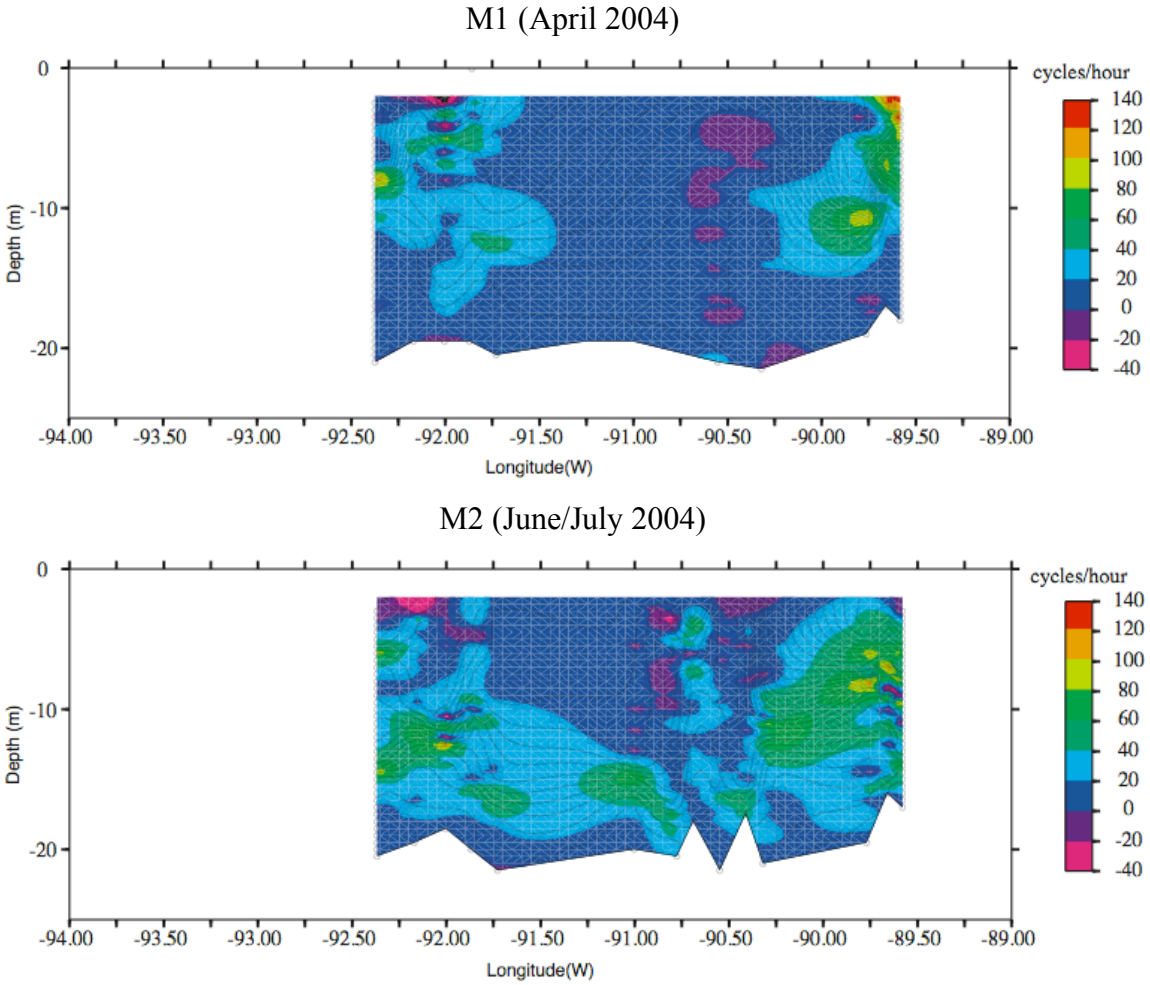

Figure 3.10. Brunt-Väisälä frequency profiles calculated using Eqn. 3.1 along the 20m isobath on MCH cruises (M1-M7) in 2004-2005. Salinity is shown as contours.

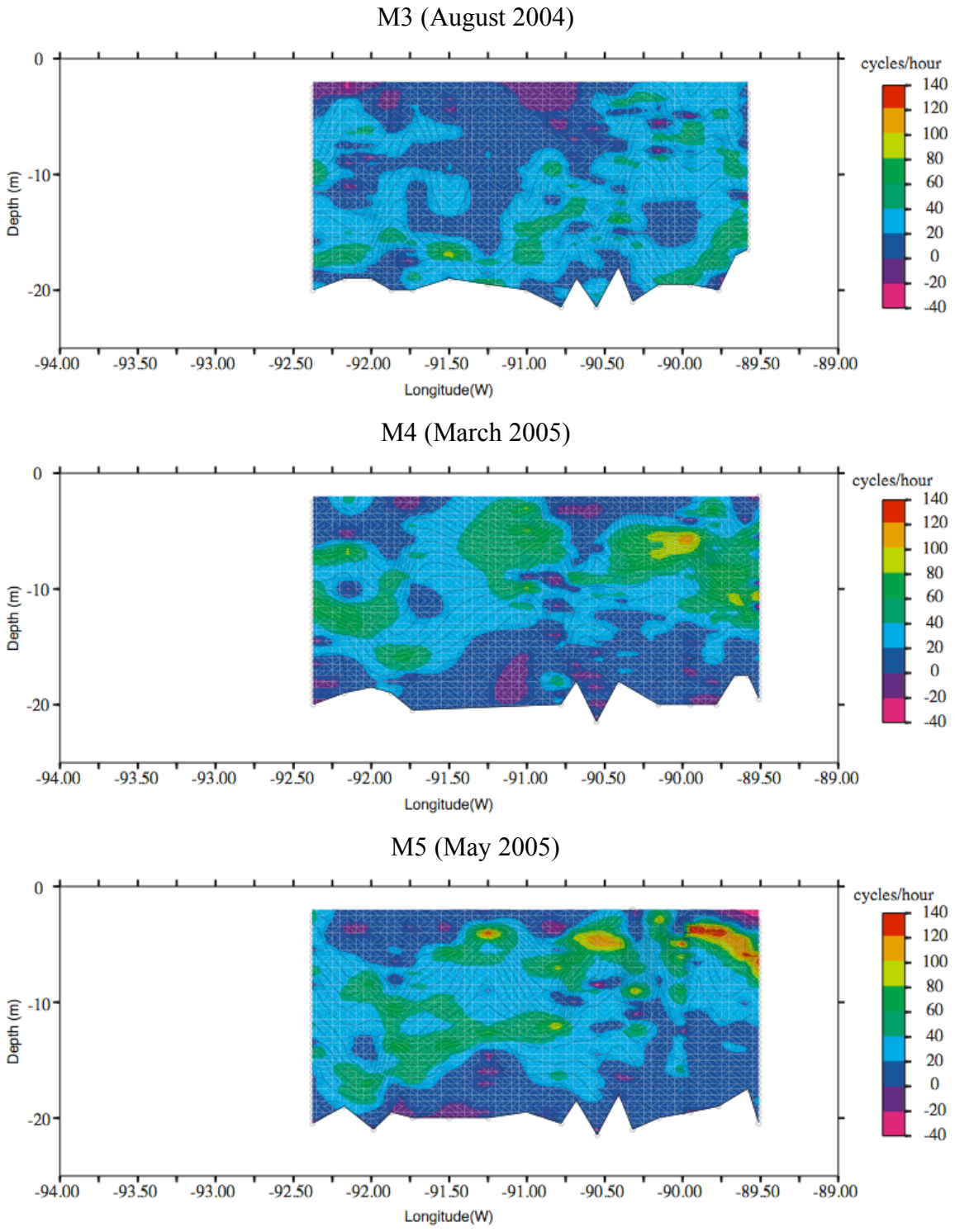

Figure 3.10. Continued.

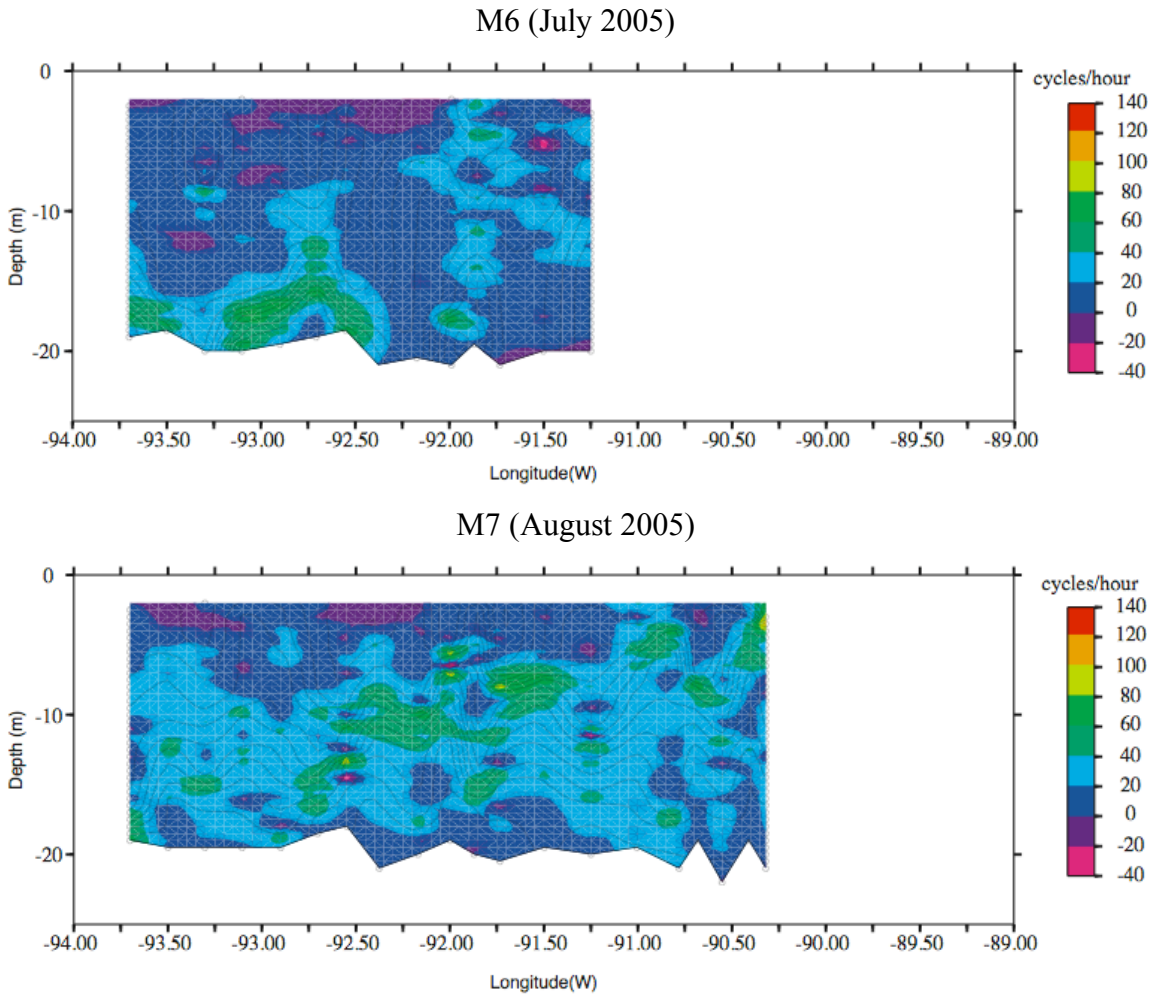

Figure 3.10. Continued.

Belabbassi [2006] showed that low-oxygen and hypoxic waters in the Northern Gulf of Mexico were found only in waters with Brunt-Väisälä maxima greater than 40 cycles per hour. Bottom dissolved oxygen versus maximum Brunt-Väisälä frequency at all stations on MCH cruses is shown in Figure 3.11. Inspection revealed that hypoxic conditions were not present in waters with Brunt-Väisälä frequency less than 40 cycles per hour. The deviations from a linear relationship where bottom dissolved oxygen concentrations decrease with increasing Brunt-Väisälä frequency are most likely

attributed to the strong current shear events, which increase mixing. Although, this is speculation because current profiles were not measured on these cruises.

To further investigate the effect of vertical stratification on the occurrences of low-oxygen and hypoxic waters, the maximum value of the Brunt-Väisälä frequency was compared with the bottom apparent oxygen utilization value at each station. The hypothesis is that a highly stratified water column facilities the formation of hypoxic waters by limiting the vertical mixing that can supply oxygen in the sub-pycnocline layer.

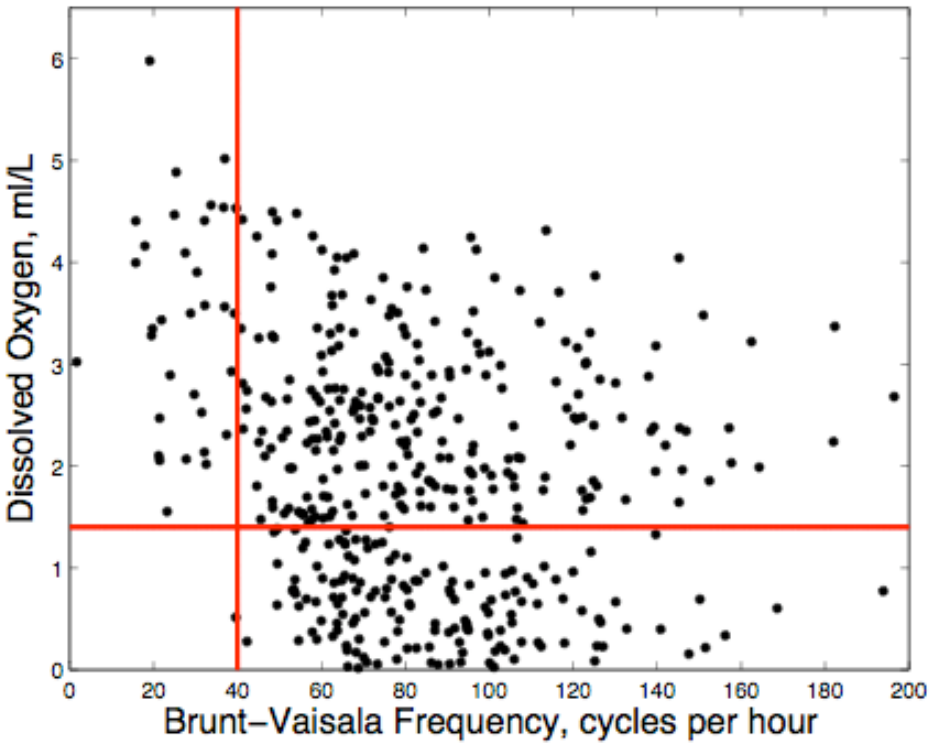

Figure 3.11. Bottom dissolved oxygen concentration versus maximum Brunt-Väisälä frequency at all stations on all MCH cruises in 2004-2005. The threshold of 1.4 $ml \cdot L^{-1}$ for hypoxia, and 40 cycles per hour are shown with horizontal and vertical red lines, respectively.

Apparent oxygen utilization (AOU) is the difference between the saturated value of dissolved oxygen and the measured value. AOU is defined by *Millero* [2005]:

$$AOU = O_2^{sat} - O_2^{obs}, \tag{3.2}$$

where O_2^{sat} is the saturated value of dissolved oxygen concentration,

O_2^{obs} is the measured dissolved oxygen concentration.

The saturated value is the concentration of dissolved oxygen in equilibrium with the atmosphere, but corrected to its value at the salinity, temperature, and pressure where the measurement was taken. The saturation value is computed at the potential temperature of water and one atm total pressure using the following expression based on the data of *Murray and Riley* [1969]:

$$\begin{aligned} \ln\left(O_2^{sat}\right) = & -173.4292 + 249.6339/(T/100) + \\ & +143.3482 \bullet \ln(T/100) - 21.8492 \bullet (T/100) + \\ & +S \bullet \left(-0.033096 + (T/100) \bullet \left(0.014259 - 0.0017 \bullet (T/100)\right)\right) \end{aligned}, \tag{3.3}$$

where T is the water temperature (Kelvin), S is the water salinity.

The constants used in the Eqn. 3.3 produce units of $ml \cdot L^{-1}$.

The AOU of a water sample represents the sum of the biological activity that the sample has experienced since it was last in equilibrium with the atmosphere. The apparent oxygen utilization is a measure of how much oxygen has been taken up by in the water column by biochemical processes.

Figures 3.12-3.17 show bottom AOU values versus maximum Brunt-Väisälä frequency at all stations on MCH cruises. Figures 3.12-3.16 have three panels each, representing different zones, that were defined geographically: close to the Mississippi River Delta (zone A), near the C6 monitoring station location operated by LUMCON and south of Terrebonne Bay (zone B), off Atchafalaya Bay, LA (zone C).

Zones D (downstream open shelf between Texas border and Atchafalaya Bay) was introduced during the cruise M6 and revisited during the cruise M7. Data collected in zone D on those two cruises was combined with the data from zone C for analysis.

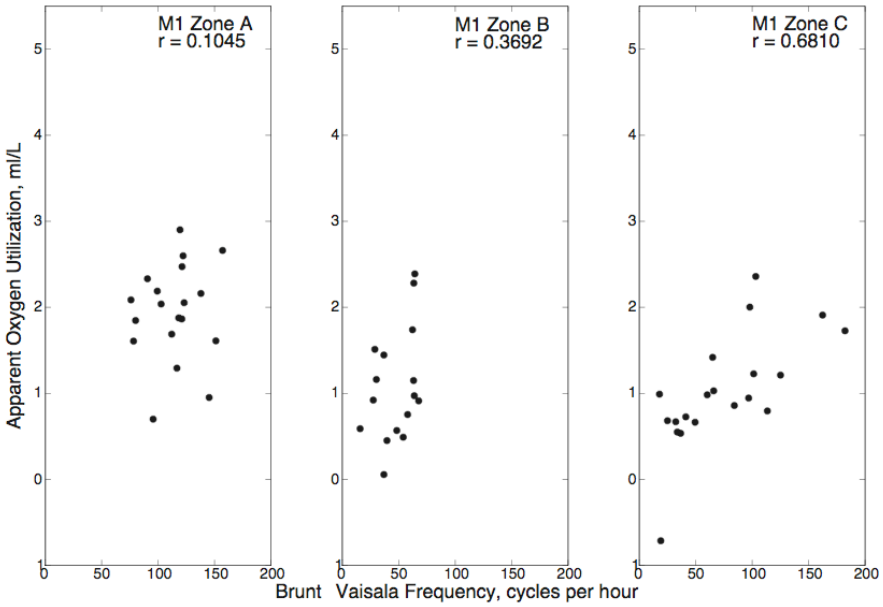

Figure 3.12. Apparent oxygen utilization vs. Brunt-Väisälä frequency for each zone at all stations on M1 cruise.

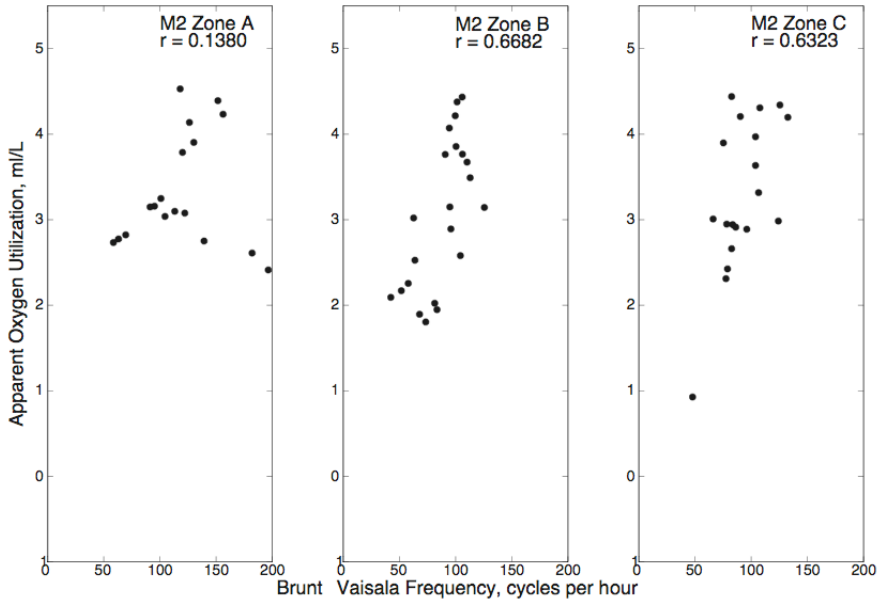

Figure 3.13. Apparent oxygen utilization vs. Brunt-Väisälä frequency for each zone at all stations on M2 cruise.

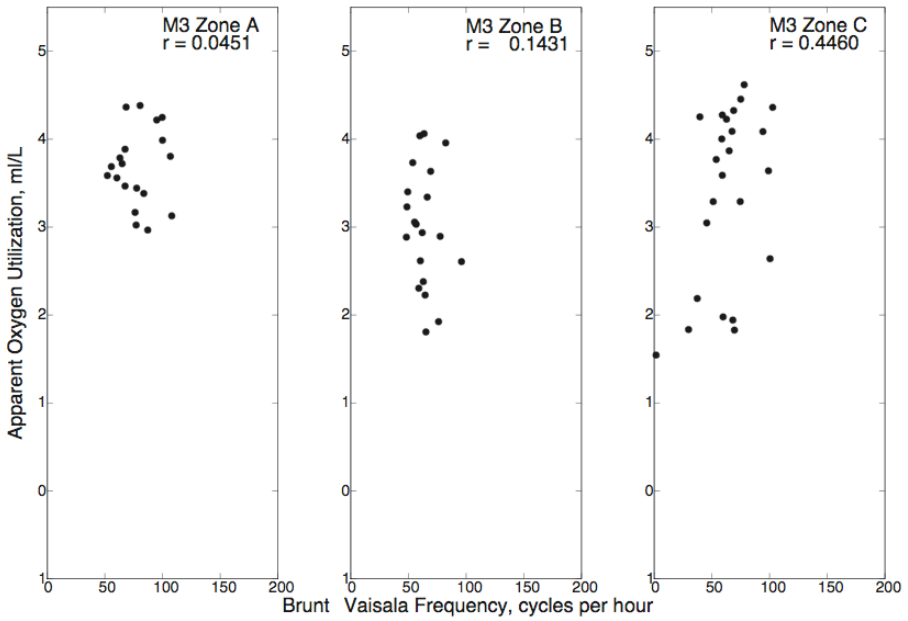

Figure 3.14. Apparent oxygen utilization vs. Brunt-Väisälä frequency for each zone at all stations on M3 cruise.

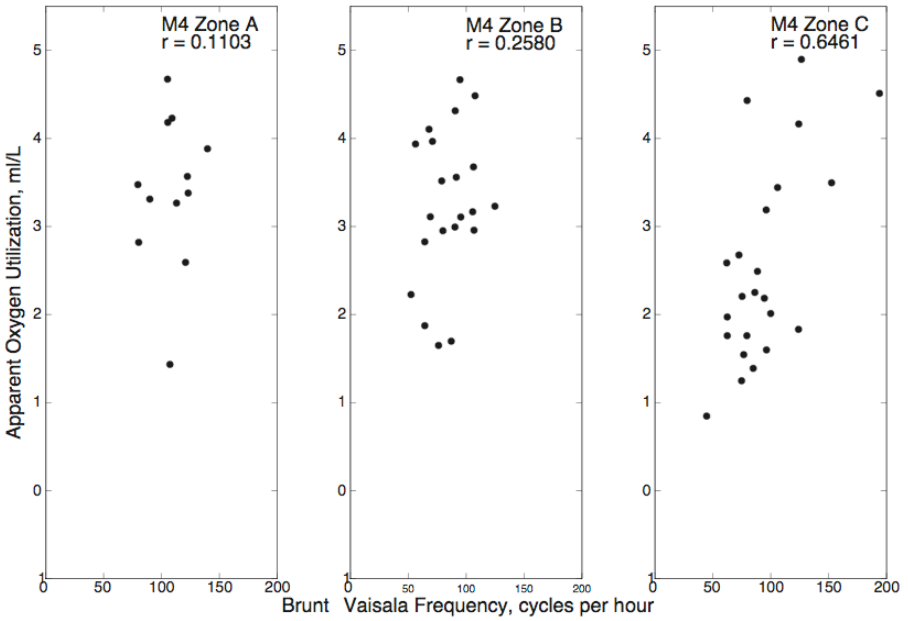

Figure 3.15. Apparent oxygen utilization vs. Brunt-Väisälä frequency for each zone at all stations on M4 cruise.

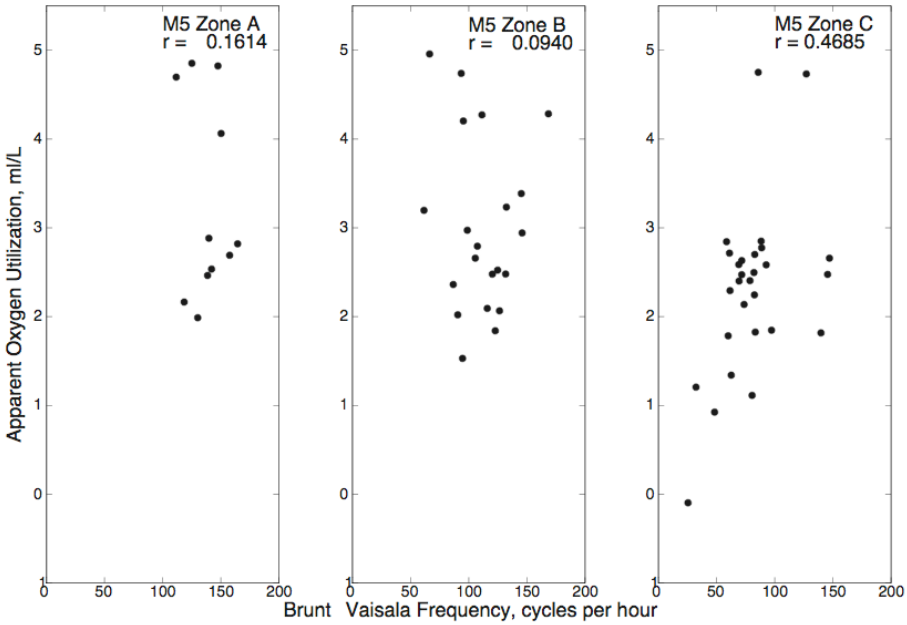

Figure 3.16. Apparent oxygen utilization vs. Brunt-Väisälä frequency for each zone at all stations on M5 cruise.

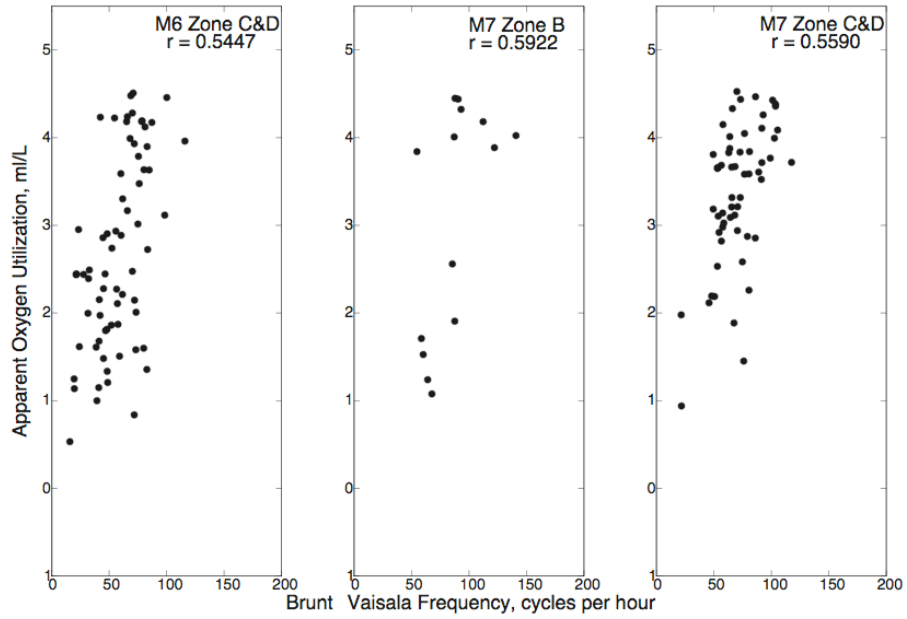

Figure 3.17. Apparent oxygen utilization vs. Brunt-Väisälä frequency for each zone at all stations on M6 and M7 cruises.

The inspection of Figures 3.12-3.17 showed that the water column was well stratified during the cruises M1-M7. There were only a few stations on cruises M1, M3, M5 and M7 with maximum Brunt-Väisälä frequency less than 40 cycles per hour. The large values of Brunt-Väisälä frequency, above 100 cycles per hour were found on every cruise in different zones. Apparent oxygen utilization also exhibits great variability between the zones and cruises. Saturated values of bottom AOU ~0.0 $ml \cdot L^{-1}$ and lower were found on cruises M1 and M5. The large values of bottom AOU, corresponding to the high oxygen uptake, were found on all cruises except M1 (Figure 3.12). Basic statistics for bottom AOU and maximum Brunt-Väisälä frequency is presented in Table 3.1.

Table 3.1. Basic statistics for the bottom apparent oxygen utilization and maximum Brunt-Väisälä frequency on MCH cruses M1-M7 in 2004-2005.

Cruise	Zone	Min AOU ($ml \cdot L^{-1}$)	Max AOU ($ml \cdot L^{-1}$)	Min BVF ($cycles \cdot h^{-1}$)	Max BVF ($cycles \cdot h^{-1}$)	Correlation, R	Significant at 95% confidence
M1	A	0.7	2.9	76.0	157.1	0.10	NO
	B	0.06	2.34	15.7	67.7	0.37	NO
	C	-0.71	2.36	17.9	182.3	0.68	YES
M2	A	2.41	4.53	58.4	196.4	0.14	NO
	B	1.81	4.43	42.3	125.7	0.67	YES
	C	0.92	4.44	47.9	132.7	0.63	YES
M3	A	2.97	4.38	52.2	108.0	0.05	NO
	B	1.81	4.06	48.4	96.0	-0.14	NO
	C	1.54	4.62	1.69	102.7	0.45	YES
M4	A	1.43	4.67	79.7	139.7	0.11	NO
	B	1.65	4.67	52.4	124.8	0.26	NO
	C	0.85	4.9	44.6	193.9	0.65	YES
M5	A	1.99	4.85	111.6	164.3	-0.16	NO
	B	1.53	4.96	61.6	168.6	-0.09	NO
	C	-0.1	4.75	25.4	146.9	0.47	YES
M6	C&D	0.53	4.51	15.74	115.8	0.54	YES
M7	B	1.08	4.45	54.6	140.8	0.59	YES
	C&D	0.94	4.52	21.4	117.6	0.56	YES

Apparent oxygen utilization and Brunt-Väisälä frequency are not well correlated in zone A on cruises M1-M5 (left panels of Figures 3.12-3.16). Estimated correlation coefficients are small and not significant at the 95% confidence level. Zone B shows a better correlation between the two parameters, however, only on cruises M2 (middle panel of Figure 3.12) and M7 (middle panel of Figure 3.17) those values are significant at 95% of confidence level. Correlations between the bottom AOU and maximum Brunt-Väisälä frequency are larger in zone C on all cruises. Cruises M1 (right panel of Figure 3.12), M2 (right panel of Figure 3.13), and M4 (right panel of Figure 3.15) show that ~40% of the variance in bottom AOU in zone C can be explained by variations in maximum Brunt-Väisälä frequency. This value is ~30% on cruises M6 (left panel of Figure 3.17) and M7 (right panel of Figure 3.17), and ~20% on cruises M3 (right panel of Figure 3.14) and M5 (right panel of Figure 3.16).

During MCH cruises the occurrences of low-oxygen and hypoxic waters, represented as waters with high AOU values, were related to the local vertical stratification mostly in zone C and D. These results of analysis support the *Rowe and Chapman* [2002] idea, discussed in Chapter II, that different processes control the dissolved oxygen level in different physical regimes. However, delineation of the regions, based on the distance from the source of freshwater and nutrients, is not entirely valid as those zones can be variable in space and time. In general, the bottom AOU increases with the increase in Brunt-Väisälä frequency and vice versa. This mechanism is well illustrated by the wave-like disturbances seen in the vertical distributions of salinity and dissolved oxygen concentrations along the shelf (Figures 3.1 and 3.8). Strong stratification caps the bottom water layer restricting the supply of dissolved oxygen down to the bottom from the surface layer. As stratification weakens due to the vertical mixing it allows for injecting the well-oxygenated waters from the surface into the bottom layer.

Temperature, salinity, and dissolved oxygen concentrations records, collected on MCH cruises, demonstrated that meander seen in horizontal sections along the shelf, is a persistent characteristic of the Louisiana shelf. Other data such satellite imagery (Figure

1.4) also support this observation. This meander also manifests in the vertical sections along the shelf as wave-like disturbances of the water properties. The origin of the meander and its influence on the distribution of dissolved oxygen concentrations along the shelf is investigated in the next chapter.

CHAPTER IV

NUMERICAL MODEL SIMULATIONS

The examination of various data, collected on MCH cruises, in Chapter III showed that the alongshore distribution of water properties on Louisiana shelf is affected by propagation of the dynamic instabilities. These instabilities disturb the water column and result in the wave-like structure of the physical and biochemical parameters. The Regional Ocean Modeling System (ROMS) was configured to perform a series of numerical experiments in an idealized coastal domain in order to investigate the nature of instabilities observed on the Louisiana shelf. Idealized numerical simulations simplify the overall complex coastal system, and help to separate the processes such topographic steering and freshwater discharge, that may be responsible for the generation of dynamic instabilities. The inclusion of a chemical tracer, representing dissolved oxygen concentration, into the model allows to investigate how the local physical processes can affect the distribution of the chemical and biological properties of the water.

In this chapter, I describe the series of numerical experiments produced for this dissertation. The objectives of the experiments are: 1) to understand the influence of the freshwater discharge and bottom topography on the development of dynamic instabilities, and 2) to investigate the effect of dynamic instabilities and shoaling topography on the distribution of dissolved oxygen concentrations in the water column. The results of numerical experiments will be compared against the MCH data sets in later chapter.

The model was run for a time period of 45 days. Output fields of salinity, density, dissolved oxygen deficit, and other parameters were saved for further analysis.

The nomenclature used to describe and identify the numerical experiments is as follows. Two bottom topographies will be discussed: cases with no shoals will be called “smooth”, and cases with shoals will be called “bumpy”. The terms “steep-sloped” and “gradually-sloped” describe the relative value of continental shelf slope, 0.0007 and

0.0005 respectively. Those cases with the freshwater forcing of 7500 $m^3 \cdot s^{-1}$ are designated as "moderate discharge" while those with 15000 $m^3 \cdot s^{-1}$ will be designated as "large discharge". Each experimental case can be conveniently identified from its unique descriptor word combination, e.g., the smooth steep-sloped with large discharge case, the bumpy gradually-sloped with moderate discharge case, etc. This convention is applied to all twelve numerical experiment cases shown in Table 2.4.

4.1 Salinity distribution across and along the shelf

A standard set of figures showing the temporal evolution of the salinity is presented for each of the twelve experiments. Each individual figure contains a sequence of several panels that are ordered in time, from left to right and top to bottom. In every panel, the flow enters from the right and exits on the left of the figures. The salinity fields are represented in contour plots.

a. The smooth gradually-sloped no freshwater forcing case: the Control Case

The control case is presented by a combination of smooth gradually-sloped bottom topography and no freshwater forcing (see Table 2.4 for details). Horizontal fields of surface and bottom salinity at several time steps are shown in Figure 4.1. Vertical sections of salinity at similar times along the 15 m isobath are shown in Figure 4.2.

The eight panels in Figure 4.1 show surface and bottom salinity for time steps 1, 14, 28, and 56 which correspond to the initial conditions, 3.5, 7, and 14 days of simulations.

A simple visual observation reveals that salinity field undergoes only the minor changes during this run. The horizontal salinity front exhibited only slight onshore/offshore movements in response to the wind forcing. Salinity gradient changes very little with distance offshore. Six panels in Figure 4.2 show the vertical water column salinity distribution along the shelf at 15 m depth. The alongshore sections of salinity demonstrate slight weakening of vertical gradient, possibly due to the wind

forcing, energy transfer and mixing. No instabilities were developed throughout the simulation time period.

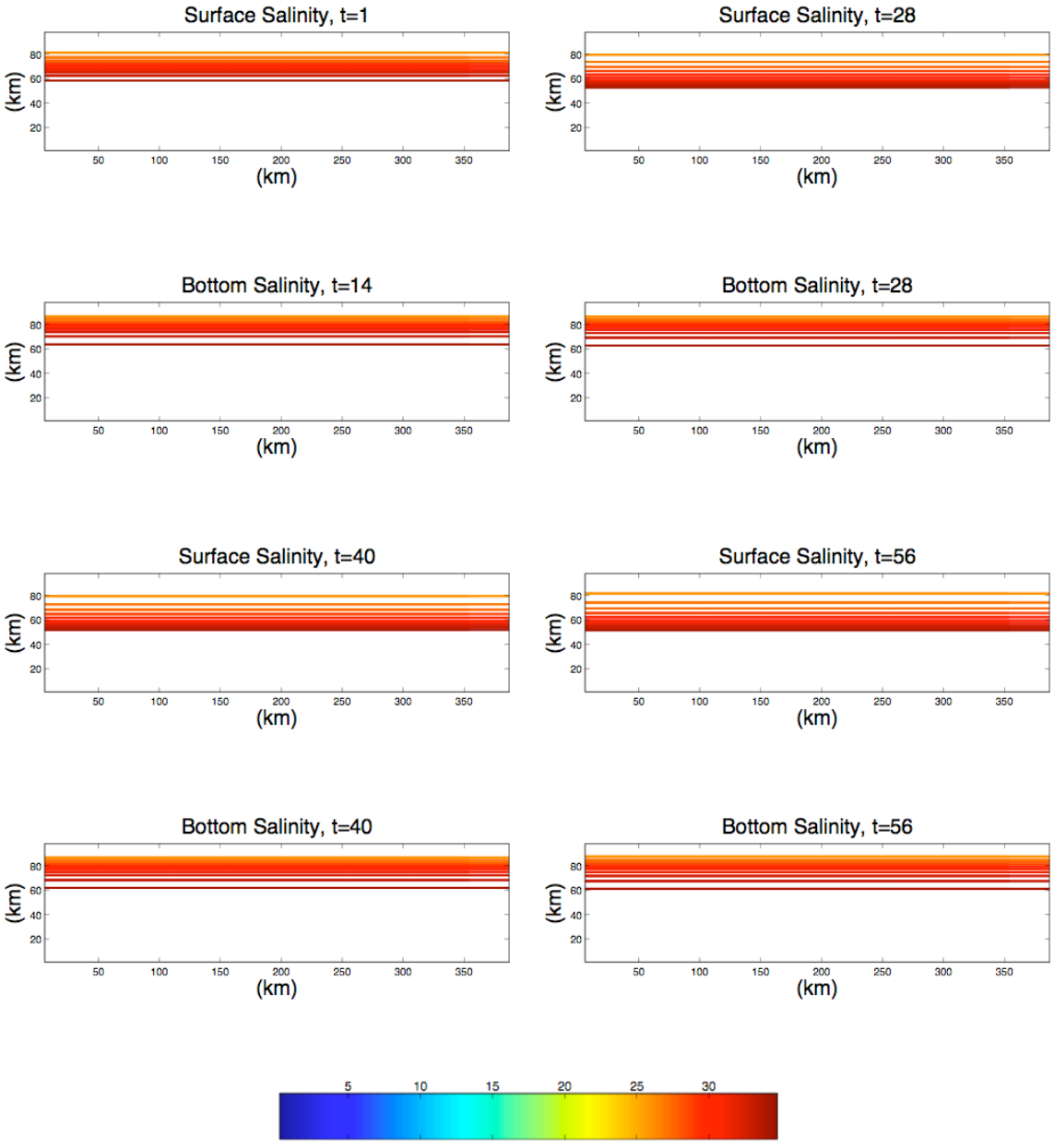

Figure 4.1. Surface and bottom salinity for smooth gradually-sloped no freshwater forcing case *a*. t units are equal to 1=6 hours.

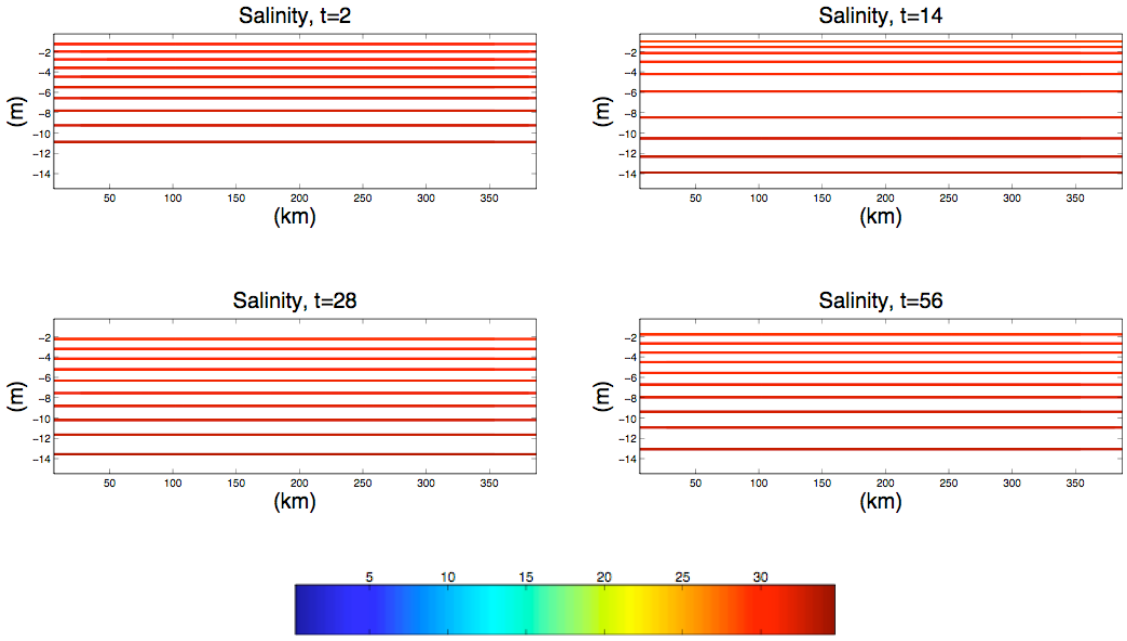

Figure 4.2. Salinity along the 15 m isobath for smooth gradually-sloped no freshwater forcing case *a*. t units are equal to 1=6 hours.

b. The smooth steep-sloped no freshwater forcing case

In this experiment the continental shelf slope was changed to a steeper value of 0.0007. Horizontal fields of surface and bottom salinity at several time steps are shown in Figure 4.3. Vertical sections of salinity at similar times along the 20 m isobath are shown in Figure 4.4.

Both horizontal and vertical salinity profiles look very similar to those of the Control Case seen in *a* above.

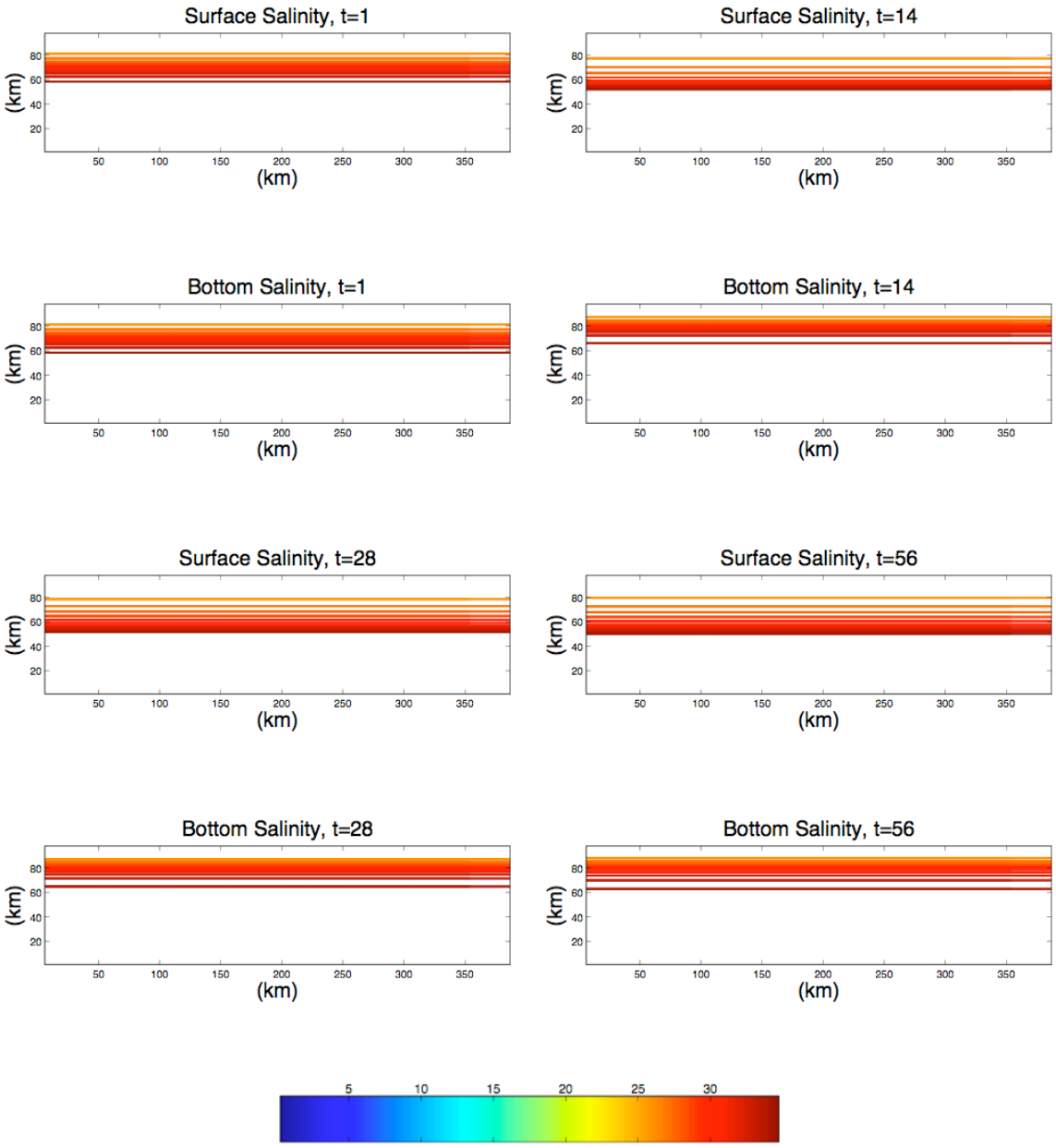

Figure 4.3. Surface and bottom salinity for smooth steep-sloped no freshwater forcing case *b*. t units are equal to 1=6 hours.

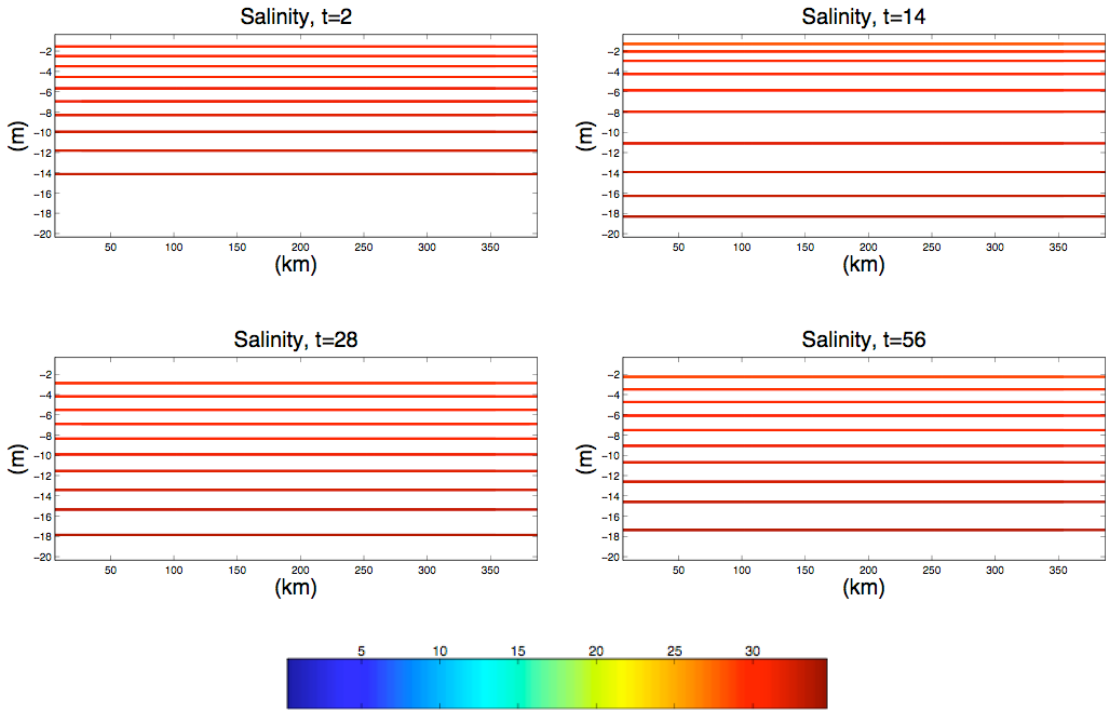

Figure 4.4. Salinity along the 20 m isobath for smooth steep-sloped no freshwater forcing case *b*. t units are equal to 1=6 hours.

c. The bumpy gradually-sloped no freshwater forcing case

In this experiment, topographic features were introduced into the model domain. The features were represented as three distinct shoals. The shoals were constructed as Gaussian bumps of half-width of 5 km and extended upward into the water column to a maximum of 5 m. The centers of the shoals were positioned 50 km apart alongshore, and 10 km from the coast. Horizontal fields of surface and bottom salinity at several time steps are shown in Figure 4.5. Vertical sections of salinity at the same times along the 15 m isobath are shown in Figure 4.6.

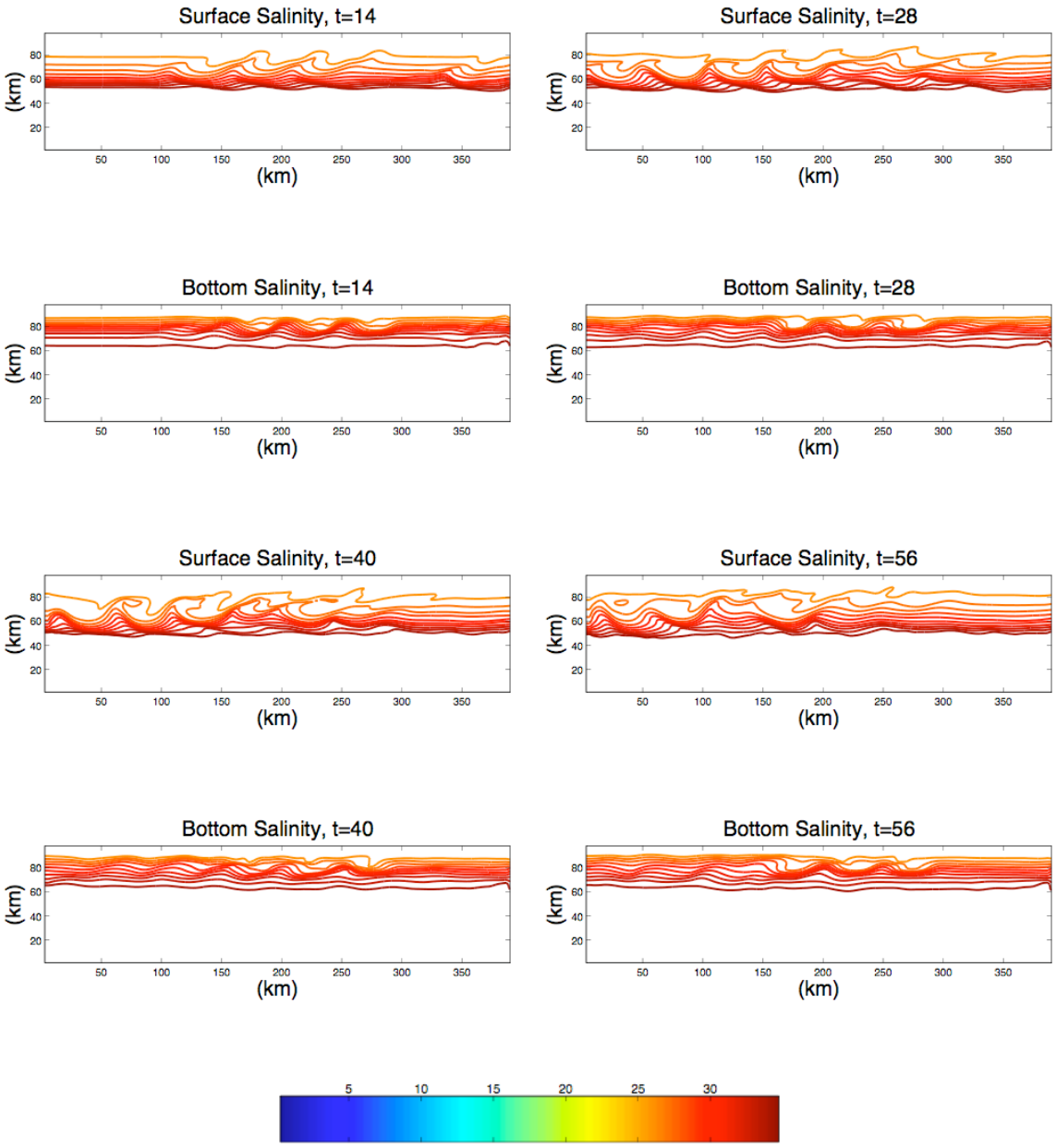

Figure 4.5. Surface and bottom salinity for bumpy gradually-sloped no freshwater forcing case *c*. t units are equal to 1=6 hours.

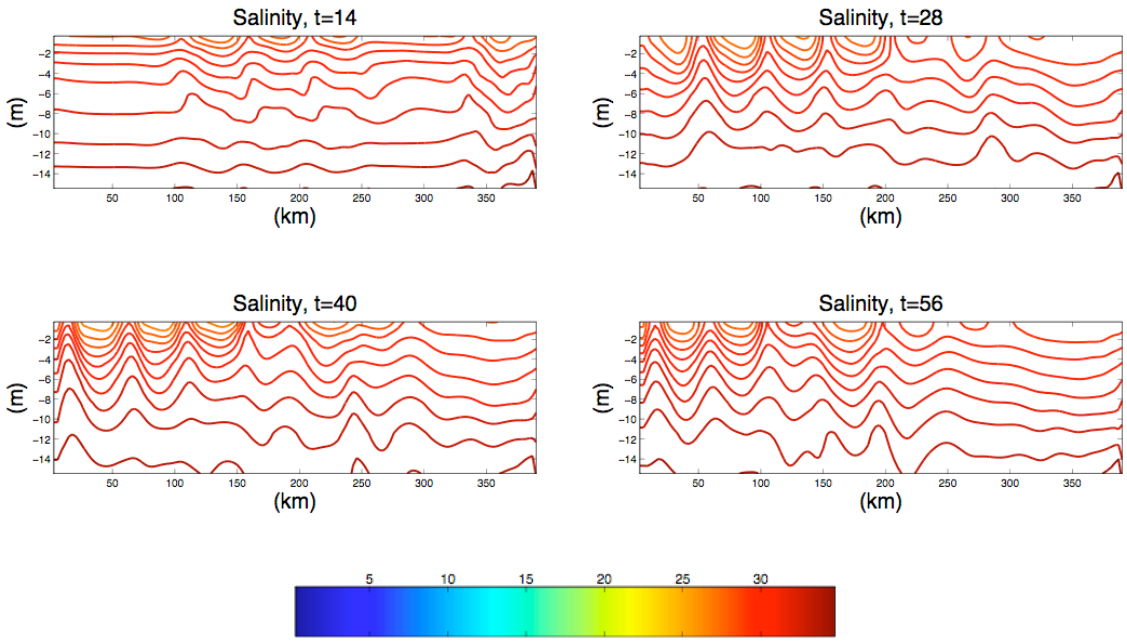

Figure 4.6. Salinity along the 15 m isobath for bumpy gradually-sloped no freshwater forcing case *c*. t units are equal to 1=6 hours.

The eight panels in Figure 4.5 show surface and bottom salinity for time steps 14, 28, 40 and 56 which correspond to 3.5, 7, 10, and 14 days of simulation time period. The development of an alongshelf meander can be seen in the surface salinity contours where the flow passes over the shoals. As the experiment progresses in time the meander's shape become more irregular in response to the wind mixing and topographic steering. The meander in the horizontal distribution of bottom salinity appears to be more confined to the shoals profile, as the wind mixing does not affect the bottom layer because of frictional effects.

As seen in vertical sections the wave is also present in the water column along the shelf (Figure 4.6). The estimated wavelength is ~50 km which is consistent with the alongshore spacing of the shoals. Vertical sections show a gradual increase in the amplitude of the wave from the beginning of the experiment to 10 days. After 10th day it stays quasi-steady and vertical amplitude (peak to trough) is ~3 m in the 15 m of the total water depth.

The results of this experiments show that introduction of a rough topography into the model domain can produce dynamic instabilities in the along and cross shelf salinity fields.

d. The bumpy steep-sloped no freshwater forcing case

For this experiment, a steeper continental shelf slope of 0.0007 was used to initialize the model. Horizontal fields of surface and bottom salinity at several time steps are shown in Figure 4.7. Vertical sections of salinity at the same times along the 20 m isobath are shown in Figure 4.8.

The development of the dynamic instabilities, seen in the horizontal and vertical salinity profiles, is very similar to that in the Case *c*, described above. The main difference is the vertical range of the wave amplitude. The amplitude reaches ~6 m in the 20 m of total water depth after two weeks of simulation.

This case shows that an increase of the continental shelf slope value leads to the stronger instability amplitudes.

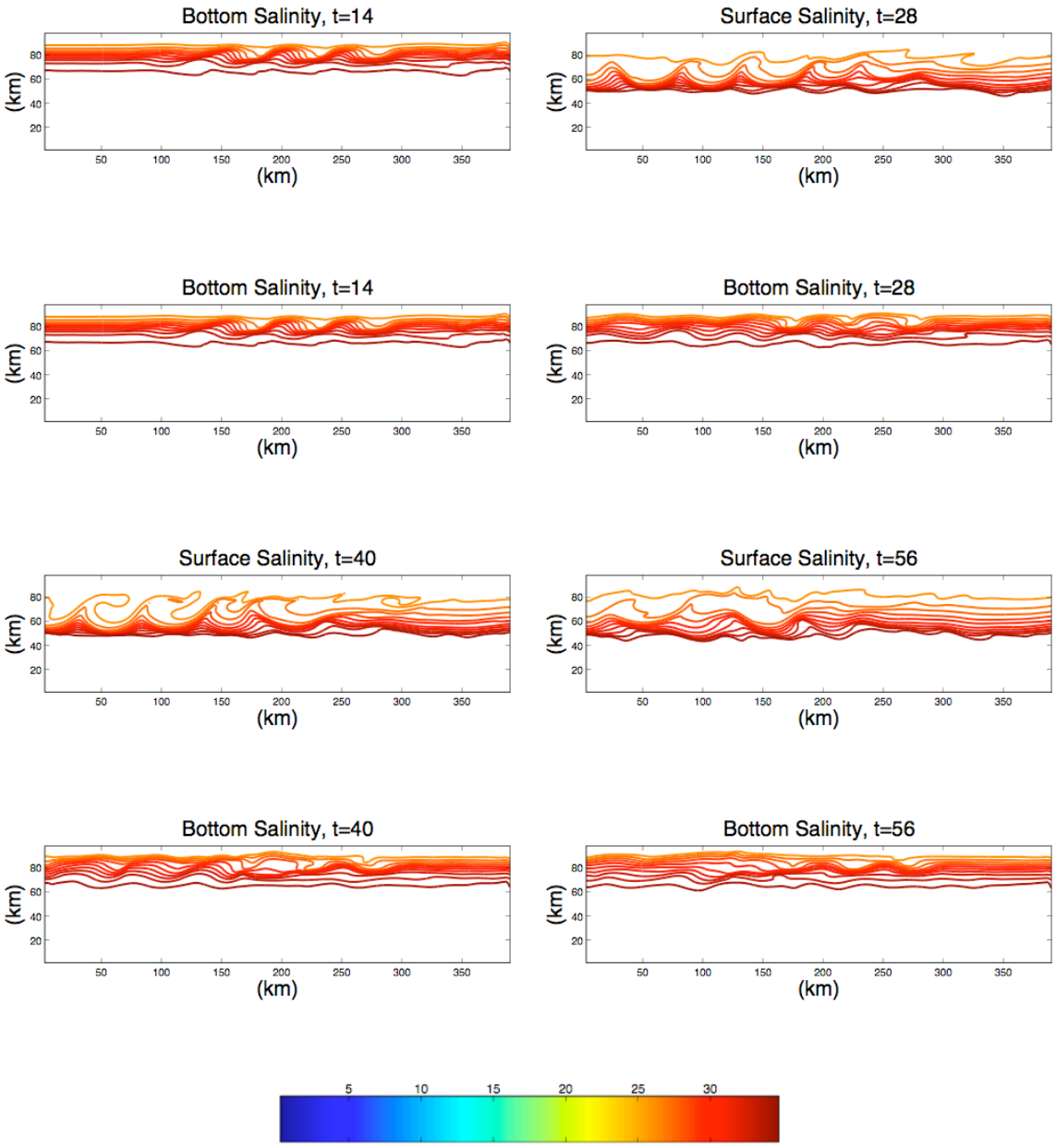

Figure 4.7. Surface and bottom salinity for bumpy steep-sloped no freshwater forcing case *d*. t units are equal to 1=6 hours.

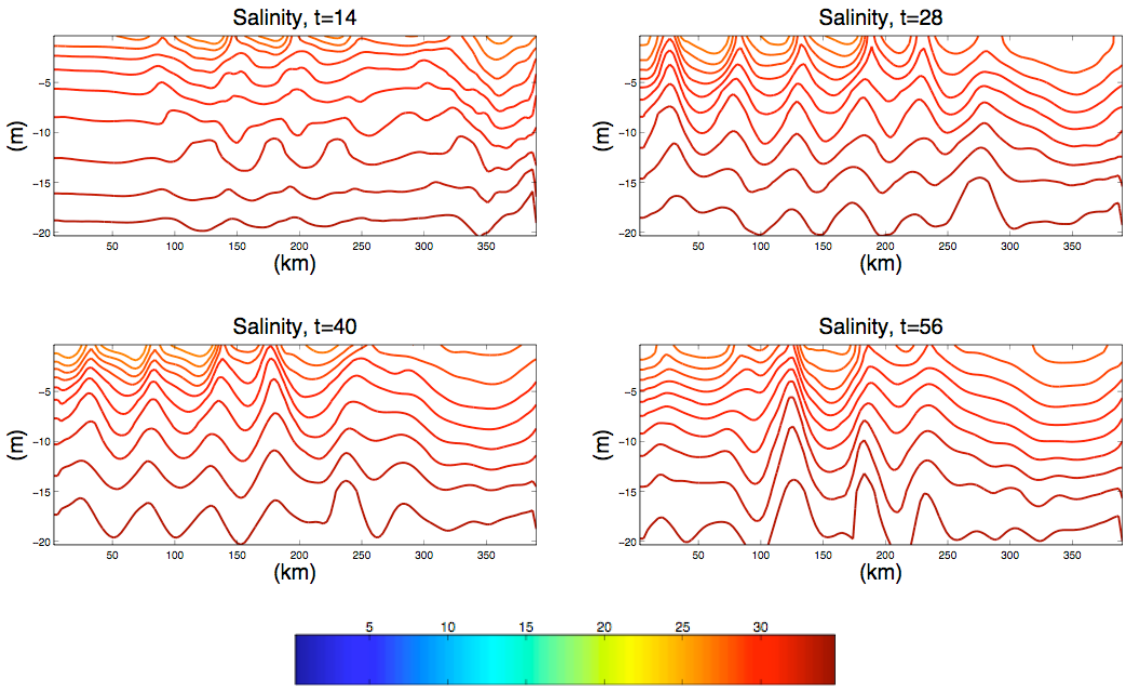

Figure 4.8. Salinity along the 20 m isobath for bumpy steep-sloped no freshwater forcing case *d*. t units are equal to 1=6 hours.

e. The smooth gradually-sloped with moderate discharge case

This case consists of initializing the model with smooth gradually-sloped topography and introducing a constant but moderate freshwater discharge into the domain (see Table 2.4 for details). Horizontal fields of surface and bottom salinity at several time steps are shown in Figure 4.9. Vertical sections of salinity at the same times along the 15 m isobath are shown in Figure 4.10.

Upon entering the domain, the freshwater plume stretches downcoast along the shelf following the main direction of the flow to the left. The newly introduced freshwater intensifies the salinity gradient across the shelf, forming a density front which when combined with the wind mixing results in the formation of the instabilities on the outer edge of the plume. Though weaker, the plume signature also can be seen in the bottom salinity plots. Unlike the surface, there is only a minor interaction between the

plume and initial salinity front at the bottom. Salinity contours near the bottom show only slight perturbations in the horizontal structure.

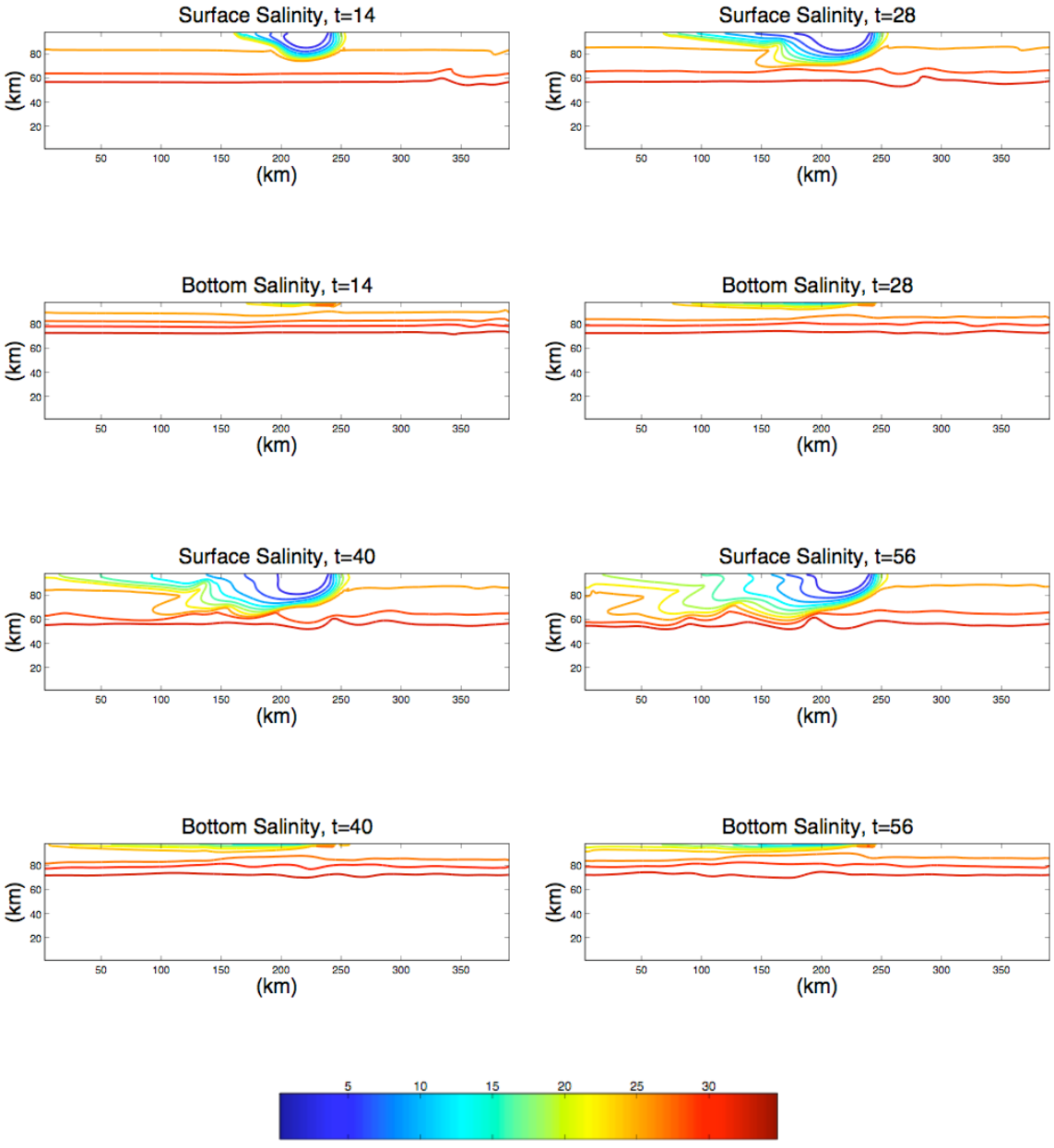

Figure 4.9. Surface and bottom salinity for smooth gradually-sloped with moderate discharge case *e*. t units are equal to 1=6 hours.

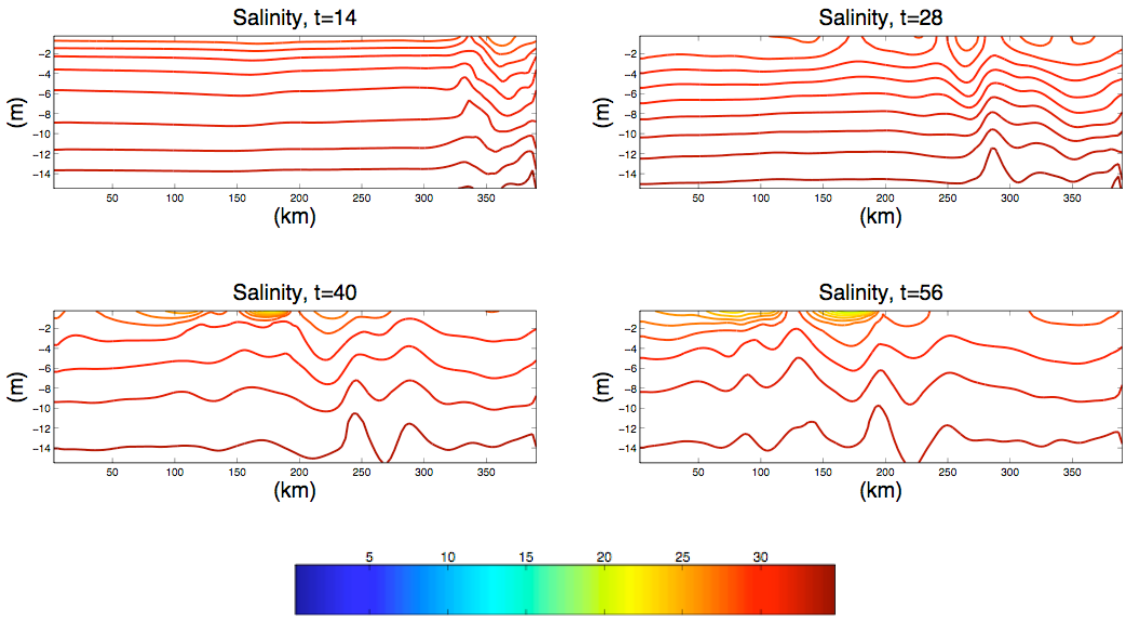

Figure 4.10. Salinity along the 15 m isobath for smooth gradually-sloped with moderate discharge case *e*. t units are equal to 1=6 hours.

Vertical distribution of salinity along the shelf shows the wave development as well. However, wavelength and amplitude of the wave are quite variable, and have a range of 30 -100 km along the coast and 1- 4 m in the 15 m of total depth.

Inclusion of the freshwater discharge increases the density gradient, and is sufficient to produce instabilities. The meander shows strong temporal variability.

f. The smooth steep-sloped with moderate discharge case

Use of a steeper value for the continental shelf slope (see Table 2.4 for details) in this experiment brings a noticeable change in the spatial scales of instabilities. Horizontal fields of surface and bottom salinity at several time steps are shown in Figure 4.11. Vertical sections of salinity at the same times along the 20 m isobath are shown in Figure 4.12.

The meander is more pronounced in both horizontal and vertical sections of the shelf. The estimated wavelength of the feature is ~50 km along the shelf; the amplitude

varies from 3-5 m in the 20 m of the total water depth. The meander is also apparent in the salinity contours near the bottom after 10 days of model run.

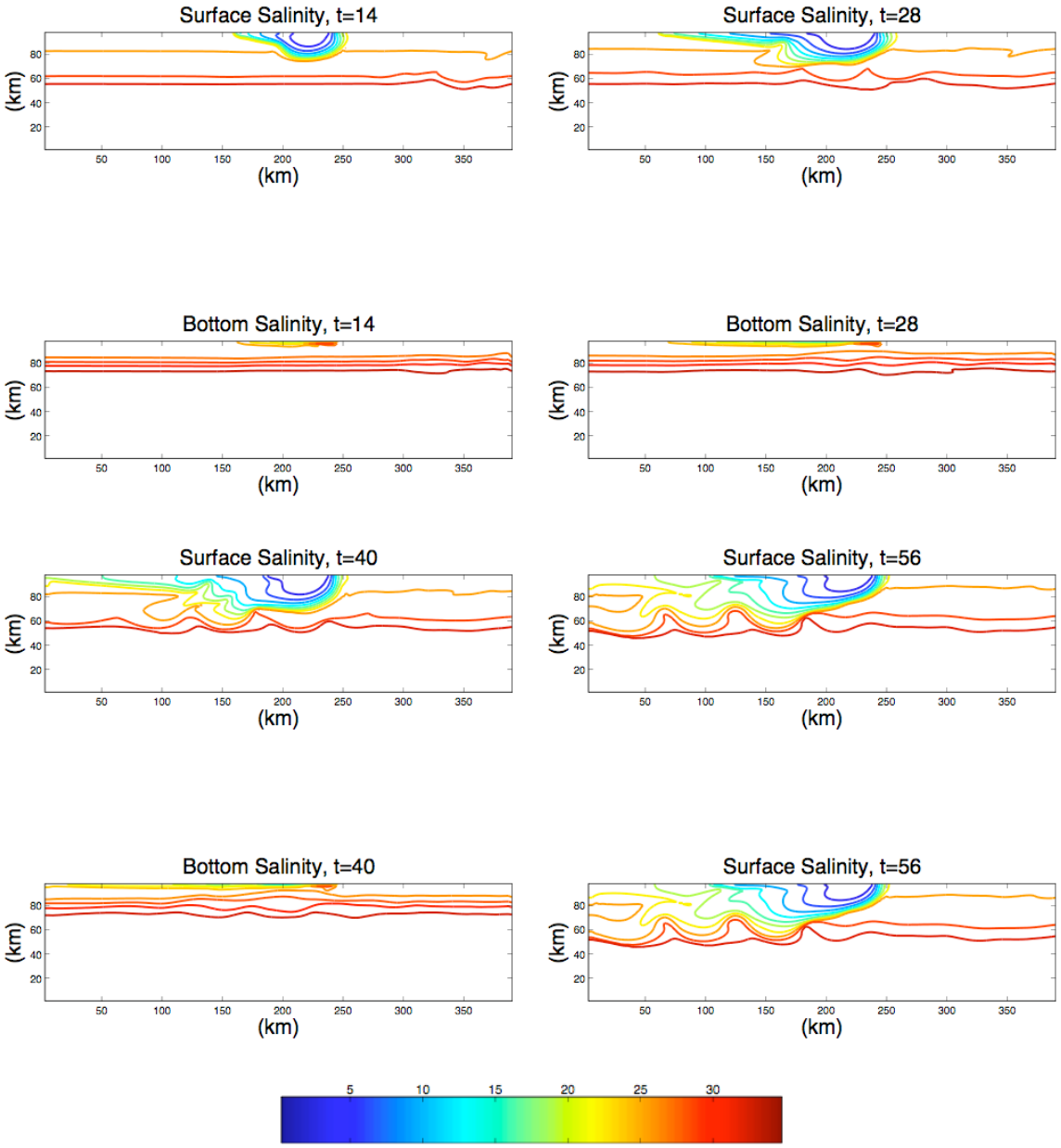

Figure 4.11. Surface and bottom salinity for smooth steep-sloped with moderate discharge case *f*. t units are equal 1=6 hours.

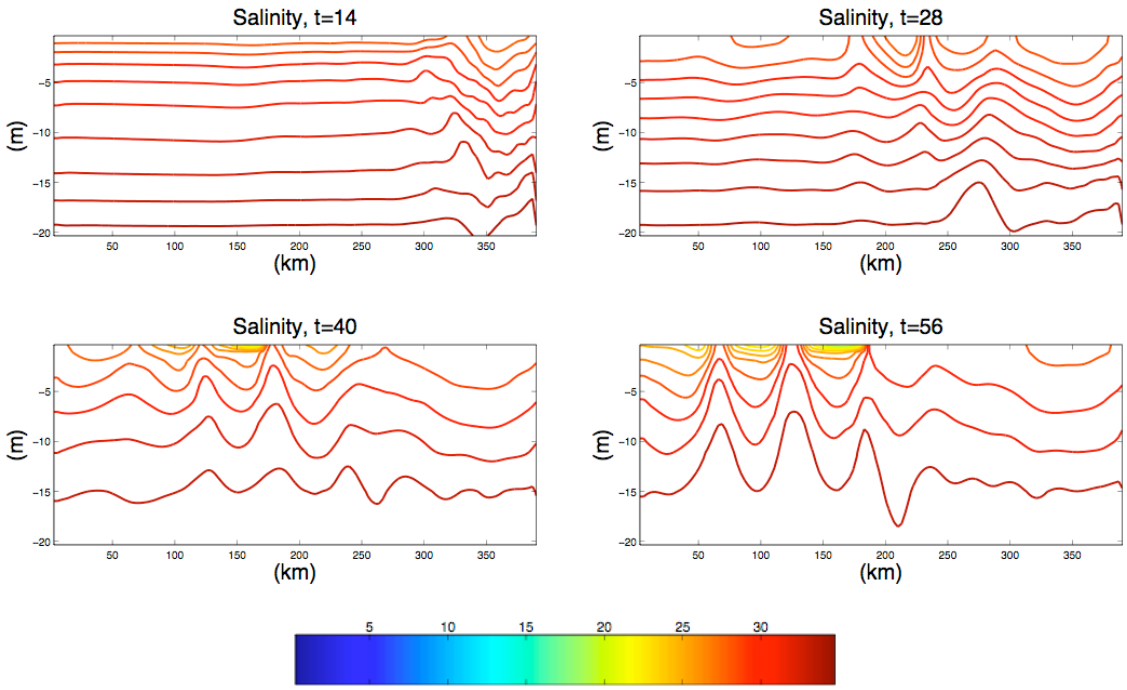

Figure 4.12. Salinity along the 20 m isobath for smooth steep-sloped with moderate discharge case *f*. t units are equal 1=6 hours.

An increase of the continental shelf slope value leads to the stronger instability amplitudes and more persistent meander.

g. The smooth gradually-sloped with large discharge case

This case consists of initializing with the smooth gradually-sloped topography and introducing a constant but large freshwater discharge (see Table 2.4 for details). Horizontal fields of surface and bottom salinity at several time steps are shown in Figure 4.13. Vertical sections of salinity at the same times along the 15 m isobath are shown in Figure 4.14.

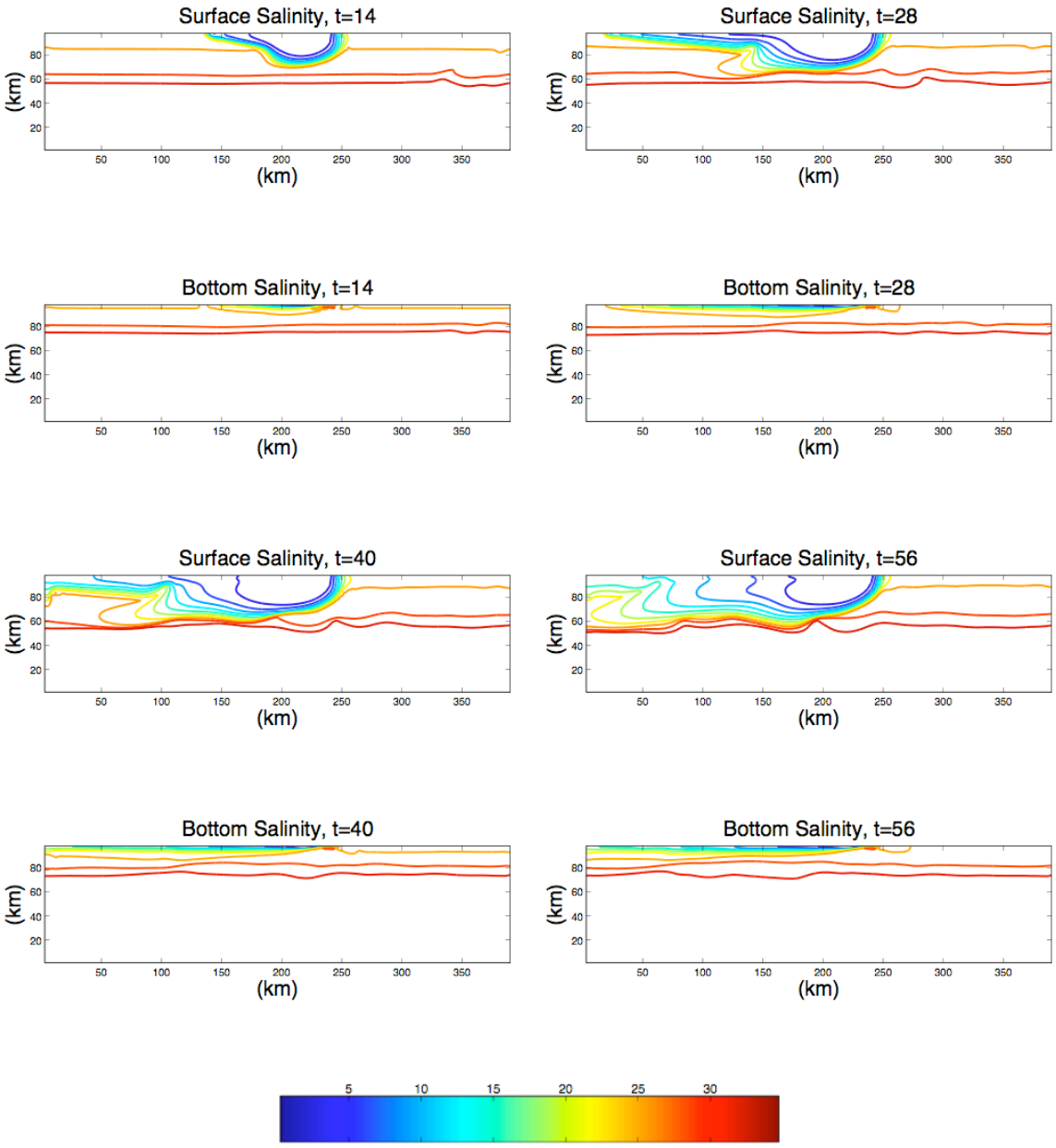

Figure 4.13. Surface and bottom salinity for smooth gradually-sloped with large discharge case *g*. t units are equal 1=6 hours.

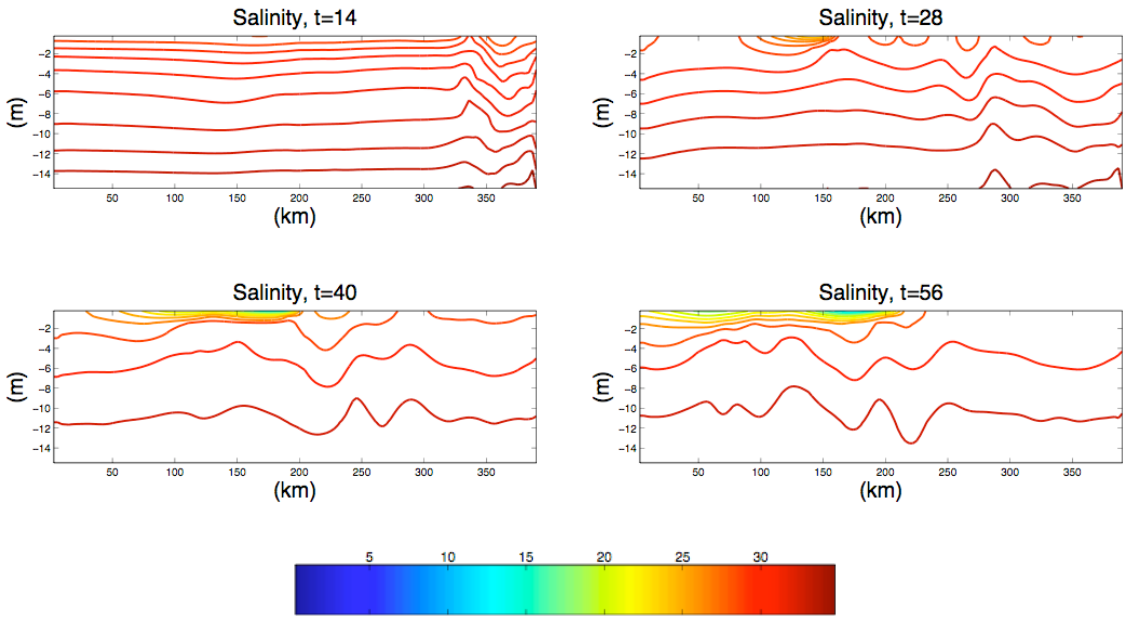

Figure 4.14. Salinity along the 15 m isobath for smooth gradually-sloped with large discharge case *g*. t units are equal 1=6 hours.

The amount of the freshwater produces stronger gradient for the salinity front but does not appear to affect the spatial or temporal scales of the instabilities seen in Case *e*. Note that the area of interest for this experiment is located close to the discharge point;, and instabilities might vary further downstream away from the source. The results of the experiment are very similar to that with the moderate freshwater discharge (Case *e*). There is a presence of instabilities, as it is seen in the surface salinity contours, on the outer edge of the plume. However, salinity contours at the bottom show only a slight evidence of those.

This experiments demonstrates that freshwater discharge rate does not affect instabilities near the injection point.

h. The smooth steep-sloped with large discharge case

This experiment is the same as Case *f* except here freshwater discharge is increased to 15000 $m^3 \cdot s^{-1}$. Horizontal fields of surface and bottom salinity at several time

steps are shown in Figure 4.15. Vertical sections of salinity at the same times along the 20 m isobath are shown in Figure 4.16.

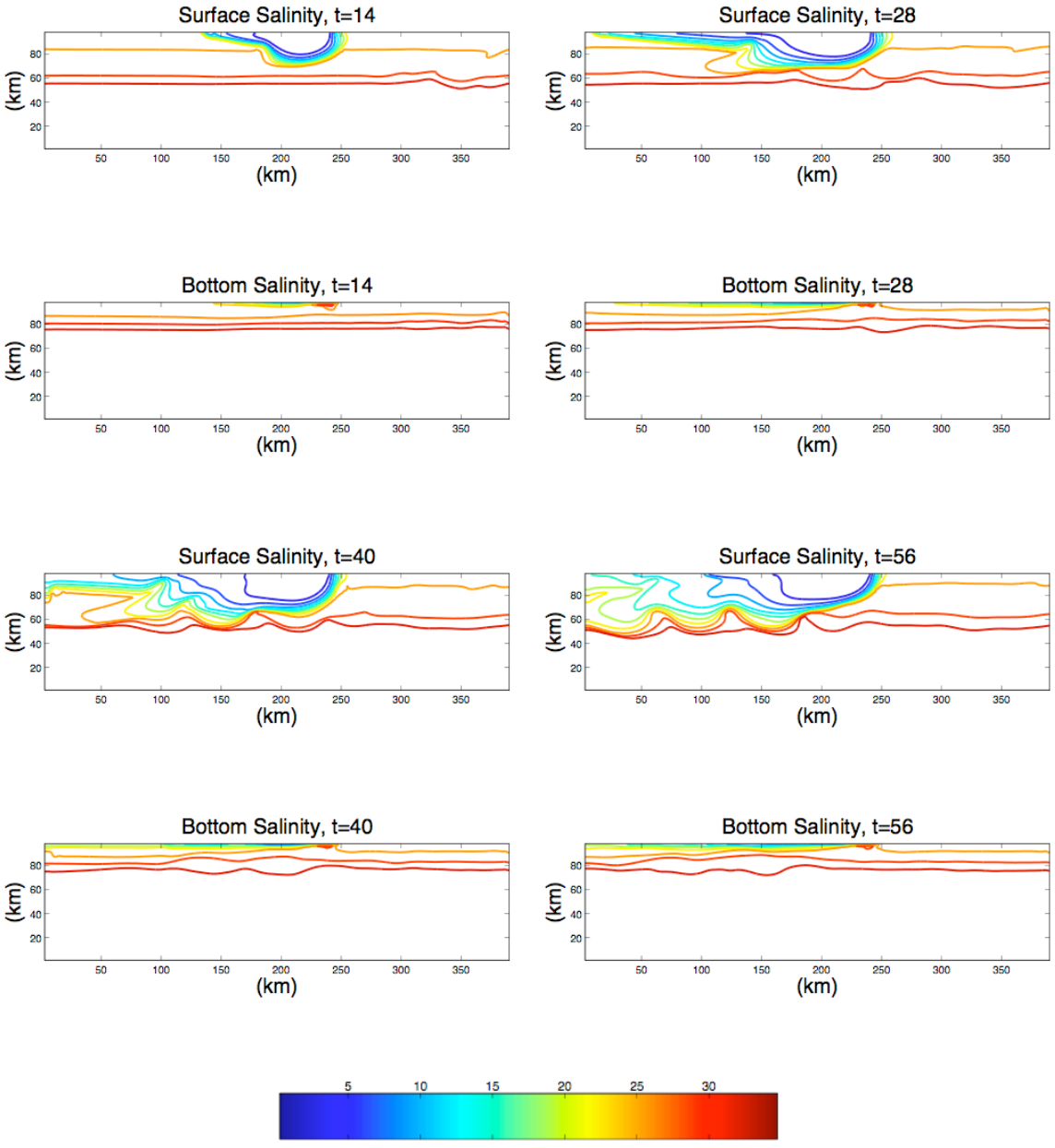

Figure 4.15. Surface and bottom salinity for smooth steep-sloped with large discharge case *h*. t units are equal 1=6 hours.

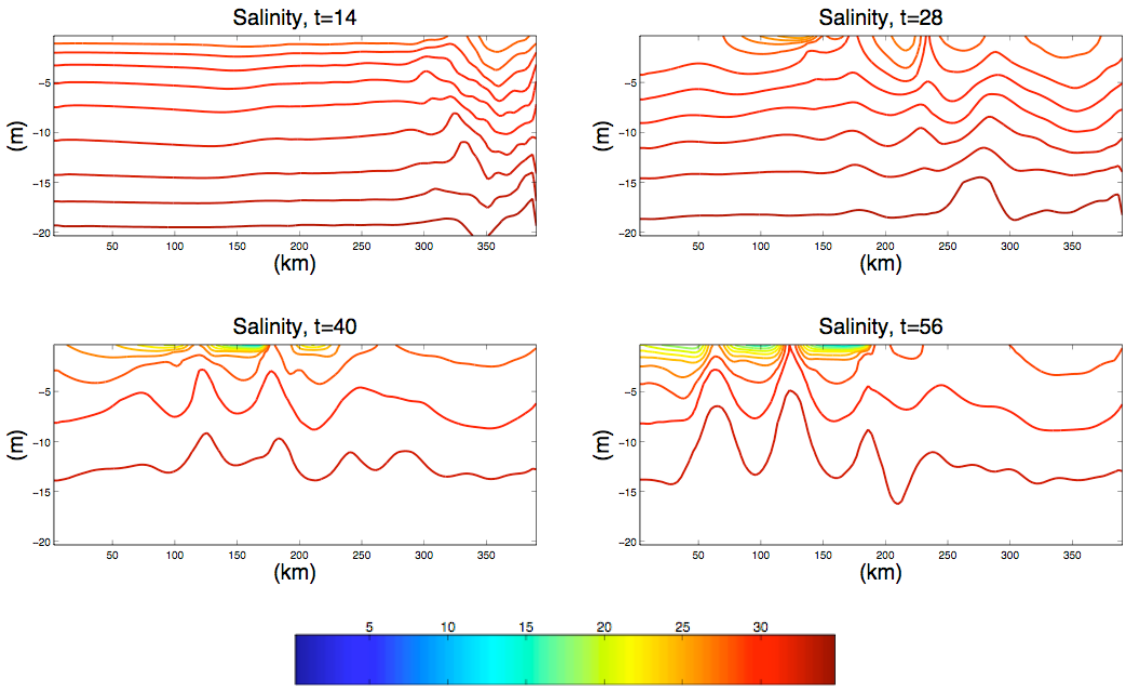

Figure 4.16. Salinity along the 20 m isobath for smooth steep-sloped with large discharge case *h*. t units are equal 1=6 hours.

Surface salinity contours show the temporal sequence of the interaction between the plume and initial salinity front, resulting in the formation of dynamic instabilities on the interface. The spatial scale of horizontal meander is ~50 km along the coast. The evolution of the meander can be also seen in the vertical section along the shelf. After two weeks of the model run, the amplitude of the wave reaches its maximum at ~6 m in the 20 m of the total water depth. As seen for the gradually-sloped cases, the increase in the freshwater forcing does not impact the spatial or temporal scales of observed instabilities.

As shown in this experiment, doubling the freshwater discharge does not impact the structure of instability.

i. The bumpy gradually-sloped with moderate discharge case

This experiment consists of initializing with the gradually-sloped bottom topography with shoals and introducing a constant but moderate freshwater discharge (see Table 2.4 for details). Horizontal fields of surface and bottom salinity at several time steps are displayed in Figure 4.17. Vertical sections of salinity at the same times along the 15 m isobath are shown in Figure 4.18.

The eight panels of Figure 4.17 show the temporal sequence of instability development. There are two forcings for the formation of the meander: topographic steering caused by the shoals and an increase in the salinity gradient due to the freshwater input. At t=14 (3.5 days) the meander caused by flow propagating over the shoals is separate from the disturbances on the outer edge of the plume caused by salinity differences. Surface salinity contours at t=28 (7 days) show some evidence of interaction of the two forcings, and after the t=40 (10) days of simulation the superposition of instabilities caused by these sources is clearly seen. The meander apparent in the salinity fields near the bottom, however, appears to be due to the shoaling topography. The plume is trapped behind the shoals and does not contribute to the meander variability in the bottom layer.

Vertical cross-sections reflect a dual nature of instabilities as well. Salinity contours look more irregular at t=40 (10 days) and t=56 (14 days) in comparison with those at t=28 (7 days).

The outcome of this experiment is that inclusion of the two different forcings such shoaling topography and freshwater discharge results in superposition of the states.

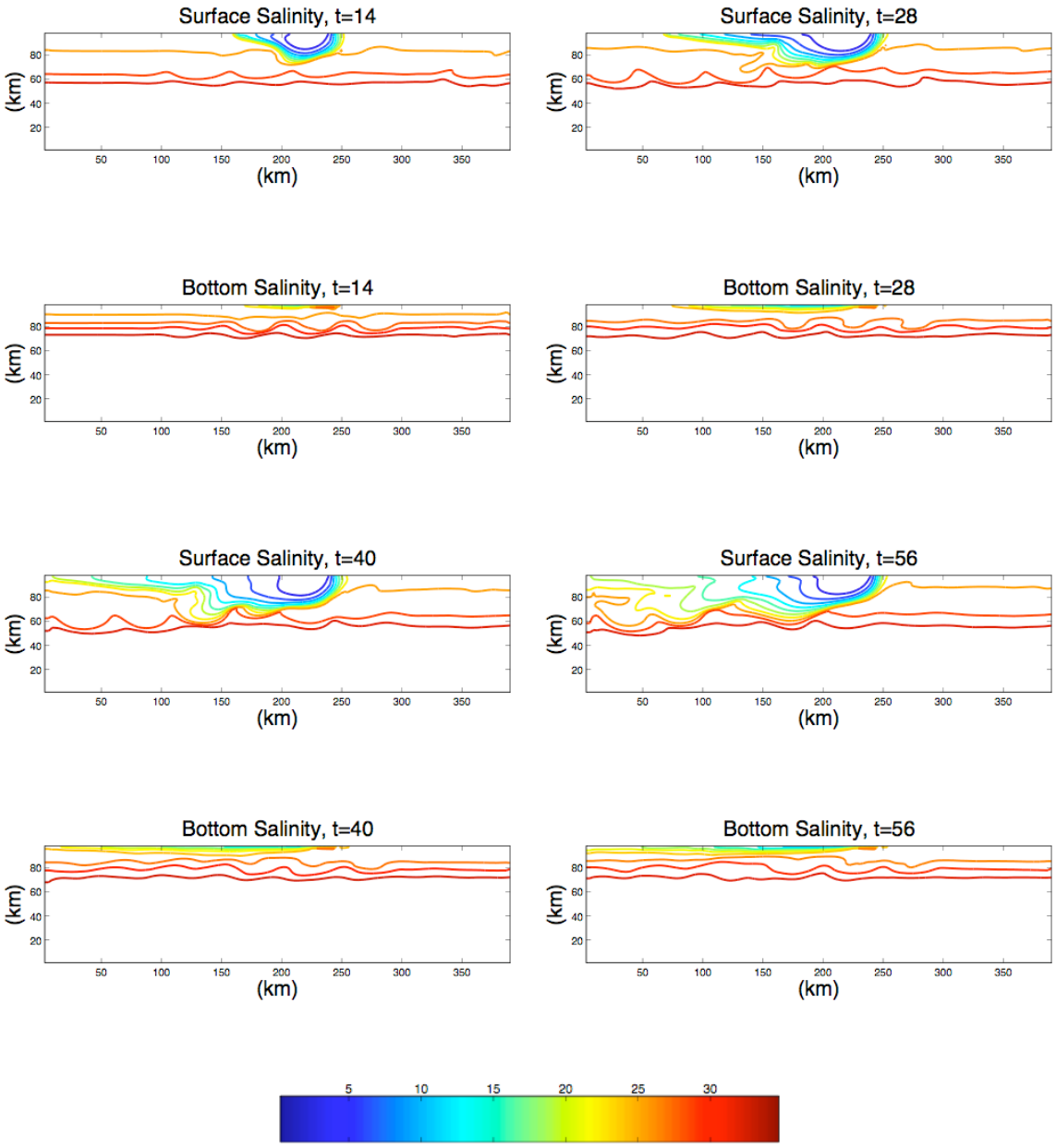

Figure 4.17. Surface and bottom salinity for bumpy gradually-sloped with moderate discharge case *i*. t units are equal 1=6 hours.

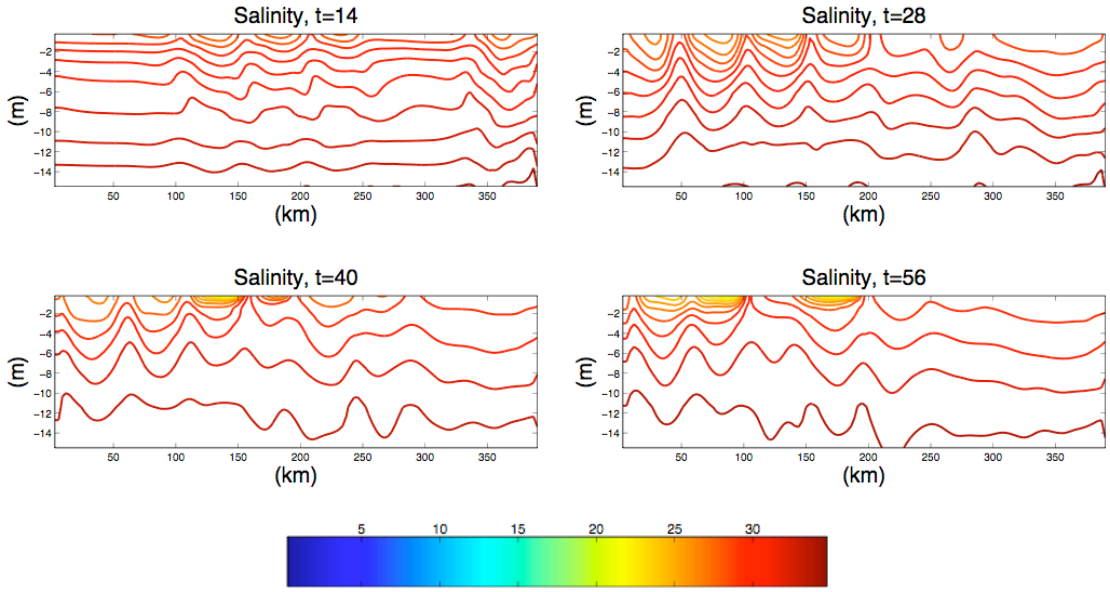

Figure 4.18. Salinity along the 15 m isobath for bumpy gradually-sloped with moderate discharge case *i*. t units are equal 1=6 hours.

j. The bumpy steep-sloped with moderate discharge case

A steeper shelf slope is used in this experiment than Case *i* (see Table 2.4 for details). Horizontal fields of surface and bottom salinity at several time steps are displayed in Figure 4.19. Vertical sections of salinity at the same times along the 20 m isobath are shown in Figure 4.20.

The mechanism of alongshore meander development is same as it is described in the Case *i*. The distinct feature of this case is that a steeper slope allows for the plume to propagate further offshore, which results in the interference of the plume with instabilities caused by shoals near the bottom and downcoast. This is especially evident on the two lower panels of Figure 4.19.

Vertical distribution of salinity shows the wave-like disturbances along the shelf and throughout the water column. The estimated wavelength is ~50 km with the wave amplitude up to ~6 m in the 20 m of the total water depth.

A steeper continental shelf slope leads to the stronger interaction between instabilities produced by two forcings, and generally leads to the larger amplitudes of instability.

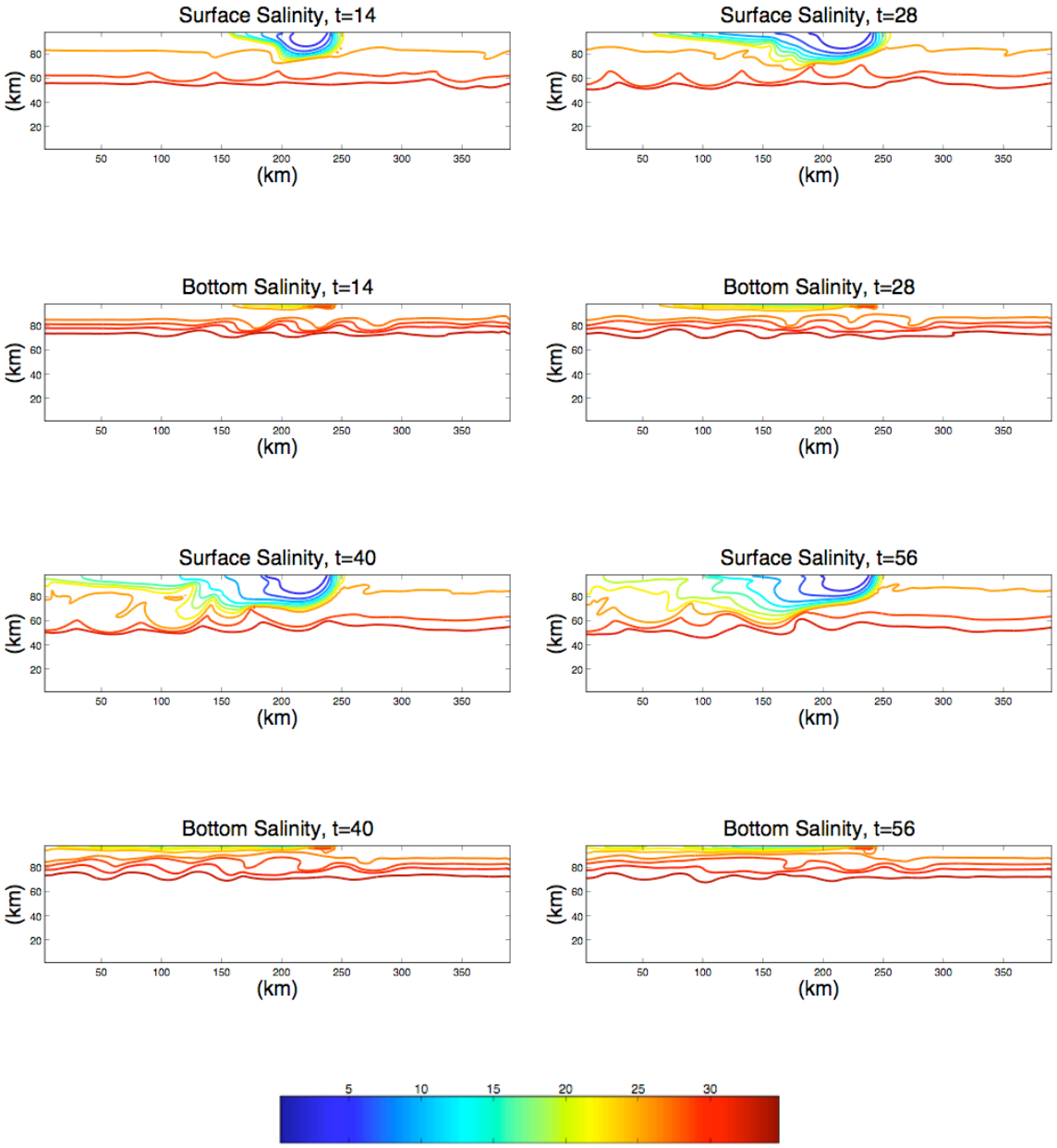

Figure 4.19. Surface and bottom salinity for bumpy steep-sloped with moderate discharge case *j*. t units are equal 1=6 hours.

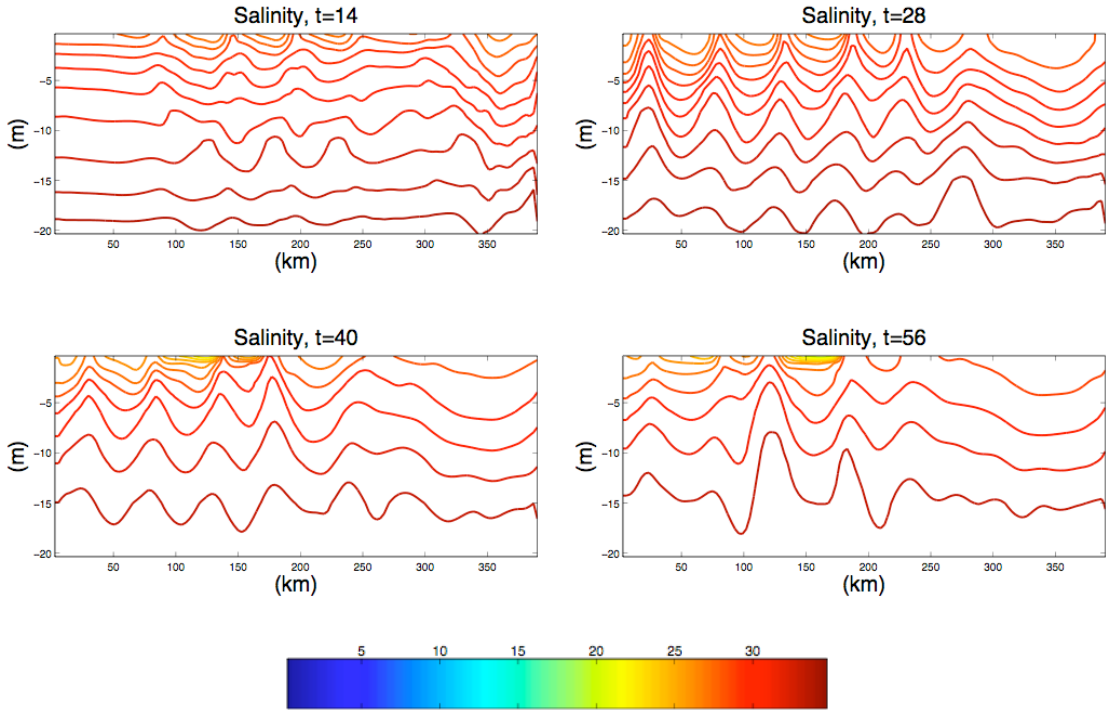

Figure 4.20. Salinity along the 20 m isobath for bumpy steep-sloped with moderate discharge case *j*. t units are equal 1=6 hours.

k. The bumpy gradually-sloped with large discharge case

This experiment is the same as the Case *i* but with the large freshwater discharge (see Table 2.4 for details). Horizontal fields of surface and bottom salinity at several time steps are shown in Figure 4.21. Vertical sections of salinity at the same times along the 15 m isobath are shown in Figure 4.22.

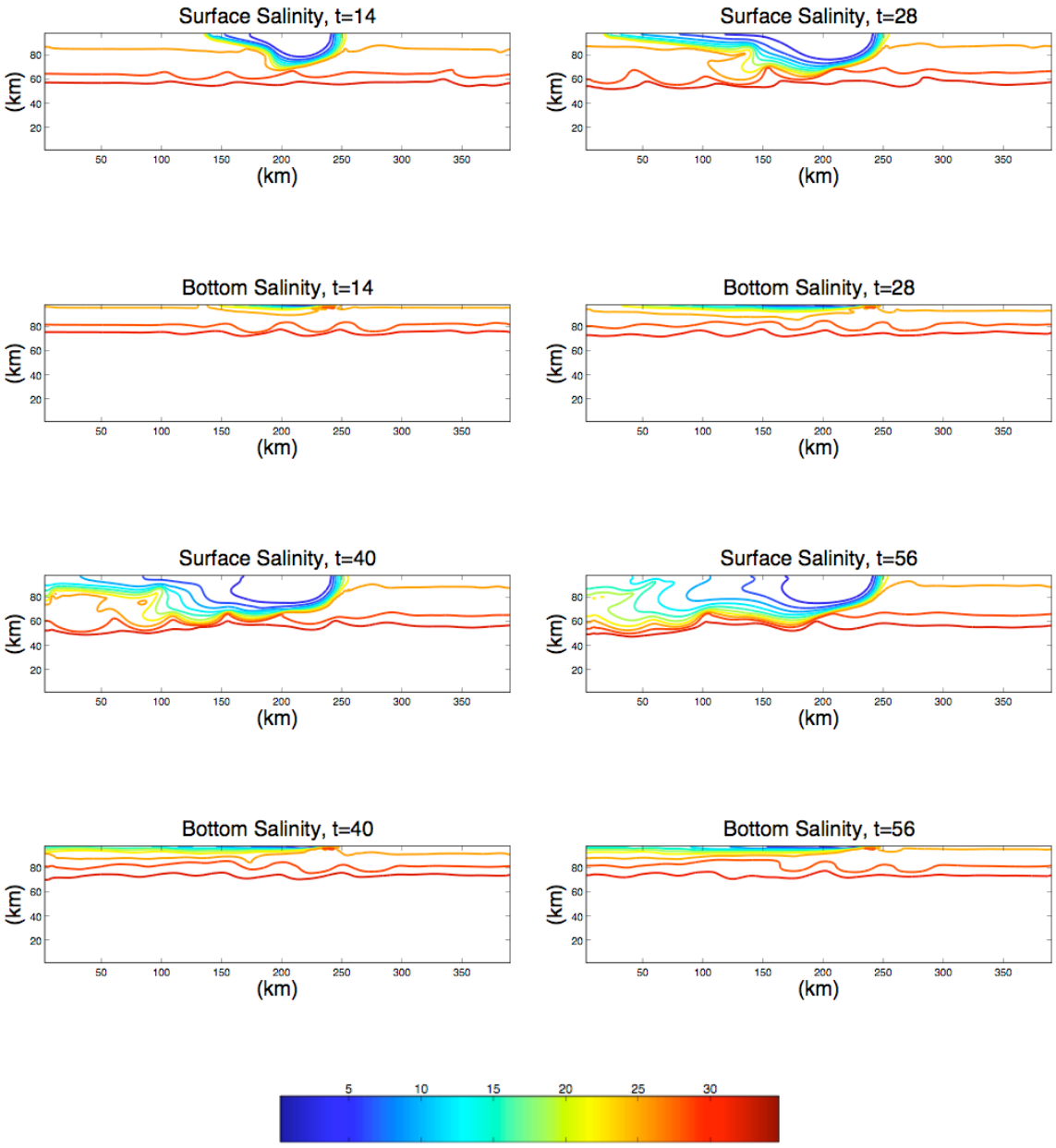

Figure 4.21. Surface and bottom salinity for bumpy gradually-sloped with large discharge case *k*. t units are equal 1=6 hours.

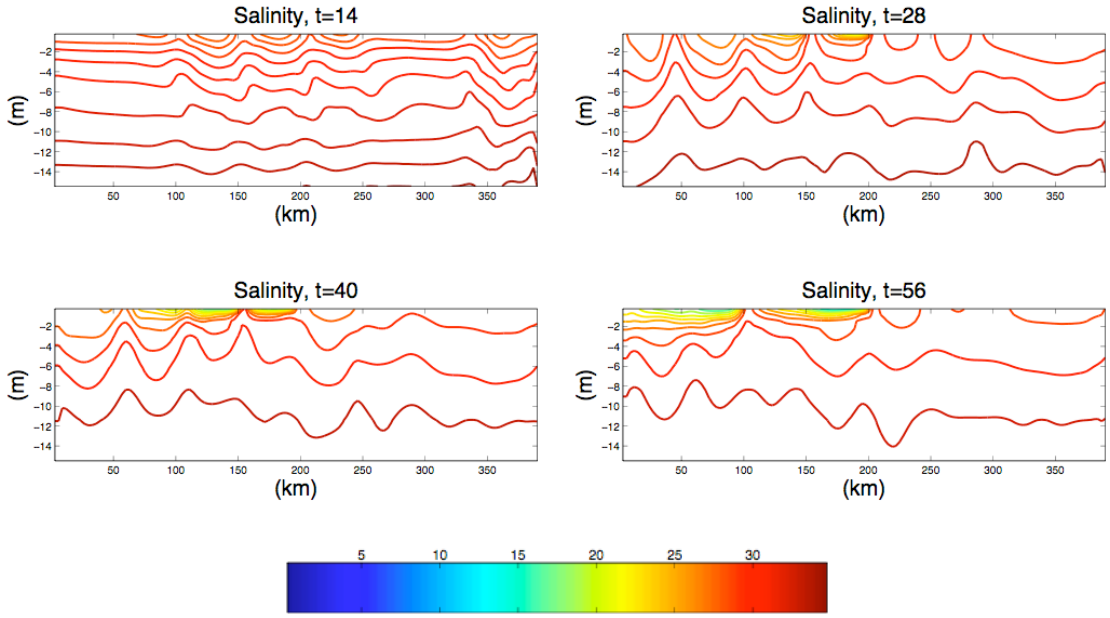

Figure 4.22. Salinity along the 15 m isobath for bumpy gradually-sloped with large discharge case *k*. t units are equal 1=6 hours.

As it was noted before, the change in the freshwater forcing does not appear to affect the formation of the instabilities and their spatial scales. The results of this experiment are comparable to those in Case *i*. The larger volumes of freshwater cause the bigger salinity differences in the bottom layer, and yet, there is a little interaction between the plume and meander produced by flow over the shoaling topography. Large volumes of less saline water are present in the vertical along shelf section, but have no effect on the spatial scales of instabilities as those are very much alike as in Case *i* with the moderate freshwater discharge.

As noted above in Case *h*, doubling of the freshwater discharge does not affect the structure of instability near the injection point.

l. The bumpy steep-sloped with large discharge case

This case consists of initializing with the steep-sloped shoaling topography and introducing a large freshwater discharge (see Table 2.4 for details). Horizontal fields of

surface and bottom salinity at several time steps are shown in Figure 4.23. Vertical sections of salinity at the same times along the 20 m isobath are shown in Figure 4.24.

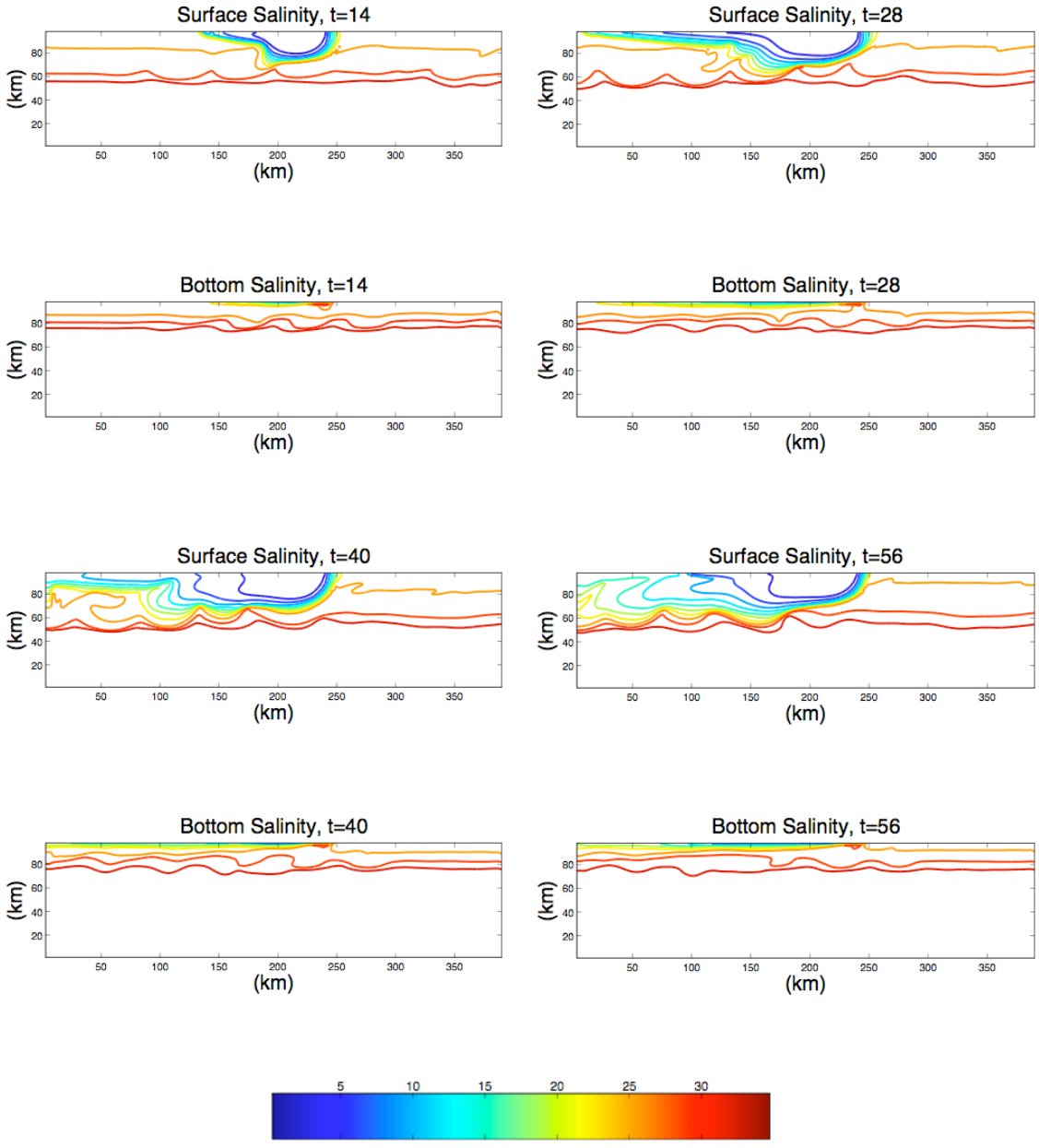

Figure 4.23. Surface and bottom salinity for bumpy steep-sloped with large discharge case *l*. t units are equal 1=6 hours.

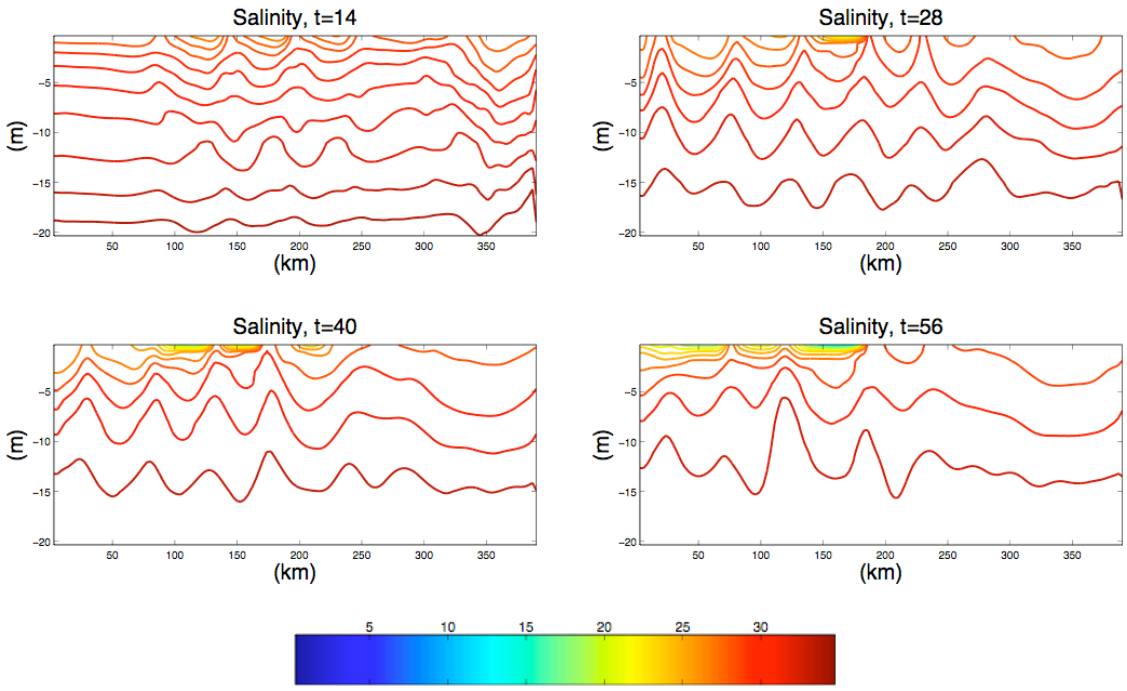

Figure 4.24. Salinity along the 20 m isobath for bumpy steep-sloped with large discharge case *l*. t units are equal 1=6 hours.

Similarly, to the cases with more gentle continental shelf slope (Cases *i* and *k*), the change in the freshwater forcing has a minor effect on the formation and evolution of instabilities along the shelf. The results of this experiment are very similar to the outcome of the case with the same topography configuration and moderate freshwater discharge (Case *j*). However, as it was mentioned above, the steeper slope contributes to the greater offshore spread of the plume.

As noted above in Case *h*, doubling of the freshwater discharge does not affect the structure of instability near the injection point.

4.2 Relative importance of bottom topography and freshwater forcing on the development of dynamic instabilities along the shelf

Twelve numerical experiments were performed in order to evaluate a relative importance of the variable bottom topography and freshwater forcing on the development, evolution, and scales of the dynamic instabilities.

No instabilities developed along and across the spatial extent of the model domain in the absence of the freshwater forcing for the cases with smooth topography (Cases *a* and *b*). Those two cases differ from each other in a used value of the continental shelf slope. Both values of slope used in this study in combination with other chosen parameters (initial salinity gradient, wind) demonstrated their insufficiency to support the formation of the instabilities.

The inclusion of the shoals into the bottom topography showed the development of the dynamic instabilities as the flow passed over the shoals and downstream (Cases *c* and *d*). The disturbances were present in the horizontal and vertical structure of the water property, e.g. salinity. Vertical cross-section along the shelf revealed the wave-like disturbances throughout the water column. The horizontal meander initiated by the shoals underwent further deformation due to the wind mixing, although weak (~1 $m \cdot s^{-1}$). As the influence of the wind mixing diminished with the depth, the shape of meander closely resembled the shape and sizing of the shoals. A variation of continental shelf slope for these cases resulted in a change of the wave amplitudes in the vertical distribution with being larger for the steeper value of slope. The estimated wavelength of the meander is ~50 km along the shelf, which is consistent with the spacing of the shoals.

Introduction of the fresh water onto shelf resulted in the greater salinity differences, and as the consequence in the formation of the unstable salinity fronts along the plume edge. Freshwater forcing (moderate and large) used in the experiments (Cases *e-h*), alone was sufficient to originate the instabilities. The spatial scales of the meander were variable with the wavelength of ~30-100 km along the shelf and wave amplitude of

1-6 m in the water column. The range depends more on the steepness of the shelf slope than on the volume and rate of the fresh water injected onto the shelf.

Combination of the freshwater forcing and shoaling topography (Cases *i-l*) showed the interaction between instabilities produced by different mechanisms: topographic steering due to the shoals and buoyancy transfer due to the density gradient. A close inspection of salinity contours near the bottom revealed that more gentle shelf slope causes plume to be trapped inshore behind the shoals. A change in the shelf slope to steeper value allowed for plume to move further offshore and interfere with the meander produced by irregularities in the topography. The estimated wavelength of the meander was ~50 km along the shelf with the wave amplitude varied ~1-6 m in the water column.

Variation in the freshwater discharge magnitude does not appear to alter the development, sustainment, and scales of instabilities for any of the studied cases (*e-l*).

4.3 Dissolved oxygen deficit distribution along the shelf

To evaluate the influence of instabilities, which are produced by freshwater forcing and topographic steering, on the distribution of dissolved oxygen at the bottom, six cases out of twelve described above were chosen. The rationale for the selected cases (*c-f* and *i-j*) follows from the conclusions discussed above. The cases with shoaling topography and freshwater discharge correspond closest to the conditions found on the shelf and present the most interest for the further analysis. Currents extracted from the numerical experiments were used to advect the tracer representing the dissolved oxygen deficit. Dissolved oxygen is removed from the water column according to Eqn. 2.1. Note that the purpose of the numerical experiments is to understand the spatial distribution of the tracer rather than produce real values of the water property.

A standard set of figures showing the temporal evolution of the dissolved oxygen is presented for each of the six experiments. Each individual figure contains a sequence of several panels that are ordered in time, from left to right and top to bottom. In every

panel, the flow enters from the right and exits on the left of the figures. The salinity fields are represented in plots as contours.

c. The bumpy gradually-sloped no freshwater forcing case

This numerical experiment setup consists of the variable topography with the gradual continental shelf slope (see Table 2.4 for details). Vertical sections of dissolved oxygen deficit along the 15 m isobath at several times are displayed in Figure 4.25.

The six panels in Figure 4.25 show water column distribution of dissolved oxygen deficit for time steps 14, 28, 56, 70, 94, and 120 which correspond to the 3.5, 7, 14, 17.5, 23.5, and 30 days of simulations. Panels were chosen from animations of the model runs and best represent the processes described.

Distribution of dissolved oxygen deficit exhibits strong temporal and spatial variability in response to the development of instabilities. It is clearly seen, at t=14 (3.5 days), that a band of dissolved oxygen deficit at the bottom has broken into patches along the shelf. Locations of gaps in the dissolved oxygen deficit field correspond to the appearance of a vertical variability outlined by salinity contours. As the simulation progresses in time, the wave-like structure of the distribution of the dissolved oxygen in the water column is apparent. The wavelength and amplitude of the feature are highly variable throughout the run and are ~25-50 km alongshore and ~2-6 m in the total of 15 m water depth. The panel showing the results of experiment at t=28 (7 days) illustrates that the peaks and troughs in oxygen deficit distribution coincide with the peaks and troughs in salinity pattern. The same panel also shows areas of the high oxygen deficit, originated at the bottom, are being detached from the bottom band and carried downstream and upward by the currents. The further inspection of the oxygen deficit distributions at t=56 (14 days) and t=70 (17.5 days) reveals that larger areas with high oxygen deficit tend to appear in the regions with stronger density gradients, i.e. downstream. However, the peaks and troughs of oxygen deficit distribution are no longer in phase with the wave seen in salinity contours. This is possibly due to the difference in the respiration and instability transfer time scales. As the currents produced

by instability weaken, as seen at t=120 (30 days), the oxygen deficit in the lower water column increases as there is no source for its replenishment.

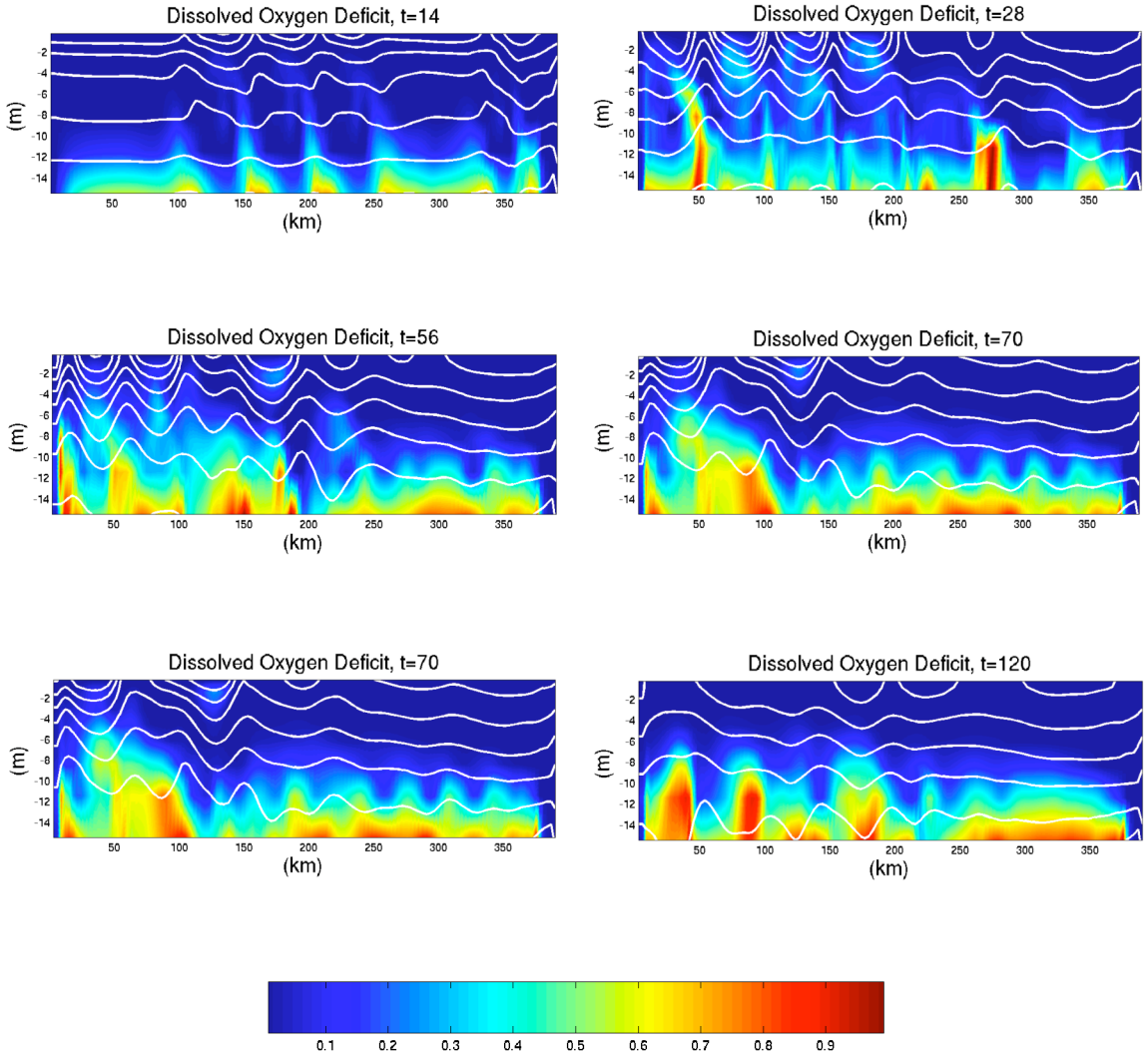

Figure 4.25. Dissolved oxygen deficit and salinity contours along the 15 m isobath for bumpy gradually-sloped no freshwater forcing case *c*. t units are equal 1=6 hours.

Vertical distribution of the dissolved oxygen deficit retains a wave-like structure throughout the simulation time with its peaks and troughs concurred with salinity pattern at the beginning of the run. Large areas of the high dissolved oxygen deficit emerge in the strongly stratified regions. Vertical mixing as a result of instabilities in the buoyancy driven flow induces the bottom band of high oxygen deficit to break into patches and dissipate.

d. The bumpy steep-sloped no freshwater forcing case

A steeper value for the continental shelf slope is used in this experiment (see Table 2.4 for details). Vertical sections of dissolved oxygen deficit along the 20 m isobath at several times are shown in Figure 4.26.

The six panels in Figure 4.26 show water column distribution of dissolved oxygen deficit for the same time steps as in Case *c,* described above.

The mechanism responsible for the distribution of the dissolved oxygen deficit in the water column along the shelf is the similar to that found in Case *c*. However, a steeper topography leads to the stronger amplitudes of instabilities and less temporal variability. The persistence of the wave throughout the simulation up to t=120 (30 days) actively contributes to the movement downstream and/or upward, and dissipation of patches with the high oxygen deficit. As a result of this action, the areas with the high oxygen deficit are much smaller than those in Case *c*.

Steep topography allows for the rapid flushing of the system and dispersion of low-oxygen waters.

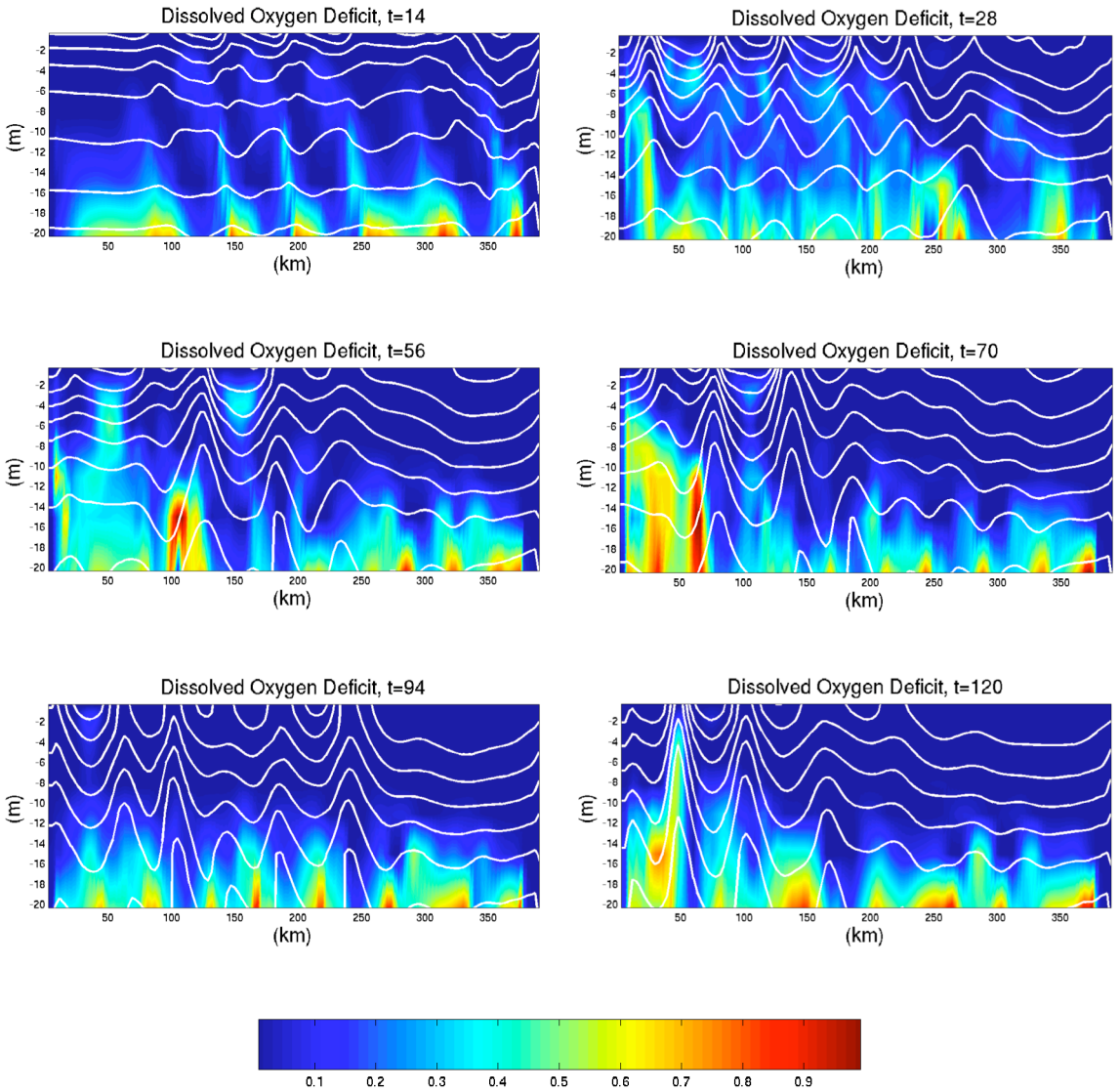

Figure 4.26. Dissolved oxygen deficit and salinity contours along the 20 m isobath for bumpy steep-sloped no freshwater water forcing case *d*. t units are equal 1=6 hours.

e. The smooth gradually-sloped with moderate discharge case

This numerical experiment consists of initializing the model with the smooth gradually-sloped topography and introducing a constant but moderate freshwater discharge into the model (see Table 2.4 for details). Vertical sections of dissolved oxygen deficit along the 15 m isobath at several times are shown in Figure 4.27.

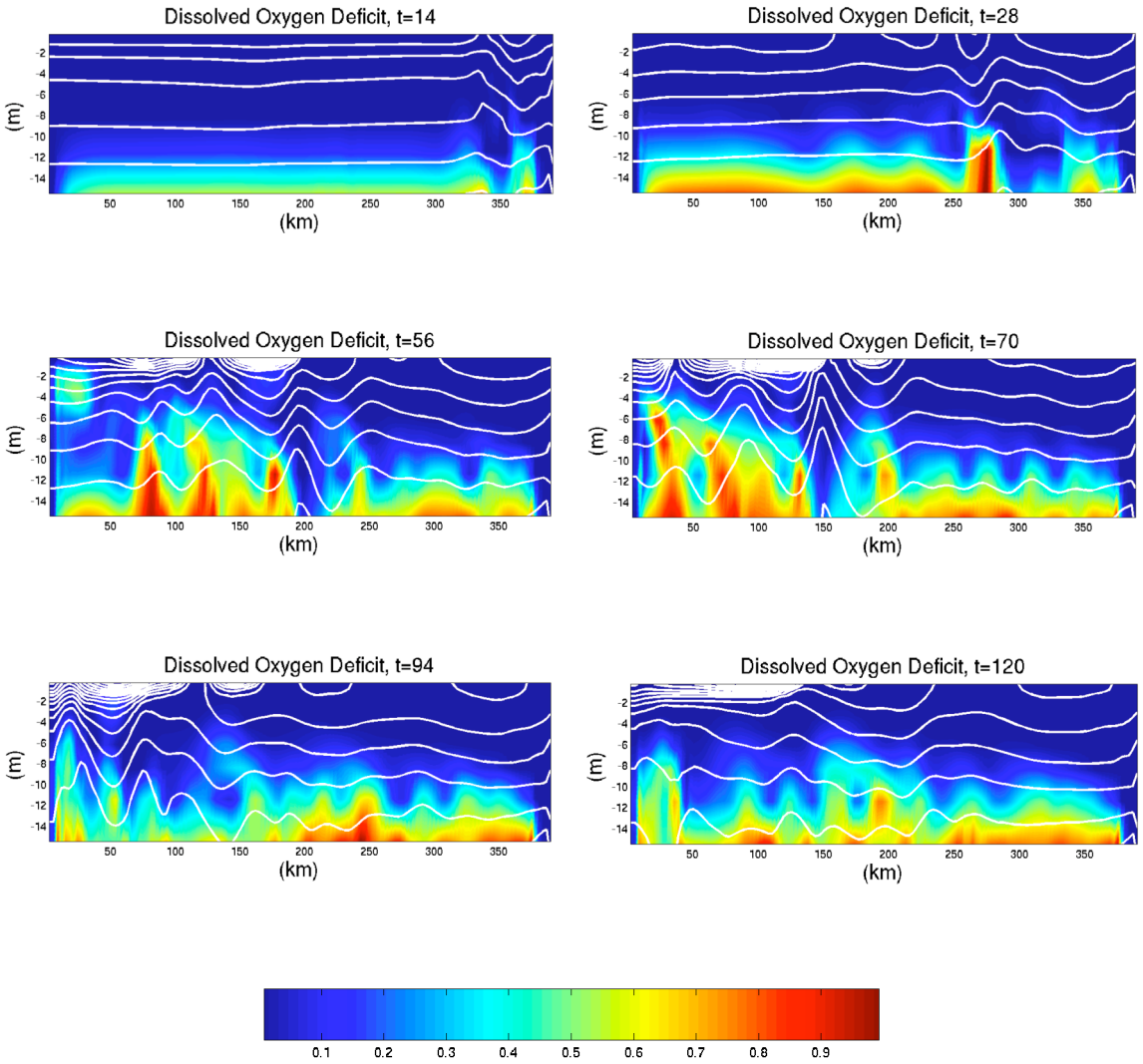

Figure 4.27. Dissolved oxygen deficit and salinity contours along the 15 m isobath for smooth gradually-sloped with moderate discharge case *e*. t units are equal 1=6 hours.

As described in Section 4.1, instabilities in this experiment develop due to the salinity differences introduced by the spread of river plume offshore. As seen in the upper left panel at t=14 (3.5 days) the absence of instabilities allows for the establishment of a continuous band of waters with dissolved oxygen deficit along the shelf. At t=28 (7 days) the response of the dissolved oxygen structure to the water column disturbances is seen. At all other time steps, the dissolved oxygen deficit distribution is highly variable and reflects the wave-like structure produced by

instability. The vertical displacements of dissolved oxygen deficit reach up to ~9 m in the 15 m total water depth. Areas with the high oxygen deficit tend to grow spatially under the strongly stratified regions, i.e. downstream under the river plume. These areas are seen in the panels showing t=56 (14 days) and t=70 (17.5 days). A close inspection of the wave, seen in the dissolved oxygen deficit distribution, and the wave in salinity field, reveals a phase shift as simulation progresses in time.

The absence of topographic steering delays the break down and dissipation of high oxygen deficit areas as instabilities only develop with the offshore spread of plume. High oxygen deficit areas tend to form under the river plume where the strong stratification occurs.

f. The smooth steep-sloped with moderate discharge case

A steeper value for the continental shelf slope is used in this experiment (see Table 2.4 for details). Vertical sections of dissolved oxygen deficit along the 20 m isobath at several times are shown in Figure 4.28.

The results of this experiment are similar to those in Case *d*. The main difference is that the steeper shelf slope leads to the larger amplitudes of instabilities and hence more intensive ventilation of the water column.

i. The bumpy gradually-sloped with moderate discharge case

This experiment consists of initializing with the bumpy gradually-sloped topography configuration and introducing a constant but moderate freshwater discharge into the model (see Table 2.4 for details). Vertical sections of dissolved oxygen deficit along the 15 m isobath at several times are shown in Figure 4.29.

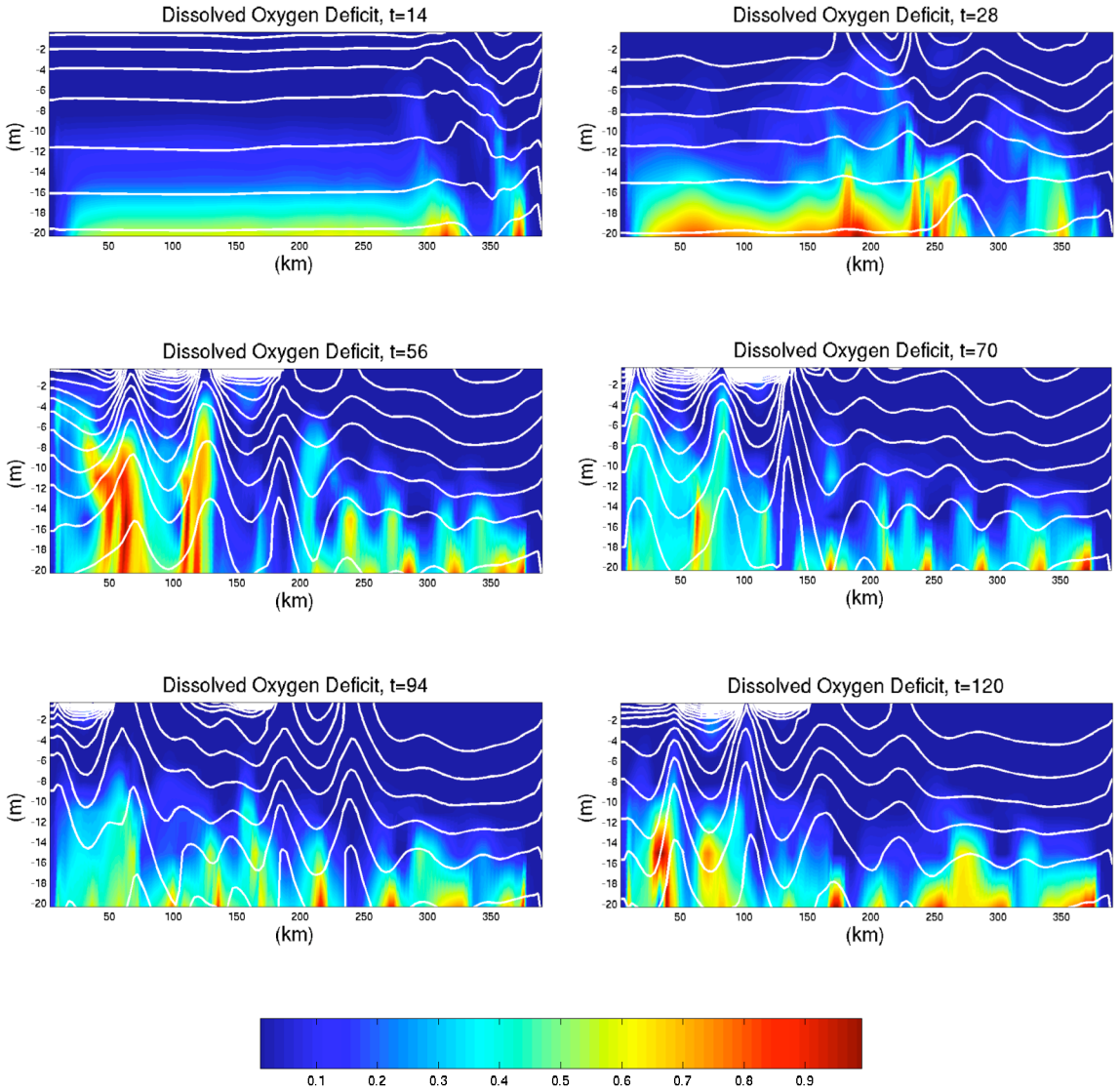

Figure 4.28. Dissolved oxygen deficit and salinity contours along the 20 m isobath for smooth steep-sloped with moderate discharge case *f*. t units are equal 1=6 hours.

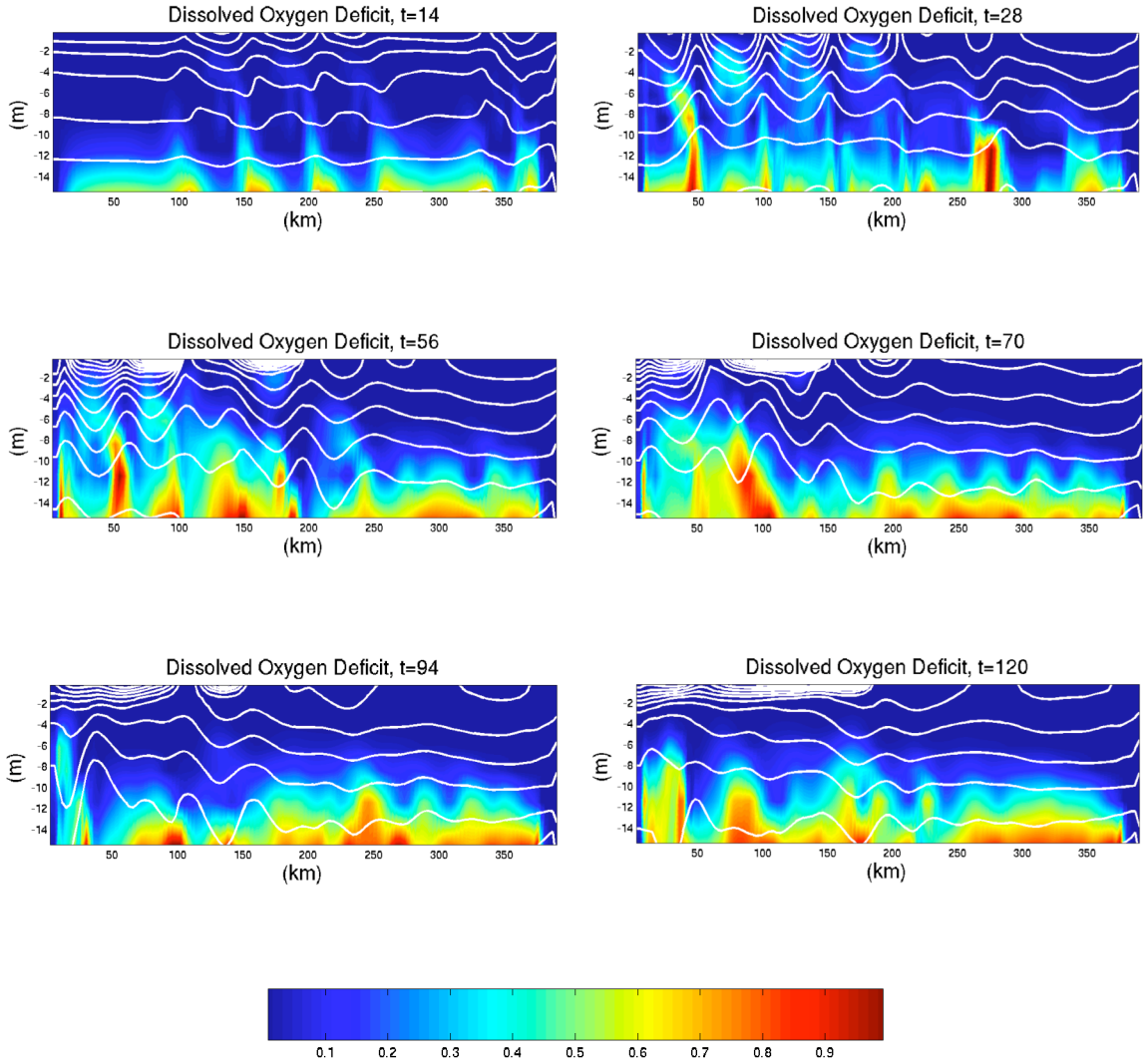

Figure 4.29. Dissolved oxygen deficit and salinity contours along the 15 m isobath for bumpy gradually-sloped with moderate discharge case *i*. t units are equal 1=6 hours.

Similarly to the other cases with shoaling topography, the distribution of dissolved oxygen deficit in this experiment exhibits a wave-like behavior right from the beginning of the simulation. The process of formation and dissipation of the high oxygen deficit areas is similar to those as described in cases with gradual continental shelf slope *c* and *e*.

j. The bumpy steep-sloped with moderate discharge case

This experiment is the same as Case *i* except here a steeper value of the continental shelf slope in used. Vertical sections of dissolved oxygen deficit along the 20 m isobath at several times are shown in Figure 4.30.

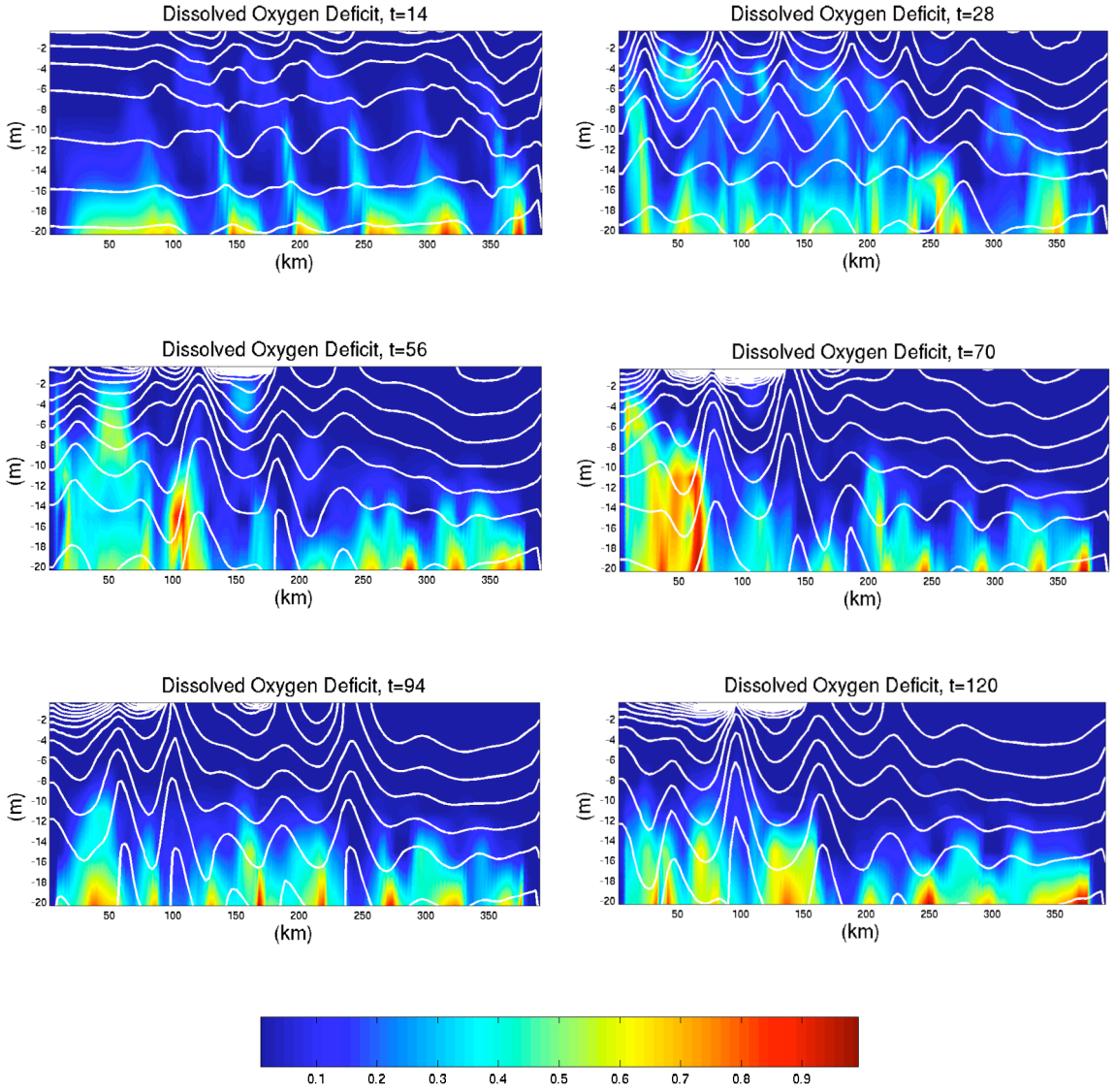

Figure 4.30. Dissolved oxygen deficit and salinity contours along the 20 m isobath for bumpy steep-sloped with moderate discharge case *j*. t units are equal 1=6 hours.

The outcome of the experiment is similar to the Case *d*. However, the inclusion of the freshwater discharge into the model increases stratification, which intensifies the dissolved oxygen deficit under the plume. The comparison with Case *i* show that an increase of the continental shelf slope results in more ventilation of the water column and therefore contributes to the dissipation of low-oxygen waters.

Distribution of the dissolved oxygen deficit along the shelf is influenced by instabilities introduced by topographic steering and freshwater forcing. The dissolved oxygen deficit intensifies in the regions under the river plume in response to the increase in stratification. A steeper value of the shelf slope increases the amplitudes of the wave in the vertical section along the shelf, and thus, promotes ventilation of the water column.

4.4 Influence of instabilities on the distribution of dissolved oxygen deficit along the shelf

Six numerical experiments were analyzed in order to investigate the effect of dynamic instabilities on spatial and temporal patterns of dissolved oxygen concentrations along the shelf.

The development of dynamic instabilities due to topographic steering or/and freshwater forcing provides a distinct mechanism for the movement and dissipation of waters with high dissolved oxygen deficit. The peaks and troughs in the vertical distribution of the dissolved oxygen along the shelf are in phase with the structure of wave seen in salinity field in the beginner stages of simulations (up to 7-14 days). However, this agreement is disrupted as experiments progress in time and superposition of disturbances caused by two different forcings occurs.

Inclusion of shoaling topography into the model domain introduces disturbances near the bottom that are immediately reflected in the oxygen deficit distribution (Cases *c-d* and *i-j*). In the absence of shoals (Cases *e-f*), dynamic instabilities depend on the offshore spread of the river plume and take up to 7 days of simulation to reach the

bottom layer and affect the distribution of dissolved oxygen at the bottom along 15 m and 20 m isobath.

Large areas of the high oxygen deficit tend to appear in the strongly stratified regions downstream.

The variation of steepness of the continental shelf slope to larger values (Cases *d*, *f*, and *j*) results in an increase in the vertical range of instability amplitudes. In turn, larger amplitudes allow for more thorough ventilation of the water column, and therefore contribute to the faster dissipation of waters with the high dissolved oxygen deficit.

In Chapter V, I will relate the conclusions drawn from the numerical experiments to observations of density and dissolved oxygen concentrations from the Louisiana Shelf.

CHAPTER V

DISCUSSION AND CONCLUSIONS

In this chapter, I compare and discuss the results of the numerical experiments and relate them to observations of density and dissolved oxygen concentrations collected on MCH cruises in 2004 and 2005. The purpose here is to identify the processes that affect the distribution of the water properties along the Louisiana Shelf, refine interpretation of the model results discussed in Chapter IV, and to outline future work. I also provide summary and conclusions of the research presented in Chapters III and IV.

5.1 Comparison of numerical experiments and observational results

The initial and boundary conditions, used in numerical experiment, Case *j*, correspond closest to the observed conditions found on the Louisiana Shelf. Therefore, Case *j* was selected as the best candidate run for the comparison with observational data. The downstream (after the injection point of the freshwater and location of shoals) region of the model domain is thought to be analogous to the region offshore off Atchafalaya Bay, LA and the open shelf region between the Texas-Louisiana border and Atchafalaya Bay.

A visual comparison of the horizontal salinity fields produced by numerical simulation (Figure 4.17) to observations of surface salinity on the Louisiana Shelf (Figure 3.3) shows that there are similarities in property distributions along and across the shelf. Both show complex structure of the density field with approximately 50 km alongshelf wavelength. The horizontal meander produced in the numerical model output is a response to the topographic steering and freshwater discharge, and suggests that the same processes control the spatial structure of the meander observed on the Louisiana Shelf during multiple cruises. The similarities of modeled (Figure 4.18) and observed (Figure 3.2) vertical sections of salinity along the coast provide the further support for this conclusion. Both, the vertical distribution of the dissolved oxygen deficit derived

from numerical simulations (Figure 4.30) and dissolved oxygen concentrations measured on MCH cruses (Figure 3.9), exhibit a wave-like structure in response to the buoyancy transfer with roughly 10 m vertical excursions and 50 km along shelf wavelength. The omnipresence of this feature throughout the modeling runs and on all cruises indicates that this is a ubiquitous characteristic of the Louisiana Shelf.

To compare the effects of stratification on bottom dissolved oxygen concentrations, the Brunt-Väisälä frequency along the 20 m isobath was calculated from model salinity and temperature fields at several time steps using Eqn. 3.1.

Bottom values of dissolved oxygen deficit versus maximum Brunt-Väisälä frequency at several time steps are shown on Figures 5.1. Data points are color-coded by the distances along the shelf with red/yellow dots being upstream (before the injection point of the freshwater and location of shoals) and blue/purple downstream (after the injection point of the freshwater and location of shoals).

The dissolved oxygen deficit distribution derived from the model shows large variability over the time that is associated with advection and enhanced mixing processes. At the beginning of the simulation (t=28; 7 days), the freshwater plume is confined to the coast near the injection point and has not had time to spread offshore to the 20 m isobath. Thus, stratification and, therefore, Brunt-Väisälä frequency tend to be low ~35-40 cycles per hour, reflecting the values set by the initial salinity gradient. A closer inspection of the distribution in Figure 5.1(*a*) reveals that data points can be divided into two groups. The first group is a narrow vertical strip with a range of the dissolved oxygen deficit at the Brunt-Väisälä frequency equal to ~30-35 cycles per hour, i.e., corresponding most closely to the initial stratification values of the model. This group (red/yellow dots) represents the water column in the upstream region (distances > 200 km) and can be neglected in further comparison since this region is not greatly influenced by variable topography and/or freshwater discharge. Data points (blue/purple dots), representing the downstream region (distances < 200 km), exhibit a similar range of the dissolved oxygen deficit with increasing stratification, which is associated with the development of instabilities at the bottom as the flow passes over the shoals.

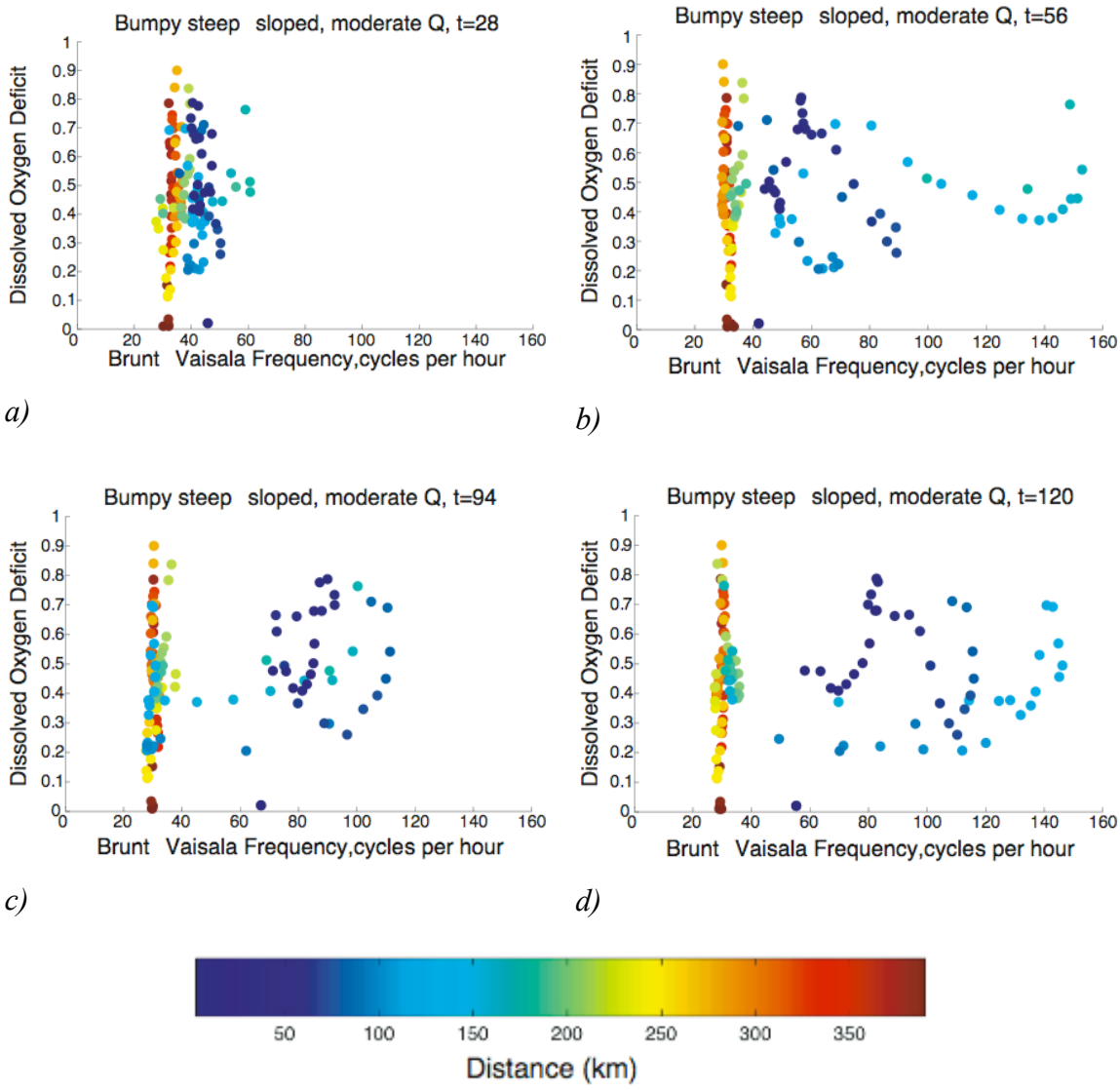

Figure 5.1. Maximum Brunt-Väisälä frequency versus bottom dissolved oxygen deficit for the bumpy steep-sloped with moderate discharge case *j* with the respiration time scale of 3 days. t units are equal 1=6 hours.

As the simulation progresses in time, the separation of the data into two distinctive groups becomes more clear, as seen in Figure 5.1(*b-d*). Although, the distribution of the data points indicate a general increase in bottom oxygen deficit with increasing Brunt-Väisälä frequency, the relationship is not linear, and manifests as loop-like features associated with the phasing of the of the physical and biological processes.

As Brunt-Väisälä frequency increases, strong pycnocline caps the bottom water layer restricting the supply of dissolved oxygen down to the bottom from the surface layer, as a result the dissolved oxygen deficit increases as well. As stratification weakens due to the vertical mixing, it allows for injecting the well-oxygenated waters from the surface downward into the bottom layer, where a decrease in the dissolved oxygen deficit is seen. The similarities in the time scales of the respiration parameterization (3 days) and buoyancy transfer processes (3-7 days) maintain the shift in the wave phase and the complexity of the patterns throughout the runs as both processes need approximately the same period of time to reach steady state.

Figures 5.2 and 5.3 illustrate how different respiration time scales produce different spatial and temporal patterns. A shorter time scale, i.e., 0.5 days (Figure 5.2) results in the rapid development of the dissolved oxygen deficit at the bottom along the shelf. Very few points in the downstream region have dissolved oxygen deficit values less than 0.6 The temporal response of the system to ventilate the lower layers is slower than the time to form the areas of high dissolved oxygen deficit. Hence, low-oxygen waters cover most of the shelf despite of the strong current events that move and contribute to the dissipation of those areas. A longer time scale (Figure 5.3) results in the opposite trend as the waters are minimally depleted throughout the run, i.e., few dissolved oxygen deficit values are greater than 0.5. Since ventilation rates set by physical processes are faster than the respiration scales the lower layers tend to remain well oxygenated. Variability of the dissolved oxygen deficit derived from the model with the respiration time scale of 3 days (Figure 5.1) resembles closest the distribution of the dissolved oxygen concentrations observed on MCH cruises. I expect that any changes to the structure and timing of stratification and water column stability can lead to significant changes to the character and structure of the lower layer (near bottom) dissolved oxygen deficit.

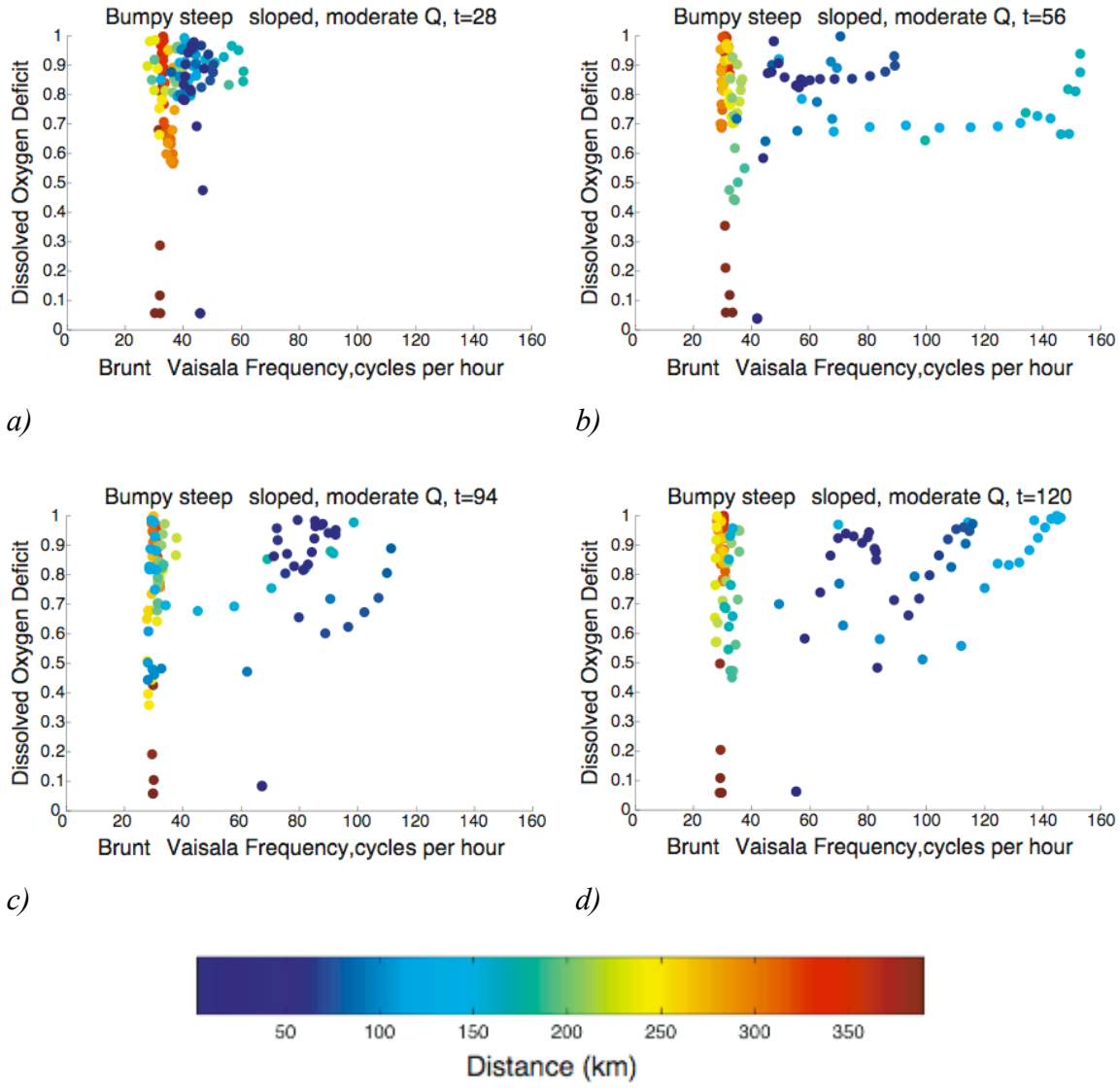

Figure 5.2. Maximum Brunt-Väisälä frequency versus bottom dissolved oxygen deficit for the bumpy steep-sloped with moderate discharge case *j* with the respiration time scale of 0.5 days. t units are equal 1=6 hours.

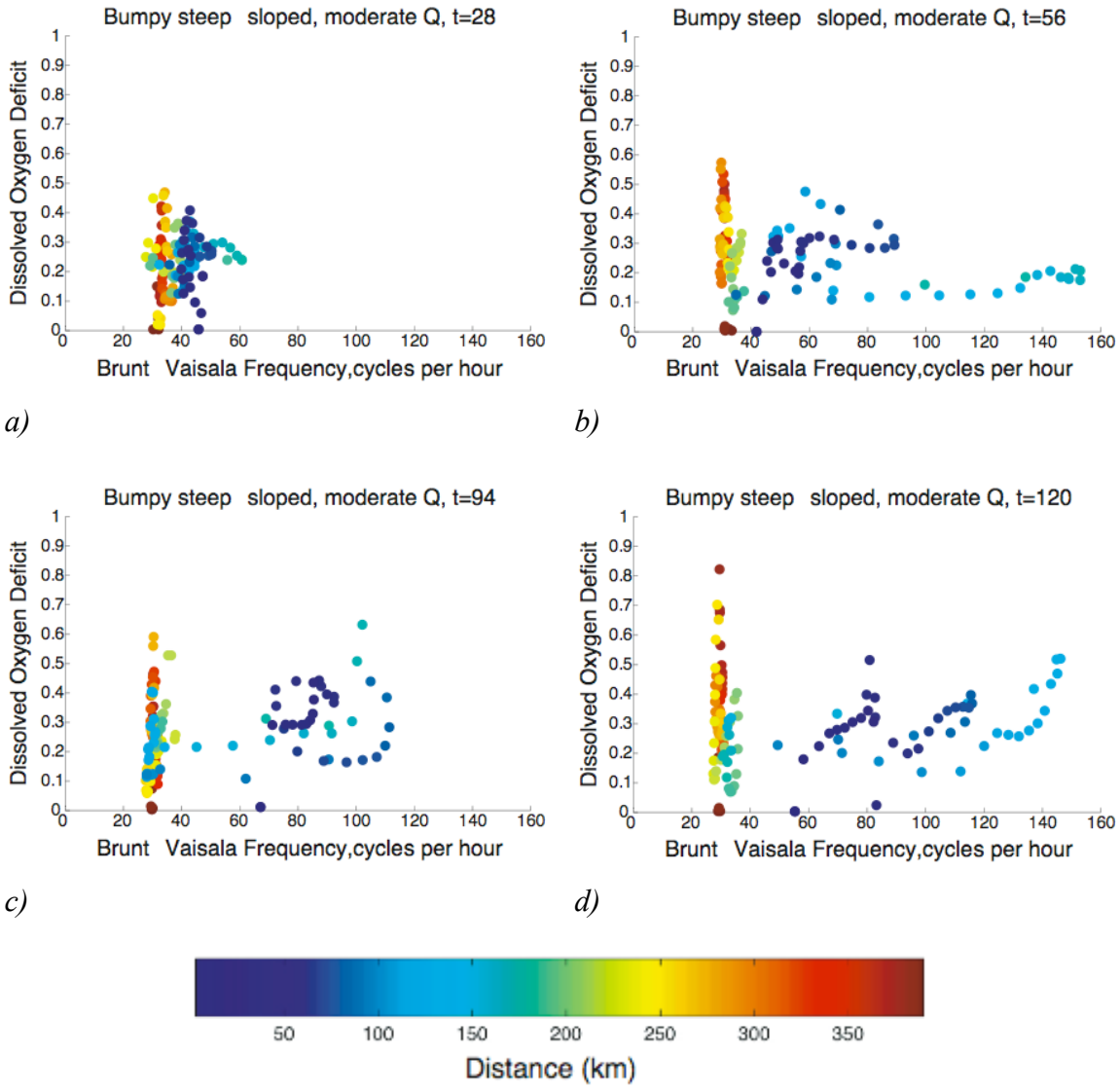

Figure 5.3. Maximum Brunt-Väisälä frequency versus bottom dissolved oxygen deficit for the bumpy steep-sloped with moderate discharge case *j* with the respiration time scale of 7 days. t units are equal 1=6 hours.

5.2 Summary and conclusions

MCH data sets were used to describe and analyze the alongshore distribution of the physical and biochemical water properties on the Louisiana Shelf. Temperature, salinity, and dissolved oxygen concentrations records, collected on MCH cruises, revealed the presence of meander, seen in horizontal sections along the shelf. The alongshelf meander is also manifested vertically as a wave-like distribution of the properties in the water column. This meander appears to be a ubiquitous characteristic of the Louisiana Shelf with spatial scale approximately 50 km and less along the shelf, which is consistent with the locations of sandy shoals along the coast and the local deformation radius.

I have shown, that during MCH cruises the occurrences of low-oxygen and hypoxic waters, represented as waters with high AOU values, were related to the local vertical stratification mainly in zones C (off Atchafalaya Bay, LA) and D (shelf between Atchafalaya Bay, LA and Texas border). In general, the bottom AOU increases with the increase in Brunt-Väisälä frequency and vice versa. This mechanism is well illustrated by the wave seen in the vertical distributions of salinity and dissolved oxygen concentrations along the shelf. Strong stratification caps the bottom water layer restricting the ventilation of dissolved oxygen from the surface layer down to the bottom. As stratification weakens due to the vertical mixing processes it allows for the injection of the well-oxygenated waters from the surface into the bottom layer. Hypoxic conditions were not present in waters with Brunt-Väisälä frequency less than 40 cycles per hour. Although, this explanation implies a linear relationship between AOU and Brunt-Väisälä frequency, the observational data show considerable variability, especially in the region in the vicinity of zones C and D.

The origin of the meander and its influence on the distribution of dissolved oxygen concentrations along the shelf was investigated using numerical modeling. Twelve numerical experiments were performed to evaluate the relative importance of the variable bottom topography and freshwater forcing on the development, evolution, and scales of the dynamic instabilities.

For the cases with smooth topography, no instabilities developed along and across the spatial extent of the model domain in the absence of the freshwater forcing. Those two cases differ from each other in a used value of the continental shelf slope. Both values of slope used in this study in combination with other chosen parameters (initial salinity gradient, wind) demonstrated their insufficiency to support the formation of the instabilities.

The inclusion of the shoals into the bottom topography showed the development of the dynamic instabilities as the flow passed over the shoals and downstream. Vertical cross-sections along the shelf revealed wave-like disturbances throughout the water column. Introduction of the fresh water onto shelf resulted in greater salinity differences, and, as a consequence in the formation of the unstable salinity fronts along the plume edge. Freshwater forcing (moderate and large) used in the experiments, alone was sufficient to originate the instabilities. The combination of the freshwater forcing and shoaling topography showed the interaction between instabilities produced by different mechanisms: topographic steering due to the shoals and buoyancy transfer due to the density gradient.

Varying the continental shelf slope resulted in a change of the vertical wave amplitudes with larger amplitudes for the steeper slopes. Inspection of salinity contours near bottom revealed that a more gentle shelf slope causes the plume to be trapped inshore behind the shoals. A change in the shelf slope to a steeper value allowed for the plume to move further offshore and interfere with the topographically induced meander. Varying the magnitude of freshwater discharge does not appear to alter the development, sustainment, and scales of instabilities near the injection point for any of the studied cases.

Six numerical experiments were analyzed in order to investigate the effect of dynamic instabilities on spatial and temporal patterns of dissolved oxygen concentrations along the shelf.

Inclusion of shoaling topography into the model domain introduces disturbances near the bottom that are immediately reflected in the oxygen deficit distribution. In the

absence of shoals, dynamic instabilities depend on the offshore spread of the river plume. The development of dynamic instabilities due to topographic steering or/and freshwater forcing provides a unique mechanism for the movement and dissipation of waters with high dissolved oxygen deficit. The peaks and troughs in the vertical distribution of the dissolved oxygen along the shelf are in phase with the peaks and troughs of the wave seen in the density structure in the beginner stages of simulations. However, this agreement is disrupted as the numerical experiments progress in time and a superposition of disturbances caused by two different forcings occurs. A loop-like relationship between Brunt-Väisälä frequency and dissolved oxygen deficit reflects the response of biochemical properties to the changes in density field. The time scales of the respiration parameterization (~3 days) and buoyancy transfer processes (~5-7 days) contribute to the shift in phasing and the complexity of the patterns seen at later times.

The variation of steepness of the continental shelf slope to larger values results in an increase in the vertical range of instability amplitudes. In turn, larger amplitudes allow for more thorough ventilation of the water column, and thus affect the bottom dissolved oxygen concentrations.

Comparison of results of the numerical modeling runs to observations of density and dissolved oxygen concentrations on the Louisiana Shelf supports the idea that physical processes such as topographic steering and/or freshwater forcing influence the alongshore distribution of physical and biochemical properties on the Louisiana Shelf. Indeed, it suggests that the time scales, associated with the physical processes that are responsible for water column stability and ventilation, are similar to the time scales associated with the benthic respiration rates. Further, the model represents the mechanisms affecting the location and dissipation of low-oxygen waters in the regions analogous to zones C and D of the Louisiana Shelf by reproducing the characteristic features of variability of water properties along the shelf.

Although, this study shows how physical processes can affect biochemical processes on the Louisiana Shelf, further investigations can be carried out in order to advance and broaden our understanding of the system. Suggestions for future work,

intended to continue this study, include expanded observational and numerical components:

Observational component

- An addition of the prolonged time series observations at several stations along the shelf;
- Acquisition of current profiles with sufficient vertical resolution to measure shear;

Modeling component

- Modification of the benthic respiration function, and inclusion of the water column respiration and photosynthesis;
- Analysis of the time series derived from the model simulations with moored time series of temperature, salinity, and dissolved oxygen concentrations from the shelf.

REFERENCES

Barth, J. A. (1989), Stability of a coastal upwelling front, *J. Geophys. Res., 94* (C8), 10,844-10,856.

Belabbassi, L. (2006), Examination of the relationship of river water to occurrences of bottom water with reduced oxygen concentrations in the Northern Gulf of Mexico, Ph.D. diss., Tex. A&M Univ., College Station.

Bennekom, A. J. Van, and F. J. Wetsteijn (1990), The winter distribution of nutrients in the southern bight of the North Sea (1961–1978) and in the estuaries of the Scheldt and the Rhine/Meuse, Neth., *J. Sea Res., 25,* 75–87.

Boesch, D. F., and N. N. Rabalais (1991), Effects of hypoxia on continental shelf benthos; comparisons between the New York Bight and the Northern Gulf of Mexico, in *Modern and Ancient Continental Shelf Anoxia*, edited by R. V. Tyson and T. H. Pearson, pp. 27-34, Geological Society Special Publication, London, England.

Boyd, R., and S. Penland (1988), A Geomorphologic model for Mississippi delta evolution, in *Transactions - Gulf Coast Association of Geological Societies*, vol. *72*(9), pp. 443-452.

Brunner, A. C., J. M. Beall, S. J. Bentley, and Y. Furukawa (2006), Hypoxia hotspots in the Mississippi Bight, *J. Foraminiferal Res., 36*(2), 95-107.

Brunt, D. (1927), The period of simple vertical oscillations in the atmosphere, *Q. J. Roy. Meteorol. Soc., 53*, 30-32.

Carter, R. A., H. F. McMurray, and J. L. Largier (1987), Thermocline characteristics and phytoplankton dynamics in Agulhas Bank waters, in *The Benguela and comparable ecosystems*, edited by A. I. L. Payne, L. A. Gulland, and K. H. Brink, pp. 327-336, Special volume of S. Afr. J. Mar. Sci., 5.

Chapman, D. C. (1985), Numerical treatment of cross-shelf open boundaries in a barotropic ocean model, *J. Phys. Oceanogr., 15*, 1060-1075.

Chapman, P., and L. V. Shannon (1987), Seasonality in the oxygen minimum layers at the extremities of the Benguela system, in *The Benguela and Comparable Ecosystems*, edited by A. I. L. Payne, L. A. Gulland, and K. H. Brink, pp. 85-94, Special volume of S. Afr. J. Mar. Sci., 5.

Chen, C., R. O. Reid, and W. D. Nowlin, Jr. (1996), Near-inertial oscillations over the Texas-Louisiana shelf, *J. Geophys. Res., 101*(C2), 3509-3524.

Cho, K., R. O. Reid, and W. D. Nowlin (1998), Objectively mapped stream function fields on the Texas-Louisiana shelf based on 32 months of moored current meter data*, J. Geophys. Res.*, *103*(C5), 10,377-10,390.

Clarke, A. J., and K. H. Brink (1985), The response of stratified, frictional flow of shelf and slope water to fluctuating large-scale, low-frequency wind forcing, *J. Phys. Oceanogr.*, *15*, 439-453.

Cochrane, J.D., and F. J. Kelly (1986), Low-frequency circulation on the Texas-Louisiana continental shelf, *J. Geophys. Res*., *91*(C9),10,645-10,658.

Conley, D. J., C. Humborg, L. Rahm, O. P. Savchuk, and F. Wolfe (2002), Hypoxia in the Baltic Sea and basin scale changes in phosphorus biogeochemistry, *Environ, Sci. Tech., 36*, 5315-5320.

Cruz-Kaegi, M. E., and G. T. Rowe (1992), Benthic biomass gradients on the Texas-Louisiana shelf, in *Proceedings, Nutrient Enhanced Coastal Ocean Productivity Workshop*, pp. 145-149, Texas A&M Sea Grant Publication, Galveston, TX, TAMU-SG-92-109.

Dagg, M, R. Benner, S. Lohrenz, and D. Lawrence (2004), Transformation of dissolved and particulate materials on continental shelves influenced by large rivers: plume processes, *Cont., Shelf Res., 24*, 833-858.

Degens, E. T., S. Kempe, and J. E. Richey (1991), *Biogeochemistry of Major World Rivers,* pp. 356, John Wiley and Sons, New York.

Demaison, G. J., and G. T. Moore (1980), Anoxic environments and oil source bed genesis, *AAPG Bull. 64*(8), 1179-1209.

Diaz R. J. (2001), Overview of hypoxia around the world*, J. Environ. Qual., 30*(2), 275-281.

Diaz, R. J. and R. Rosenberg (1995), Marine benthic hypoxia - review of ecological effects and behavioral responses on macrofauna, *Oceanography and Marine Biology, Annual Review*, *33*, 245-303.

DiLorenzo, E. (2003), Seasonal dynamics of the surface circulation in the southern California Current System, *Deep-Sea Res., Part II, 50*, 2371-2388.

DiMarco, S. F. (2007b), Mechanisms Controlling Hypoxia on the Louisiana Shelf, Final Report, Dept. of Oceanography, Texas A&M Univ., College Station, TX.

DiMarco, S. F., and R. O. Reid (1998), Characterization of the principal tidal constituents on the Texas-Louisiana shelf, *J. Geophys. Res.*, *103* (C2), 3093-3110.

DiMarco, S. F., P. Chapman, N. Walker, R. D. Hetland (2007a), Does local topography controls hypoxia on the Texas-Louisiana shelf, *Science*, submitted.

DiMarco, S.F., F. J. Kelly, J. Zhang, and N. L. Guinasso, Jr., (1995), Directional Wave Spectra on the Louisiana-Texas Shelf During Hurricane Andrew, *J. Coastal Res., SI-21*, 217-233.

DiMarco, S.F., Howard, M.K., and R.O. Reid, (2000), Seasonal variation of wind-driven diurnal cycling on the Texas-Louisiana continental shelf, *Geophys. Res. Lett., 21*(7), 1017-1020.

Dinnel S. P., and W. J. Wiseman Jr. (1986), Fresh water on the Louisiana and Texas shelf, *Cont. Shelf Res., 6*(6), 765-784.

Dinniman, M. S., J. M. Klinck, and W. O. Smith Jr. (2003), Cross shelf exchange in a model of the Ross Sea circulation and biogeochemistry, *Deep-Sea Res., Part II, 50*, 3103-3120.

Earles, R. (2000), The Gulf of Mexico Dead Zone: Impact on Fisheries, Prepared by the National Center for Appropriate Technology for the Mississippi Riverwise Partnership, Fayetteville, AR.

Etter, P. C., M. K. Howard, and J. D. Cochrane (2004), heat and freshwater budgets of the Texas-Louisiana shelf, *J. Geophys. Res., 109*, C02024, doi:10.1029/2003JC001820.

Flather, R. A. (1976), A tidal model of the northwest European continental shelf, *Memoires de la Societe Royale des Sciences de Leige 6*(10), 141-164.

Gaston, G. R. (1985), Effects of hypoxia on macrobenthos of the inner shelf off Cameron, Louisiana, *Estuar. Coast. Shelf Sci., 20*, 603-613.

Geyer, W. R., P.S. Hill, and G.C. Kineke (2004), The transport, transformation and dispersal of sediment by buoyant coastal flows, *Cont. Shelf Res., 24*(7–8), 927–949.

Glausiusz, J. (2000), Dead Zone, *Discover, 21(3)*, 22.

Glenn, S., R. Arnone, T. Bergmann, W. P. Bissett, M. Crowley, J. Cullen, J. Gryzmski, D. Haidvogel, J. Kohut, M. Moline, M. Oliver, C. Orrico, R. Sherrell, T. Song, A. Weidemann, R. Chant, and O. Schofield (2004), Biogeochemical impact of summertime coastal upwelling on the New Jersey Shelf, *J. Geophys. Res.*, *109*,C12S02, doi: 10.1029/2003JC002265.

Gray, J. S., R. S. Wu, and Y. Y. Or (2002), Effect of hypoxia and organic enrichment on the coastal marine environment, *Mar. Ecol. Progr. Series, 238*, 249-279.

Haidvogel, D.B., H.G. Arango, K. Hedstrom, A. Beckmann, P. Malanotte-Rizzoli, and A.F. Shchepetkin (2000), Model evaluation experiments in the North Atlantic basin: Simulations in nonlinear terrain-following coordinates, *Dynamics of Atmospheres and Oceans, 32*, 239-281.

Haine, T. W., and J. Marshall (1997), Gravitational, symmetric, and baroclinic instability of the oceanic mixed layer, *J. Phys. Oceanogr., 28*, 634-658.

Harper, D. E., L. D. McKinney, R. R. Salzer, and R. J. Case (1981), The occurrence of hypoxia bottom water off the upper Texas coast and its effects on the benthic biota, *Contrib. Mar. Sci., 24*, 53-79.

Harris, A. E., J. G. Ragan, and J. H. Green (1976), Oxygen depletion in coastal waters, *Sea Grant Summ. Rep. Proj*., *No. R/BOD*,1, 161 pp.

Hetland, R. D., and S. F. DiMarco (2008), How does the character of oxygen demand control the structure of hypoxia on the Texas–Louisiana continental shelf, *J. Mar. Sys., 70*, 49-62.

Hsu, S. A. (1998), A relationship between the Bowen ratio and sea-air temperature difference under unstable conditions at sea, *J. Phys. Oceanogr., 28*, 2222-2226.

Ichiye, T. (1962), Circulation and water mass distribution in the Gulf of Mexico, *Geofisica Internacional, 2*(3), 47-76.

Joyce, S. (2000), The dead zones: oxygen-starved coastal waters, *Environ. Health Perspect., 108(3)*, A120-A125.

Justic, D., N. N. Rabalais, and R. E. Turner (2002), Modeling the impacts of decadal changes in riverine nutrient fluxes on coastal eutrophication near the Mississippi River Delta, *Ecological Modelling*, *152*, 33-46.

Kalnay, E. (2006), *Atmospheric Modeling, Data Assimilation and Predictability*, pp. 341, Cambridge Univ. Press, New York.

Kamykowski, D, and S. Zentara (1990), Hypoxia in the world ocean as recorded in the historical data set, *Deep Sea Res.,37*(12),1861-1874.

Leben, R. R. (2005), Altimeter-derived Loop Current metrics, in *Circulation in the Gulf of Mexico: Observations and Models*, pp. 181-201, Geophys. Monogr., vol. 161, Amer. Geophys. Union.

Lentz, S. J., and K. R. Helfrich (2002), Buoyant gravity currents along a sloping bottom in a rotating fluid, *J. Fluid Mech*., *464*, 251-278.

Lohrenz, S. E., G. L. Fahnenstiel, and D. G. Redalje (1994), Spatial and temporal variations in photosynthesis parameters in relation to environmental conditions in coastal waters of the Northern Gulf of Mexico, *Estuaries, 17*, 779-795.

Marchesiello, P., J.C. McWilliams, and A. Shchepetkin (2001), Open boundary conditions for long-term integration of regional ocean models, *Ocean Modelling, 3*, 1-20.

Martin, C. M., T. Morton, T. Dobrynsk, and B. Valentine (1996), Estuaries on the Edge: the Vital Link between Land and Sea, Report by American Oceans Campaign, pp. 297, Washington DC.

Millard, R. C., W. B. Owens, and N. P. Fofonoff (1990), On the calculation of the Brunt-Väisälä frequency, *Deep Sea Res., 37*, 167-181.

Millero, F. J. (2005), *Chemical Oceanography*, pp. 496, CRC Press Taylor & Francis Group, Boca Raton, FL.

Milliman, J. D., and R.H. Meade (1983), World-wide delivery of river sediment to the oceans, *J. Geol., 91*(1), 1–21.

Murray, C. N., and J. P. Riley (1969), The solubility of gases in distilled water and seawater. 2. Oxygen, *Deep Sea Res., 16*, 311-320.

Neill, C.F., and M. A. Allison (2005), Subaqueous deltaic formation on the Atchafalaya Shelf, Louisiana, *Mar. Geol., 241*, 411-430.

Nowlin Jr., W. D., A. E. Jochens, S. F. DiMarco, R. O. Reid, and M. K. Howard (2005), Low-frequency circulation over the Texas-Louisiana continental shelf, in *Circulation in the Gulf of Mexico: Observations and Models*, pp. 219-240, Geophys. Monogr., vol. 161, Amer. Geophys. Union.

Nowlin, W. D., Jr., A. E Jochens, R. O. Reid, and S. F. DiMarco (1998), Texas-Louisiana Shelf Circulation and Transport process Study, Synthesis Report: Volume I, OCS Study/MMS 1998-0036, U. S. Department of the Interior, Minerals Management, Service, Gulf of Mexico OCS Region, New Orleans, LA.

Nowlin, W. D., Jr., A. E. Jochens, S. F. DiMarco, R. O. Reid, and M. K. Howard (2001), Deepwater Physical Oceanography Reanalysis and Synthesis of Historical Data: Synthesis Report, pp. 528, OCS Study MMS 2001-064, U.S. Dept. of the Interior, Minerals Management Service, Gulf of Mexico OCS Region, New Orleans, LA.

Oetking, P., R. Back, R. Watson, and C. Merks (1974), Hydrography on the Nearshore Continental Shelf of South Central Louisiana: Final Report of Offshore Ecology Investigation for Gulf Universities Research Consortium, Galveston, Texas, Southwest Research Institute, Corpus Christi, TX, Project No.03-3720.

Oguz, T. (2006), Hypoxia and Anoxia in the Black Sea, *Geophysical Research Abstracts*, Vol. 8, SRef-ID: 1607-7962/gra/EGU06-A-04829, European Geosciences Union, Institute of Marine Sciences, Middle East Technical University, Erdemli, Turkey.

Orlanski, I. (1969), The influence of bottom topography on the stability of jets in a baroclinic fluid, *J. Atmos. Sci., 26*, 1216-1232.

Osterman L. E., R. Z. Poore, P. W. Swarzenski, and R. E. Turner (2005), Reconstructing a 180 yr record of natural and anthropogenic induced low-oxygen conditions from Louisiana continental shelf sediments, *Geology, 33*(4), 329-332.

Peliz, A., J. Dubert, D. B. Haidvogel, and B. Le Cann (2003), Generation and unstable evolution of a density-driven Eastern Poleward Current: The Iberian Poleward Current, *J. Geophys. Res., 108*(C8), 3268, doi:10.1029/2002JC001443.

Pokryfki, L., and R. E. Randall (1987), Nearshore hypoxia in the bottom water of the Northwestern Gulf of Mexico from 1981 to 1984, *Mar. Environ. Res., 22*, 75-90.

Rabalais, N. N., and D. E. Harper, Jr. (1992), Studies of benthic biota in areas affected by moderate and severe hypoxia, in *Proceedings, Nutrient Enhanced Coastal Ocean Productivity Workshop*, pp. 150-153, Texas A&M Sea Grant Publication, Galveston, TX, TAMU-SG-92-109.

Rabalais, N. N., R. E. Turner, D. Justic, Q. Dortch, and W. J. Wiseman Jr. (1999), Characterization of Hypoxia: Topic 1. Report for the Integrated Assessment on Hypoxia in the Northern Gulf of Mexico, NOAA, *Coastal Ocean Program Decision Analysis Series*, *No.15*, NOAA Coastal Ocean Program, Silver Spring, MD.

Rabalais, N. N., R. E. Turner, and D. Scavia (2002a), Beyond science into policy: Gulf of Mexico Hypoxia and Mississippi River, *Bioscience, 52*(2), 129-142.

Rabalais, N. N., R. E. Turner, B. K. Sen Gupta, D. F. Boesch, P. Chapman, and M. C. Murrell (2007), Hypoxia in the Northern Gulf of Mexico: Does Science Support the Plan to Reduce, Mitigate, and Control Hypoxia?, *Estuaries and Coasts, 30*(5), 753-772.

Rabalais, N. N., R. E. Turner, and W. J. Wiseman (2001), Hypoxia in the Gulf of Mexico, *J. Environ. Qual., 30*, 320-329.

Rabalais, N. N., R. E. Turner, and W. J. Wiseman Jr. (2002b), Gulf of Mexico hypoxia, a.k.a. "The Dead Zone", *Annu. Rev. Ecol. Syst., 33,* 235–263.

Rabalais, N. N., R. E. Turner, W. J. Wiseman, and D. F. Boech (1991), A brief summary of hypoxia on the Northern Gulf of Mexico continental shelf: 1985-1988, in *Modern and Ancient Continental Shelf Anoxia*, pp. 35-47, edited by R. V. Tyson and T. H. Pearson, Geological Society Special Publication, London, England.

Ragan, J. G., A. H. Harris, and J. H. Green (1978), Temperature, salinity and oxygen measurements of surface and bottom waters on the continental shelf off Louisiana during portions of 1975 and 1976, *Prof. Pap. Biol, 3*, 1-29.

Ritter, C., and P. A. Montagna (1999), Seasonal hypoxia and models of benthic response in a Texas Bay, *Estuaries, 22*, 7-20.

Rowe G. T. (2001), Seasonal hypoxia in the bottom waters off the Mississippi River delta*, J. Environ. Qual., 30*, 281-290.

Rowe, G. T., and P. Chapman (2002), Continental shelf hypoxia: some nagging questions; commentary, *Gulf of Mex. Sci., 20*(2), 153-160.

Scavia, D., N. N. Rabalais, R. E. Turner, D. Justic, and W. J. Wiseman, Jr. (2003), Predicting the response of Gilf of Mexico hypoxia to variations in Mississippi River nitrogen load, *Limnol. Oceanogr., 43*(8), 951-956.

Schroeder, W. (1977), The impact of the 1973 flooding of the Mobile River system on the hydrography of Mobile Bay and east Mississippi Sound, *NE Gulf Sci., 1*(2), 68-76.

Seiler, R., G. Guillen, and A. M. Landry, Jr. (1991), Utilization of the upper Houston ship channel by fish and macroverterbrates with respect to water quality trends, in *Proceedings, Galveston Bay Characterization Workshop, February 21-23*, edited by F. S. Shopley and R. W. Kiesling, pp. 39-45, Galveston Bay National Estuary Program Publication GBNEP-6.

Shchepetkin, A.F. and J.C. McWilliams (1998), Quasi-monotone advection schemes based on explicit locally adaptive dissipation, *Mon. Wea. Rev*., *126*, 1541-1580.

Shchepetkin, A.F. and J.C. McWilliams (2003), A method for computing horizontal pressure-gradient force in an oceanic model with a non-aligned vertical coordinate, *J. Geophys. Res., 108*(C3), 3090, doi:10.1029/2001JC001047.

Shchepetkin, A.F. and J.C. McWilliams (2005), The regional ocean modeling system: a split-explicit, free-surface, topography-following coordinates ocean model, *Ocean Modelling, 9,* 347-404.

Simpson J. H. (1997), Physical processes in the ROFI regime, *J. Mar. Sys., 12*, 3-15.

Solis, R. S., and G. L. Powell (1999), Hydrography, mixing characterisctics, and residense times of Gulf of Mexico estuaries, in *Biochemistry of Gulf of Mexico estuaries*, edited by T. S. Bianchi, J. R. Pennock, and R. R. Twilley, pp. 29-61, John Wiley and Sons, New York.

Song, Y. T., and D. B. Haidvogel (1994), A semi-implicit ocean circulation model using a generalized topography-following coordinate system, *J. Comput. Phys., 115*, 228-244.

Stoddard, D. J., and J. J. Welsh (1986), Modeling oxygen depletion in the New York Bight: the water quality impact of a potential increase of waste inputs, in *Urban Wastes in Coastal Marine Environments*, Vol. 5, edited by D. A. Wolfe and T. P. O'Connor, pp. 92-102, Krieger Publishing Company, Malabar, FL.

Sturges, W., and A. Lugo-Fernandez (2005). *Circulation in the Gulf of Mexico: Observations and Models*, pp. 360, Geophys. Monogr., vol. 161, Amer. Geophys. Union.

Sturges, W., and R. Leben (2000), Frequency of ring separation from the Loop Current in the Gulf of Mexico: a revised estimate, *J. Phys. Oceanogr., 30*, 1814-1819.

Turner, R. E., and N. N. Rabalais (1994), Coastal eutrophication near the Mississippi River Delta, *Nature, 386*, 619-621.

Turner, R. E., and N. N. Rabalais, E. M. Swenson, M. Kasprzak, and T. Romaire (2005), Summer hypoxia in the northern Gulf of Mexico and its prediction from 1978 to 1995, *Mar. Environ. Res., 59*, 65-77.

U.S. Environmental Protection Agency (1999), The Ecological Condition of Estuaries in the Gulf of Mexico, U.S. Environmental Protection Agency, Office of Research and Development, National Health and Environmental Effects Research Laboratory, Gulf Ecology Division, Gulf Breeze, FL, EPA 620-R-98-004.

Väisälä, V. (1925), Uber die Wirkung der Windschwankungen auf die Pilotbeobeachtungen, *Soc. Sci. Fenn. Commentat. Phys.-Mat., 219*, 19-37.

Waller, R. S. (1998), Extent of hypoxia in areas east of the Mississippi River to Mobile Bay, 1998, Hypoxia Effects Workshop, Baton Rouge, LA.

Walsh, J. J. (1998), *On the Nature of Continental Shelves*, pp. 520, Academic Press, Inc., New York.

Wang, W., W. D. Nowlin, and R.O. Reid (1998), Analyzed surface meteorological fields over the Northwestern Gulf of Mexico for 1992-2004: mean, seasonal, and monthly patterns, *Mon. Wea. Rev., 126* (11), 2864-2883.

Wei, H. , Y. He, Q. Li, Z. Liu, and H. Wang (2007), Summer hypoxia adjacent to the Changjiang Estuary, *J. Mar. Sys., 67* (3), 292-303.

Wilkin, J. L., H. G. Arango, D. B. Haidvogel, C. S. Lichtenwalner, S. M. Durski, and K. S. Hedstrom (2005), A regional ocean modeling system for the long-term ecosystem observatory, *J. Geophys. Res., 110*, C06S91, doi:10.1029/2003JC002218.

Williams, S. J., M. A. Arsenault, B. J. Buczkowski, J. A. Reid, J. G. Flocks, M. A. Kulp, S. Penland, and C. J. Jenkins (2006), Surficial sediment character of the Louisiana offshore Continental Shelf region: a GIS Compilation, U.S. Geological Survey Open-File Report 2006-1195, online at http://pubs.usgs.gov/of/2006/1195/index.htm.

Wiseman, W. J., N. N. Rabalais, R. E. Turner, S. Dinnel, and A. MacNaughton (1997), Seasonal and interannual variability within the Louisiana coastal currents: stratification and hypoxia, *J. Mar. Sys., 12*, 237-248.

Wolfe, C. L., and C. Cenedese (2006), Laboratory experiments on eddy generation by a buoyant coastal current flowing over variable bathymetry, J. *Phys. Oceanogr., 36*, 395-411.

Wu R. S. S., B. S. Zhou, D. J. Randall, N. Y. S. Woo, and P. K. S. Lam (2003), Aquatic hypoxia is an endocrine disruptor and impairs fish reproduction, *Environ. Sci. Technol., 37*, 1137-1141.

Xue, H, and G. Mellor (1992), Instability of the Gulf Stream front in the South Atlantic Bight, *J. Phys. Oceanogr., 23*, 2326-2350.

Yin, K., Z. Lin, and Z. Ke (2004), Temporal and spatial distribution of dissolved oxygen in the Pearl River Estuary and adjacent coastal waters, *Cont. Shelf Res., 24*(16*)*, 1935-1948.

Zhang, X., S. F. DiMarco, D. C. Smith, IV, M. K. Howard, A. E. Jochens, and R. D. Hetland (2008), Near-resonant oceanic response to sea breeze on a stratified continental shelf, *J. Geophys. Res.,* submitted.

Zimmerman, R. J., and J. Williams (1995), Trends in shrimp catch in the hypoxia area of the northern Gulf of Mexico, in *Proceedings of the First Gulf of Mexico Hypoxia Management Conference*, pp. 64-75, Kenner, LA.

VITA

Name: Valeriya Kiselkova

Address: Department of Oceanography
c/o Dr. S. F. DiMarco
Texas A&M University
College Station, TX 77843-3146

Email Address: kiselkova@yandex.ru

Education: B.S., Civil Engineering, Far Eastern State Technical University, 1998

M.S., Civil Engineering, Far Eastern State Technical University, 2000

Ph.D., Oceanography, Texas A&M University, 2008